Max-Planck-Institut
für Meteorologie

MAX-PLANCK-GESELLSCHAFT

International Max Planck Research School
on Earth System Modelling

Towards a scale aware cloud process parameterization for global climate models

Vera Schemann

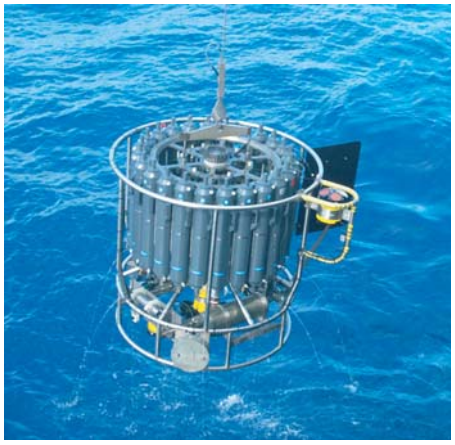

Berichte zur Erdsystemforschung 145/2014

Reports on Earth System Science

Hinweis

Die Berichte zur Erdsystemforschung werden vom Max-Planck-Institut für Meteorologie in Hamburg in unregelmäßiger Abfolge herausgegeben.

Sie enthalten wissenschaftliche und technische Beiträge, inklusive Dissertationen.

Die Beiträge geben nicht notwendigerweise die Auffassung des Instituts wieder.

Die "Berichte zur Erdsystemforschung" führen die vorherigen Reihen "Reports" und "Examensarbeiten" weiter.

Notice

The Reports on Earth System Science are published by the Max Planck Institute for Meteorology in Hamburg. They appear in irregular intervals.

They contain scientific and technical contributions, including Ph. D. theses.

The Reports do not necessarily reflect the opinion of the Institute.

The "Reports on Earth System Science" continue the former "Reports" and "Examensarbeiten" of the Max Planck Institute.

Anschrift / Address

Max-Planck-Institut für Meteorologie
Bundesstrasse 53
20146 Hamburg
Deutschland

Tel.: +49-(0)40-4 11 73-0
Fax: +49-(0)40-4 11 73-298
Web: www.mpimet.mpg.de

Layout:

Bettina Diallo, PR & Grafik

Titelfotos:
vorne:
Christian Klepp - Jochem Marotzke - Christian Klepp
hinten:
Clotilde Dubois - Christian Klepp - Katsumasa Tanaka

Berichte zur Erdsystemforschung 145/2014

Towards a scale aware cloud process parameterization for global climate models

Vera Schemann

aus Münster

Hamburg 2013

Reports on Earth System Science 145/2014

ISSN 1614-1199

Vera Schemann
Max-Planck-Institut für Meteorologie
Bundesstrasse 53
20146 Hamburg

Als Dissertation angenommen
vom Department Geowissenschaften der Universität Hamburg

auf Grund der Gutachten von
Prof. Dr. Bjorn Stevens
und
Dr. Verena Grützun

Hamburg, den 18. November 2013
Prof. Dr. Christian Betzler
Leiter des Departments für Geowissenschaften

ISSN 1614-1199

Towards a scale aware cloud process parameterization for global climate models

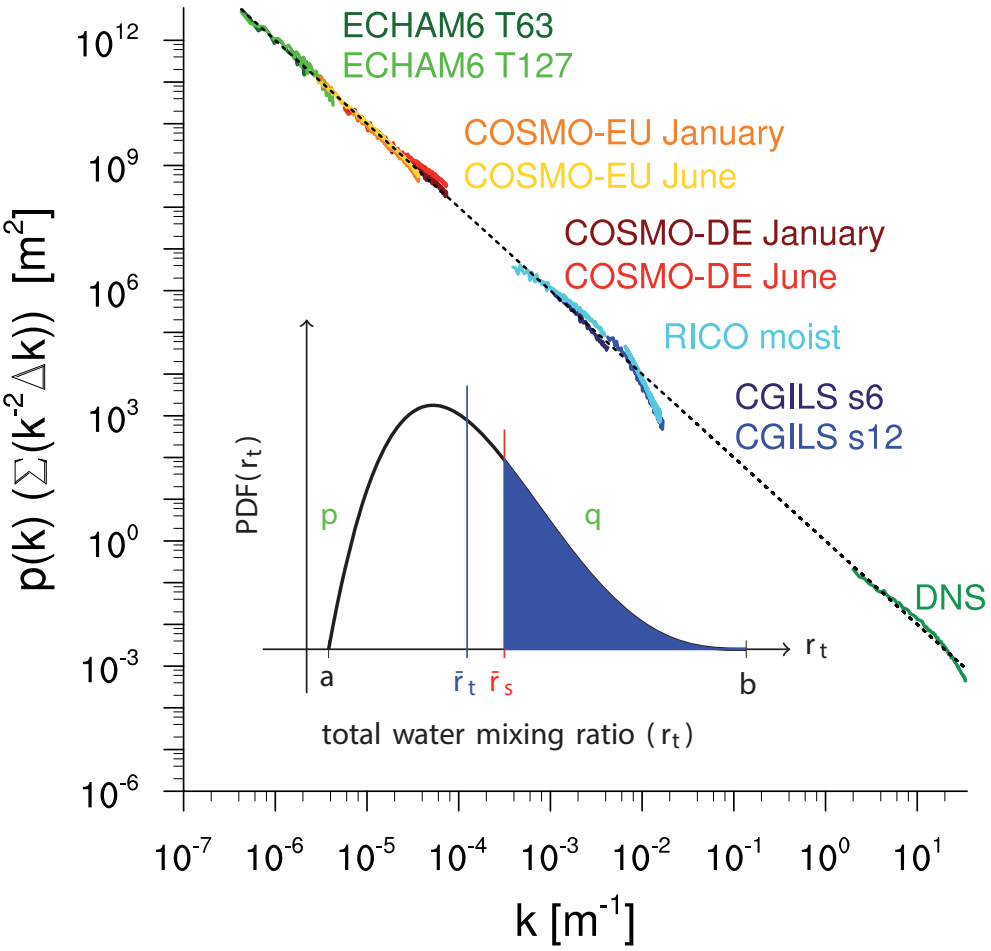

Vera Schemann

Hamburg 2013

Abstract

A state of the art statistical cloud cover scheme is investigated with respect to scale dependency and representation of subgrid-scale variability of total water. First, the expected scale dependency of total-water variance is estimated by analyzing data from a General Circulation Model (GCM), a Numerical Weather Prediction (NWP) model and Large Eddy Simulations (LES). Additionally, data from Direct Numerical Simulations (DNS) is included for parts of the analysis. The evaluation shows a consistent and continuous scaling behaviour of total-water variance over all analyzed scales. Especially for the coarser models (GCM and NWP) a consistent power law with an exponent of approximately -2 is found. The whole spectrum shows neither a spectral gap, nor evidence for a strong break in the scaling. This estimated scale dependency is found not to be represented in the statistical cloud scheme. The parameterized variance underestimates the expected subgrid-scale variability of total water and does not show any scale dependency. In order to reduce the underestimation of subgrid-scale variability of total water, three development steps for the statistical scheme are suggested. First, in cases of a negative distribution minimum, an approximation of a truncated beta distribution by the general beta distribution shows a better consistency with the cloud condensate contained in the model. Avoiding the additional evaporation of cloud condensate produced by the previous approach improves the representation of subgrid-scale variability of total water. Second, prognostic equations for the higher moments variance and skewness are implemented. These moments provide a better physical interpretation than the previously used shape parameter and distribution width. Additionally, the flexibility and the range of possible skewness values is increased and extended by allowing negative skewness. Third, a new parameterization for the contribution by convection to the higher moments is introduced. By this, the coupling to the convection parameterization is strengthened. The new source terms are formulated exclusively in the space of the moments, which provides an easier use of other distributions or closures. The development is evaluated within the ECHAM6 GCM, using the metric of critical relative humidity. By this metric, it is possible to reproduce an observed subgrid-scale variability of total water with the revised statistical schemes. The main changes can be observed by the coupling to other processes (e.g. large-scale condensation). This thesis emphasizes the need for and contributes to the development of scale-aware parameterizations and an improved coupling of statistical schemes to other processes.

Contents

Chapter 1

Introduction

Clouds play an important role for our weather and climate. Their interaction with the radiation influences the Earth's energy budget and they are also essential for the formation of precipitation. The spectrum of important scales for cloud processes is broad and ranges from the micrometer scale (cloud drops) to cloud structures at several hundreds or thousands of kilometers (e.g Stevens and Bony 2013). Due to this large spectrum, cloud modelling is still a big challenge in todays modelling of atmospheric physics and a major driver for the uncertainties in current climate change simulations (e.g., Bony and Dufresne 2005; Randall et al. 2007). The focus of this thesis is on the evaluation and improvement of the representation of humidity fluctuations – and with this clouds – in general circulation models (GCM).

General circulation models typically operate today at a resolution of several hundred kilometers ($O(100\,\mathrm{km})$) for global climate simulations. At this resolution important processes, such as convection, cannot be resolved. The use of coarse model grids can be associated with a filtering applied to the equations describing the physical processes. This filtering separates the whole spectrum of variability distributed over different scales into two parts: the resolved – the grid-scale – variability and the unresolved – the subgrid-scale – variability. As the unresolved part is nevertheless essential for the processes in the atmosphere, it is necessary to define submodels describing the amount of unresolved variability. These submodels are called parameterizations. A typical approach for a parameterization is to find a relationship between unresolved variability and the grid-scale mean values. Nowadays, parameterizations are also becoming more popular that attempt to describe the unresolved variability in a stochastic sense.

Even though clouds act on a broad spectrum of scales, the processes leading to the formation of clouds are mainly part of the unresolved variability in GCMs and need to be parameterized. For warm boundary layer clouds the assumption that clouds form as soon as the air is saturated provides a good approximation to reality. Due to the fluctuations of humidity and temperature inside a grid box of the scale $O(1-100\,\mathrm{km})$ parts of the box will already be saturated before the whole grid box, respectively the mean values, reach saturation. This fractional cloud cover can be included into the model by defining a way to represent the subgrid-scale fluctuations of humidity.

In a modelling context, humidity is often described by total water, i.e. the sum of water vapor, liquid water and ice. The subgrid-scale variability of humidity should be the zeroth order task for cloud cover parameterizations, but additionally, also the fluctuations of temperature and vertical velocity could be taken into account (Tompkins 2003). Figure 1.1 drafts the differences between an all-or-nothing approach, which neglects the subgrid-scale fluctuations of humidity and calculates the cloud cover based on the saturation of the grid box, and an approach taking the fluctuations of humidity into account, which leads to partial cloud cover.

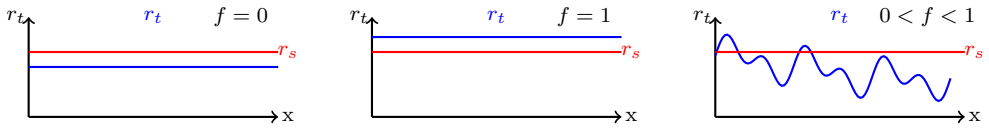

Figure 1.1: Sketch of one dimensional (x) grid box showing the differences between neglecting fluctuations of humidity (left and middle) and including fluctuations of humidity (right). Left: The total-water mean (r_t, blue) is less than the saturation value (r_s, red) that leads to zero cloud fraction ($f = 0$). Middle: The whole one-dimensional grid box is saturated ($r_t > r_s$) that leads to cloud fraction of $f = 1$. Right: If fluctuations of total water are taken into account, partial cloud cover is possible and the cloud fraction can be between 0 and 1.

How the strength of the fluctuations represented by a parameterization should change with resolution, is one of today's research questions in parameterization development. It becomes more important as methods such as grid refinement are becoming more popular. These methods use a basis coarse grid, but increase the resolution at certain regions in order to resolve more processes locally. This raises the challenge for parameterizations to be applicable and consistent over a broad range of different resolutions. In addition, many processes are interacting with each other and this needs to be represented by coupled parameterizations (e.g. Moeng and Stevens 2000; Siebesma et al. 2009). To provide a consistent representation of a certain subgrid-scale variability across all interactions with other processes is another challenge for the development and implementation of parameterizations. Both challenges – the consistent representation across scales and across processes – will be addressed for cloud cover parameterizations in this thesis, by two leading questions:

- How should the subgrid-scale variability of humidity change with resolution?
- How can a consistent representation of subgrid-scale variability of humidity in a GCM be achieved?

For the representation of subgrid-scale fluctuations of humidity, varying approaches can be found in the literature and in models. They all are assuming an underlying

probability density function (PDF) of humidity, and some additionally of temperature and vertical velocity. But they differ in the complexity and the explicitly used properties of the distribution. Based on these differences three main categories can be defined. The first category of possible cloud cover parameterizations uses an explicit prognostic equation for the cloud fraction (Tiedtke 1993). As the cloud fraction is an integrated quantity of a PDF of humidity, and maybe additionally temperature and vertical velocity, also these schemes assume a PDF, even though it is less explicit than for the other approaches. In order to improve the representation of subgrid-scale variability of humidity the focus of this dissertation is on the two following approaches which include the PDF more explicitly.

The second category is the early but still used approach of (critical) relative humidity schemes (e.g. Sundqvist 1978; Sundqvist et al. 1989). These schemes define a critical relative humidity and as soon as the relative humidity reaches this threshold, clouds start to form and grow monotonically with relative humidity. These schemes are defined by their monotonic function and the value of critical relative humidity. Both decisions are typically made independent of longitude and latitude, and also without a direct coupling to the applied resolutions. With this, strong restrictions are made on the representation of global differences and for a possible scale adaptivity. Another strong restriction is that it is impossible to form clouds before the threshold is reached. For instance in dry areas cloud water (liquid plus ice) detrained from convection would evaporate instantaneously as long as the mean relative humidity of the grid box is below the threshold. Nonetheless, these schemes represent the subgrid-scale variability in an easy and computationally efficient way and are still used in current GCMs (e.g. ECHAM6, Stevens et al. (2013)).

The description of the subgrid-scale variability of humidity with a critical relative humidity and a monotonic function is equivalent to assuming explicitly a certain probability density function (PDF) of humidity with a fixed distribution width (e.g. Smith 1990; Le Trent and Li 1991). Approaches which are based on the explicit assumption of a specific PDF family are called statistical or assumed PDF schemes and form the third category. The range of PDF families assumed in these approaches is broad and ranges from gaussian (Sommeria and Deardorff 1977) over uniform (Le Trent and Li 1991) and triangles (Smith 1990) to generalized log-normal (Bony and Emanuel 2001), beta (Tompkins 2002) and double gaussian distributions (Larson et al. 2001). Also the way how the PDF is described is diverse, and besides a fixed distribution width (e.g. Smith 1990) also diagnostic (e.g. Bony and Emanuel 2001) or prognostic equations (e.g. Tompkins 2002) are used to describe the width and shape of the PDFs. For this approach, the cloud fraction is calculated by integrating over the saturated part of the PDF. In addition, some schemes use the PDF to diagnose the amount of subgrid-scale cloud water (e.g. Larson et al. 2001), while other schemes use the PDF to describe solely the spatial variability of the cloud water produced by other parameterizations

(e.g. Bony and Emanuel 2001; Tompkins 2002). The latter approach allows an easier parameterization of the microphysical processes by separate prognostic equations for the cloud water, and the possibility of a consistent coupling between several parameterizations (e.g. convection, microphysics and cloud cover). This thesis focuses on statistical cloud schemes that use prognostic equations to describe the shape of the PDF. Furthermore, the PDF will be used to describe the spatial variability of cloud water and total water, while the amount is mainly determined by parameterizations for convection and microphysics (e.g. precipitation and condensation). A more detailed review of this type of statistical cloud schemes and especially the scheme by Tompkins (2002) will be given in chapter 2.

The opportunity of statistical cloud schemes to describe the shape of the PDF by diagnostic or prognostic equations not only allows a flexible evolution in time, but also has the potential for a sensible adjustment with resolution. The development of many parameterizations was and is based on the assumption of a spectral gap. This means that the variability is produced at large and at small scales with a gap in between. As a consequence, for the range of the gap always the same amount of subgrid-scale variability has to be parameterized independently of the exact resolution of the GCM. In the last years, more evidence was found that the assumption of a spectral gap might not be fulfilled and that varying resolutions have to be taken into account for parameterization development (e.g. de Roode et al. 2004; Jonker et al. 1999). Especially methods such as grid refinement, which provide the possibility to use several resolutions in one model setup, strengthen the need for more detailed investigations of the distribution of variability to different scales. And as a consequence they also raise the need for the development of scale-aware or scale-dependent parameterizations. Those parameterizations should take the resolution into account and potentially adjust automatically, without additional tuning. The statistical cloud schemes have the potential to fulfill these requests, but first it is important to analyze how cloud cover parameterizations and their representation of subgrid-scale variability of humidity should change with resolution. Based on observational studies, in the past some analysis of the scale dependency of water vapor variability has been performed (e.g. Kahn and Teixeira 2009; Kahn et al. 2011). But for the conserved variable total water, which is essential for cloud and large-scale condensation parameterizations, the question of scale dependency is still an open question. In chapter 3 an evaluation of the scale dependency of the variance of total water and its implication for the development of cloud cover parameterizations will be presented.

Using the amount of total water produced by other parameterizations already constitutes a first strong coupling between the parameterizations. But statistical schemes offer the possibility for more interactions, as the representation of other processes could be improved by the information about spatial variability of total water (e.g. radiation and autoconversion). But before the spatial variability of total water can be used in

other parameterizations, it is important to evaluate the representation of this variability described by the statistical schemes. Weber et al. (2011) and Quaas (2012) evaluated the statistical scheme by Tompkins (2002) and found an underestimation of produced subgrid-scale variability of total water. These studies showed the need of first improving the overall representation of subgrid-scale variability of total water, before a stronger scale dependency or more interactions with other processes could be introduced. In chapter 4 three major development steps on how to improve the representation of subgrid-scale variability with a statistical scheme based on the one by Tompkins (2002) will be presented. In chapter 5 the improvement obtained by these three steps will be measured by evaluating the critical relative humidity produced by the revised statistical cloud schemes in comparison to two reference cloud schemes and observational data.

The explicit description of subgrid-scale variability of humidity is one big advantage of the statistical cloud schemes, as it offers the possibility to use this variability in the parameterization of other processes. But besides representing the important fluctuations and subgrid-scale variabilities for one process in a reasonable way, modeling the interaction between varying unresolved processes is a big challenge on its own. The great potential of statistical cloud schemes to include their description of variability into other parameterizations also leads to constraints on their computational complexity and consistency. The consequences of the common approach to reduce the degrees of freedom in order to obtain a less complex description will be discussed exemplarily for the statistical scheme by Tompkins (2002) in chapter 4. The various interactions with other processes also raise the need to understand the dependency of the statistical scheme on the initial conditions. For the interpretation and evaluation of the statistical scheme embedded in a GCM it is essential to understand the mechanisms responsible for changes in the shape or the cloud fraction. This will be discussed theoretically in chapter 4, but is also important for the evaluation of the revised schemes in chapter 5.

Besides theoretical approaches, the analysis of high resolution Large Eddy Simulations (LES) is an important tool in the development of cloud parameterizations. Those simulations allow to investigate the interaction and evolution of certain processes on a spatial and temporal scale. Due to computational progress, the evaluation and development of parameterizations can benefit during the next years from the performance of simulations with higher resolutions on larger domains. Also in this thesis several simulations have been used to analyze possible parameterizations and to sharpen the expectations on the behaviour of the statistical cloud scheme. An overview of the included simulations will be given in chapter 2.

The development of cloud cover parameterizations that are consistent across scales and processes is a great challenge and will become more important in the coming years, with GCMs that are more flexible in their resolutions and their intended simulations. This thesis highlights the need of scale aware parameterizations by analyzing the scale

dependency of total-water variance over a large range of scales. It moreover contributes to the development of statistical cloud schemes in order to provide a consistent representation of the subgrid-scale variability of total water.

1.1 Outline and structure of the thesis

The chapters 3, 4, and 5 of the thesis are written with the intention to be readable independently, and with this they include their own introduction and conclusion. Nevertheless, especially chapter 4 and chapter 5 are strongly coupled by developing and evaluating a revised statistical cloud scheme. Chapter 3 is accepted (in press) in the Journal of the Atmospheric Sciences. For editorial consistency, some editorial changes and minor modifications have been made to the text of chapter 3. The thesis is structured in the following way:

Chapter 2 In chapter 2 a review of statistical cloud schemes and especially the statistical scheme by Tompkins (2002) is provided. Additionally, this chapter includes an overview of the models and datasets used in this thesis.

Chapter 3 In chapter 3 the scale dependency of total-water variance is investigated by using the output of a broad range of models, from a high-resolution model to a coarse global model. Based on the results, the statistical scheme of Tompkins (2002) is evaluated with respect to scale dependency.

Chapter 4 In chapter 4 three major development steps are presented in order to improve the representation of the subgrid-scale variability of total water by the statistical scheme based on Tompkins (2002). Also the common approach to reduce the degrees of freedom and its consequences is discussed. Finally, the dependency of the cloud fraction on the cloud water and skewness of the PDF is evaluated to develop a better understanding of the expected behaviour of the scheme.

Chapter 5 In chapter 5 the evaluation of the revised statistical cloud scheme, following the development steps suggested in chapter 4, is presented. The representation of the subgrid-scale variability of total water is evaluated using the metric of critical relative humidity, following Quaas (2012).

Chapter 6 The thesis closes with a general summary and conclusion of the results presented in chapters 3 to 5 and provides an outlook discussing the open questions on the way to a scale-aware cloud process parameterization.

1.2 Research questions

The overall motivation of this thesis is driven by the challenge to find a representation of subgrid-scale variability of humidity consistent across scales and processes. The two leading questions raised by this challenge, which have been mentioned earlier, will be at the basis of the whole thesis and are specified in more detail in the research questions.

Research questions:

- How should the subgrid-scale variability of total water change with resolution? And how can this information be used for the evaluation and development of parameterizations?
- How can the representation of subgrid-scale variability of total water by a statistical cloud scheme be improved?
- How does the sensitivity of the properties of the PDF depend on the chosen approach to determine the parameters? How should the parameterization respond to changes in the initial conditions?

Chapter 2

Background

In this chapter, a short review of the general idea of statistical cloud parameterizations and especially the scheme by Tompkins (2002) is presented. The statistical scheme is evaluated in chapter 3 and provides the basis for the parameterization development presented in chapter 4 and chapter 5. Furthermore, a short overview of the models and datasets used for the simulations and the evaluation in the following chapters is provided. As chapter 3 contains its own description of the datasets, the focus here is on the simulations presented in chapter 4 and chapter 5.

2.1 The approach of statistical cloud schemes

In current general circulation models (GCMs) the grid-box size varies between approximately 10 km and 200 km. In a grid box of this size, internal fluctuations of humidity or temperature lead to cloud formation before the grid box mean values reach saturation. The aim of cloud cover parameterizations is to represent these fluctuations inside a grid box and describe them in a way, that allows the calculation of partial cloud cover. One approach to represent the subgrid-scale fluctuations is to assume an underlying probability density function (PDF). This approach is called a statistical cloud scheme, or assumed PDF scheme. The most important subgrid-scale variability for the formation of partial cloud cover is caused by fluctuations of humidity (total water). Fluctuations of temperature and, to a smaller extent, vertical velocity are moreover influencing the cloud formation (e.g. Tompkins 2003). When fluctuations of multiple quantities shall be considered, joint PDFs can be used. For instance, Larson et al. (2002) introduce a joint PDF for humidity, temperature and vertical velocity. The use of a joint PDF requires more parameters and with this a larger number of equations and an increased computational effort. A more common approach is to include the fluctuations of humidity as well as the fluctuations of temperature by formulating the parameterization in terms of the *saturation deficit*, s (e.g., Tompkins 2002). This quantity is defined by

$$s = a_l(r'_t - \alpha_l T'_l) \quad , \tag{2.1}$$

where r_t' describes the fluctuations of total water and T_l' the fluctuations of liquid water temperature. The parameters are defined by $a_l = (1 + (\frac{L}{c_p})\alpha_l)^{-1}$ and $\alpha_l = (\frac{\partial r_s}{\partial T})(\bar{T}_l)$, with $\bar{T}_l$ the mean thermodynamic state, r_s the saturation vapor mixing ratio, L the latent heat of vaporization, and c_p the specific heat of dry air (Tompkins 2002).

Whether or not the fluctuations of temperature (and vertical velocity) have to be taken into account or can be neglected is highly discussed. A good overview of several studies discussing the influence of temperature fluctuations is given in Tompkins (2008). Tompkins (2003) concluded in his analysis of the impact of temperature and humidity variability on cloud cover, that the fluctuations of humidity are more important and should be the zeroth order task for parameterizations. It would however be desirable to include the fluctuations of temperature at a later point. Following this suggestion, only the PDF of total water (sum of water vapor, liquid water and ice) is used and discussed in this study. By only considering the fluctuations of total water, the two (or even three) dimensional PDF is reduced to a one dimensional PDF as outlined in Fig. 2.1.

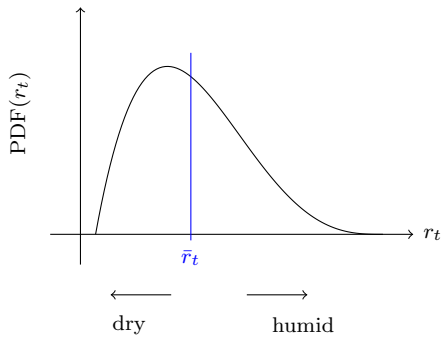

Figure 2.1: Sketch of a distribution of total water (r_t). The right side of the distribution describes the probability of high values of total water and with this the humid and potentially saturated part, while the left side represents the probability of dry and potentially unsaturated parts of the grid box.

If the distribution of total water is known, some conclusions about the atmospheric state in a grid box can immediately be drawn from the shape of the distribution. A positive skewness, which produces a tail to the right side, describes a situation, where the air inside the grid box is mainly rather dry with only a few points of high humidity. A negative skewness in contrast leads to a tail on the left side and describes a grid box that mainly consists of moist air with a few dry areas. Physically, the first situation is often connected to convection that is happening on a small area compared to the grid box size. The latter situation is mainly connected to downdrafts or subsiding regimes, that are bringing dry air into a rather moist volume. High values of skewness (negative and positive) and variance give the impression of a rather heterogeneous environment,

as a broad spectrum of total-water values is present in the volume. As the opposite, small values for skewness and variance are indicating a rather homogeneous, well mixed environment with only a small range of different total-water values inside the grid box.

Besides this general representation of the physical situation, also important properties of the grid box, as for instance the total water mean ($\bar{r}_t$), can immediately be determined by integration if the PDF is known:

$$\bar{r}_t = \int_0^\infty r_t \, \mathrm{PDF}(r_t) dr_t \tag{2.2}$$

For statistical schemes, a common assumption is, that condensation happens instantaneously when saturation is reached. This is often a good approximation for warm clouds, which consist of liquid water, but more problematic for ice clouds. Nevertheless, this assumption is also made in the following and cloud water is often used to refer to the cloud water (liquid plus ice). With this assumption and a known saturation mixing ratio (r_s), the cloud water mean ($\bar{r}_c$), the water vapor mean ($\bar{r}_v$), and the cloud fraction (f) can be calculated.

$$\bar{r}_c = \int_{r_s}^\infty (r_t - r_s) \, \mathrm{PDF}(r_t) dr_t \tag{2.3}$$

$$\bar{r}_v = \int_0^{r_s} r_t \, \mathrm{PDF}(r_t) dr_t + \int_{r_s}^\infty r_s \, \mathrm{PDF}(r_t) dr_t \tag{2.4}$$

$$f = \int_{r_s}^\infty \mathrm{PDF}(r_t) dr_t \tag{2.5}$$

Now the decision on a certain assumed PDF family has to be made. In addition, the question how to determine a certain member of this PDF family has to be answered. In the following, one way how this can be done is presented by giving a short review of the statistical scheme by Tompkins (2002). This scheme is also the basis for the analysis and development in the following chapters.

2.1.1 The statistical cloud scheme by Tompkins

In this section a review of the original Tompkins scheme implemented in the ECHAM6 GCM will be given. This review is mainly based on the original publication Tompkins (2002) and an ECMWF Seminar by Tompkins (Tompkins 2008).

The statistical scheme by Tompkins (2002) assumes the PDF family of general beta distributions. A general beta distribution is defined by four parameters, a minimum ($a \in \mathbb{R}$), a maximum ($b \in \mathbb{R}$), and two shape parameter ($p > 0$ and $q > 0$). Such a beta distribution is outlined in Fig. 2.2. The formal definition of the PDF is given by

$$f_g(x) = \frac{1}{B(p,q)} \frac{(x-a)^{p-1}(b-x)^{q-1}}{(b-a)^{p+q-1}} \quad a \leq t \leq b \quad , \tag{2.6}$$

with $p > 0$ and $q > 0$, and $a, b \in \mathbb{R}$. For a bell shaped regime, p and q have to fulfill the stronger constraint of $p > 1$, $q > 1$. $B(p, q)$ is the beta function and is defined by

$$B(p,q) = \frac{\Gamma(p)\Gamma(q)}{\Gamma(p+q)} \quad , \tag{2.7}$$

where Γ is the gamma function.

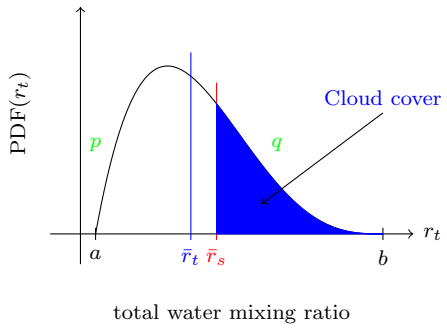

Figure 2.2: Sketch of a beta distribution of total-water mixing ratio (r_t). The cloud cover can be calculated by integrating over the saturated part ($r_t > r_s$) (see Eq. (2.11)).

As the general beta distribution is defined on the bounded interval $[a, b]$, this simplifies the general equation for the total water mean ($\bar{r}_t$, Eq. (2.3)), the cloud water mean ($\bar{r}_c$, Eq. (2.3)), the water vapor mean ($\bar{r}_v$, Eq. (2.4)) and the cloud fraction (f, Eq. (2.5)), to

$$\bar{r}_t = \int_a^b r_t \, f_g(r_t) dr_t = (b-a)\frac{p}{p+q} + a \tag{2.8}$$

$$\bar{r}_c = (b-a)\frac{p}{p+q}(q - I_x(p+1, q)) + (a - r_s)(1 - I_x(p, q)) \tag{2.9}$$

$$\bar{r}_v = (b-a)\frac{p}{p+q} I_x(p+1, q) + (a - r_s) I_x(p, q) + r_s \tag{2.10}$$

$$f = 1 - I_x(p, q) \quad \text{, with} \tag{2.11}$$

$$x = \frac{r_s - a}{b - a} \quad , \tag{2.12}$$

where $f_g(r_t)$ is used as PDF and $I_x(p, q)$ is the incomplete beta function, defined as

$$I_x(p,q) = \frac{1}{B(p,q)} \int_0^x r_t^{p-1}(1 - r_t)^{q-1} dr_t \quad . \tag{2.13}$$

Again for this the assumption has been made, that no super-saturation occurs and cloud water could include both, liquid and ice. A graphical impression of the cloud fraction described by a beta distribution, can be seen in Fig. 2.2.

The higher moments of the beta distribution can be described by:

$$\overline{r_t'^2} = \frac{(b-a)^2}{(p+q)^2}\frac{pq}{p+q+1} \qquad \text{(variance)} \tag{2.14}$$

$$\zeta = \frac{2(q-p)}{p+q+2}\sqrt{\frac{p+q+1}{pq}} \qquad \text{(skewness)} \tag{2.15}$$

At this point, two important decisions have already been made: the PDF will represent the fluctuations of total water, and the general beta distribution has been assumed as the underlying PDF family. As the next step, it is essential to define how a specific member of the PDF family will be determined. This leads to the question of input parameters and needed equations. As the general beta distribution is described by four parameters, a and b for the minimum and maximum, and p and q for the shape, four input variables or equations are needed. In theory the first four moments – mean, variance, skewness and kurtosis – could be used for this, but that would not be a trivial problem. Besides the mathematical difficulties, also from a physical point of view it is already difficult to develop a good physical understanding of the first three moments, but this would be even more challenging for the kurtosis.

Another point to take care of, is the consistency within the model. If the four parameters of one distribution are known, the cloud water can be calculated by Eq. (2.9) and the PDF could be used to diagnose the cloud water. If a prognostic equations for cloud water – or liquid and ice separately – is used in the GCM, which is the case for the ECHAM6, then it is important to include this quantity in the description of the PDF. Otherwise, the value diagnosed from the PDF could be different – and with that inconsistent – to the prognostic cloud water, that is calculated as part of the GCM. Tompkins (2002) decided to use the cloud water (Eq. (2.9)) as an input value in partially cloudy cases. Additionally the total-water mean and two equations for the shape of the PDF are used.

A grid box is defined to be partially cloudy, if a certain amount of cloud water exists ($\bar{r}_c > 0$), but not the whole grid box is saturated ($\bar{r}_v < r_s$). In clear ($\bar{r}_c = 0$) or overcast ($\bar{r}_v > r_s$) situations the cloud-water mean does not provide any information independent of the total-water mean and a different equation has to be used to determine the width of the distribution. This could be done by the variance, but Tompkins (2002) decided to use the distribution width ($b-a$) instead. For the shape of the distribution an equation for the shape parameter q is introduced, while the parameter p is set to a constant value of 2. The motivation for this restriction is based on the desire to avoid negative skewness and on the constraint $2 \leq q \leq 50$. In summary, the four input variables used in the Tompkins scheme for the determination of one specific distribution out of the family of general beta distributions in partially cloudy cases, are:

- the total water mean,

- the cloud water mean,
- the shape parameter q, representing the skewness,
- the closure $p = 2$.

The two input variables total water mean and cloud water mean are already present in the ECHAM6 GCM and described by separate prognostic equations. But for the shape parameter and for the distribution width (used in case of clear or overcast sky) new equations have to be introduced and for this either a diagnostic or a prognostic approach could be chosen. While diagnostic equations are cheaper with respect to computer power and memory, prognostic equations allow to carry a memory of the process. As many cloud structures are developing over hours and with this over timescales longer than the model timestep, Tompkins (2002) decided to introduce two additional prognostic equations, one for the shape parameter q and one for the distribution width $(b - a)$. For the skewness (and with this the shape parameter) it is still a point of discussion, if it is contained on timescales longer than a typical model timestep and should be prognostic, or if it is only operating at short timescales and should rather be diagnostic (see e.g. Klein et al. (2005)).

In a simplified way, a prognostic equation for a certain quantity, x, can be separated into three different parts, a time derivative, an advection term and local source and sink terms:

$$\frac{\partial x}{\partial t} + \mathbf{v} \cdot \bigtriangledown x = \sum_i S_i \quad , \tag{2.16}$$

with $\mathbf{v}$ being the wind and S_i source and sink terms. In case of the shape parameter q and the distribution width the advection is neglected and the prognostic equations consist only of the source and sink terms. The source and sink terms are divided into the contributions by three physical processes, the convection (conv), the turbulence (turb) and the microphysics (micro):

$$\left(\frac{\partial q}{\partial t}\right) = \left(\frac{\partial q}{\partial t}\right)_{\text{conv}} + \left(\frac{\partial q}{\partial t}\right)_{\text{turb}} + \left(\frac{\partial q}{\partial t}\right)_{\text{micro}} \tag{2.17}$$

$$\left(\frac{\partial (b-a)}{\partial t}\right) = \left(\frac{\partial (b-a)}{\partial t}\right)_{\text{conv}} + \left(\frac{\partial (b-a)}{\partial t}\right)_{\text{turb}} \tag{2.18}$$

For the distribution width, the assumption is made, that the influence of the microphysics is only implicit, as the distribution width is diagnosed in case of partial cloud cover. The parameterization of the individual source terms by Tompkins (2002) is presented in the Appendix A.1, while the motivation for the parameterizations will be explained during the introduction of prognostic equations for the higher moments skewness and variance in section 4.4.

Application of the PDF in cloud physics

Theoretically, the description of subgrid-scale variability provided by the PDF could be used in many physical processes parameterized in a GCM (e.g. autoconversion of cloud water to rain or radiation). Currently, the PDF is used for the calculation of the actual cloud fraction and for two more applications: to determine the influence of turbulence on the cloud water and water vapor, and for the large-scale condensation. Both applications will be briefly described in the following.

Influence of turbulence: The influence of turbulence on the cloud water and water vapor, is calculated by explicitely using an updated PDF. The shape parameter and the distribution width are updated with respect to the turbulence tendency (see Eq. (2.17) and Eq. (2.18), or A.1), while the mean value is assumed to stay unchanged ($\Delta r_t = 0$). Then a new value for the cloud water, or water vapor respectively, can be calculated by Eq. (2.9) or Eq. (2.10).

Large-scale condensation: Cooling or warming of a grid box and convergence or divergence of total water can also lead to changes in the cloud water. These changes (e.g. condensation or deposition) are calculated by using updated values of total water mean and saturation mixing ratio, but assuming the shape (p and q) to be unchanged. By introducing updated values for the distribution minimum $a_{n+1} = a_n + \Delta\bar{r}_t$, the total-water mean $(\bar{r}_t)_{n+1} = (\bar{r}_t)_n + \Delta\bar{r}_t$, and the saturation $(r_s)_{n+1} = (r_s)_n + \Delta r_s$ into Eq. (2.9) or Eq. (2.10) new values for the cloud water or water vapor can be calculated.

Order of calculations

In numerical models parameterizations are often applied in a certain order, even though in reality the processes would happen at the same time. This is a drawback of discretization. To give an impression of the importance of always keeping a consistent formulation, the order of calculations of the statistical scheme that is implemented in the ECHAM6 model is outlined below:

1. From the last time step or initial conditions, p, q, $\bar{r}_t$, $\bar{r}_c$, and $(b-a)$ are given.
2. The minimum a is determined:
   - for partial cloudiness ($\bar{r}_c > 0$, $\bar{r}_v < r_s$) – iteratively by combining Eq. (2.8) and Eq. (2.10) and solving for a:

$$\begin{aligned} 0 &= (r_t - a) I_x(p+1, q) + (a - r_s) I_x(p, q) + r_s - \bar{r}_v \quad \text{, with} \\ x &= \frac{p(r_s - a)}{(r_t - a)(p+q)} \end{aligned} \tag{2.19}$$

- for overcast ($\bar{r}_v \geq r_s$) or clear sky ($r_c = 0$) – diagnostically by using Eq. (2.8) and the distribution width

$$a = \bar{r}_t - (b - a)\frac{p}{p + q} \quad . \tag{2.20}$$

3. The maximum b is determined diagnostically with Eq. (2.8)

$$b = (\bar{r}_t - a)\frac{p + q}{q} + a \quad . \tag{2.21}$$

4. The cloud fraction is calculated using Eq. (2.11).
5. The tendency due to turbulence is calculated.
6. The influence of turbulence on cloud water and water vapor is calculated (section 2.1.1, turbulence).
7. The large-scale condensation is calculated (section 2.1.1, large-scale condensation).
8. The tendency due to convection is calculated.
9. The tendency due to microphysics is calculated.
10. The total tendency for the shape parameter q (Eq. (2.17)) and the distribution width $(b - a)$ (Eq. (2.18)) are calculated, and q and $(b - a)$ are updated.

It is essential, that a consistent description of the PDF is kept throughout all these steps. If for instance only one of the parameters a, b, p or q is changed between step 2./3. and step 6., an artificial evaporation or condensation of cloud water is caused. This issue will be discussed in more detail in chapter 4.

2.2 Models

2.2.1 ECHAM6 - General Circulation Model (GCM)

The parameterization development presented in this study is done in the framework of the GCM ECHAM6 (Stevens et al. 2013). The ECHAM6 is mainly developed at the Max Planck Institute for Meteorology in Hamburg, Germany. The model is based on a spectral-transform dynamical core, coupled to several physical parameterizations. The convection is parameterized using the mass flux approach of Tiedtke (1989) with modifications to the treatment of deep convection following Nordeng (1994). The model includes separated prognostic equations for the water vapor, liquid water and ice, which are based on Lohmann and Roeckner (1996). The default cloud scheme is a

(critical) Relative Humidity (RH) scheme by Sundqvist et al. (1989), with slight modifications to obtain a better representation of stratocumulus clouds. The statistical scheme by Tompkins (2002) is implemented as an optional cloud scheme. A comprehensive overview of the parameterizations used in the ECHAM6, but also its history, development and performance is given in Stevens et al. (2013). The model version used for the parameterization development in this study employs a changed radiation scheme, which is using a McICA treatment of cloud overlap (Pincus et al. 2003).

Experiments

For the experiments shown in this dissertation, Atmospheric Model Intercomparison Project (AMIP) simulations, using sea-surface temperature (SST) and sea ice of a current climate as boundary conditions, have been performed. The applied spectral resolution is T63, which corresponds roughly to a resolution of $1.9° \times 1.9°$ in longitude and latitude. The vertical resolution is defined by 47 hybrid levels, reaching a height of 0.01 hPa. The simulations in chapter 5 are performed for 14 months and output was written every 6 hours. For the analysis only the last 12 months (1 year) are included. As the processes in the atmosphere adjust relatively fast and the SSTs were prescribed, the first 2 months are considered as enough spin up time.

2.2.2 COSMO-DE - Numerical Weather Prediction Model (NWP)

For the analysis of the mesoscales (10-100 km) and for more realistic initial conditions for sensitivity studies, datasets from a numerical weather prediction model developed and maintained by the German Weather Service (Deutscher Wetterdienst, DWD) are used. The local model COSMO-DE with a 2.8 km grid spacing is basically covering the domain of Germany (see e.g. Baldauf et al. 2011). As the synoptic situation is expected to vary with seasons, datasets from varying times during a year have been analyzed. For the final analysis the set was reduced to two datasets representing two different seasons (June and January). Each time period consists of 6 hourly forecast on a length of 4 days. In chapter 3, additionally the coarser model COSMO-EU, covering Europe with a grid spacing of 7 km, is evaluated for the same time periods (January and June).

2.2.3 UCLA-LES - Large Eddy Simulations (LES)

One tool for parameterization development and evaluation, that becomes more and more important are large eddy simulations of a well defined physical situation. In this study several simulations performed with the University of California, Los Angeles Large Eddy Simulation (UCLA-LES) model, which solves the Ogura-Phillips anelastic equations (Stevens et al. 1999, 2005) are analyzed. The default parameterization of cloud microphysical processes is based on the two-moment warm rain scheme of Seifert

and Beheng (2001) with some refinements (see Stevens and Seifert (2008)). To reduce the influence of the initial conditions, for all simulations the first timesteps are excluded.

CGILS: [1] From the CFMIP-GCSS Intercomparison of Large-Eddy and Single-Column Models (CGILS) (Blossey et al. 2013) the simulations of a shallow cumulus (s6) and a stratocumulus (s12) case, both with a length of 10 days, are used. The shallow cumulus case (s6) was simulated using a 100 m grid spacing. A domain of $10 \times 10\,\mathrm{km}^2$ was filled with 96×96 points horizontally and 128 vertical levels reaching up to 6.4 km. The stratocumulus case (s12) was simulated using a 25 m grid spacing. This time the domain of $3 \times 3\,\mathrm{km}^2$ was filled with 128×128 points and 180 vertical levels reaching up to 1 km. The three dimensional fields were saved every hour.

RICO: [2] As an alternative realization of shallow cumulus, simulations based on observations made during the Rain in Cumulus over the Ocean field campaign (RICO) (Rauber et al. 2007) are included in this thesis. These simulations were performed for 30 days with hourly output on a small grid (25 m), covering a large domain (1024×1024 points). In the vertical 160 levels were used, reaching up to 4 km. In chapter 3, two different setups are analyzed which differ in the specification of free tropospheric humidity following the set up described by Stevens and Seifert (2008) and Seifert and Heus (2013). In chapter 4, only the drier simulation is used.

Deep convection: [3] In chapter 4, additionally a deep convective case is included. This case simulates a diurnal cycle of continental convection by prescribing the surface heat fluxes. This leads to shallow convection in the morning hours, that evolves towards deep convection in the afternoon. The domain is approximately 250 km × 250 km with a horizontal resolution of 250 m and 100 vertical levels reaching up to 20.7 km. The length of the simulation is one day with output written every 30 minutes. For this simulation in addition to the two-moments warm rain scheme, a two moment ice-microphysics scheme as developed by Seifert and Beheng (2006) was used. More details on this simulation can be found in Schlemmer and Hohenegger (in revision).

2.2.4 DNS - Direct Numerical Simulations

[4] In chapter 3, for part of the analysis also Direct Numerical Simulations (DNS) is included. This dataset is from a $(1024)^3$ simulation of a 3 m wide mixed layer configuration that mimics a stratocumulus-top solely driven by evaporative cooling (Mellado 2010).

[1] These simulations were performed by Thijs Heus.
[2] These simulations were performed by Axel Seifert.
[3] This simulation was performed by Linda Schlemmer.
[4] This simulation was performed by Alberto de Lozar

Chapter 3

Scale dependency of total water variance, and its implication for cloud parameterizations

The scale dependency of variance of total water mixing ratio is explored by analyzing data from a General Circulation Model (GCM), a Numerical Weather Prediction Model (NWP) and Large Eddy Simulations (LES). For clarification Direct Numerical Simulation (DNS) data is additionally included, but the focus is placed on defining a general scaling behaviour for scales ranging from global down to cloud resolving. For this, appropriate power-law exponents are determined by calculating and approximating the power density spectrum. The large-scale models (GCM and NWP) show a consistent scaling with a power-law exponent of approximately -2. For the high-resolution LES the slope of the power density spectrum shows evidence of being somewhat steeper, although the estimates are more uncertain. Also the transition between resolved and parameterized scales in a current GCM is investigated. Neither a spectral gap nor a strong scale break is found, but a weak scale break at high wavenumbers cannot be excluded. The evaluation of the parameterized total-water variance of a state of the art statistical scheme shows that the scale dependency is underestimated by this parameterization. This study and the discovered general scaling behaviour emphasize the need for a development of scale dependent parameterizations.[1]

3.1 Introduction

The parameterization of cloud processes, including fractional cloud cover, is known to be the principal driver of uncertainties in simulations of climate change (e.g., Bony and Dufresne 2005; Randall et al. 2007). Although different parameterizations use different approaches, all rest on assumptions about the subgrid-scale variability of total

[1]This chapter has been preliminary accepted by the Journal of the Atmospheric Sciences as: Schemann, V., B. Stevens, V. Grützun, and J. Quaas, 2013: Scale dependency of total water variance, and its implication for cloud parameterizations. J. Atmos. Sci. doi:10.1175/JAS-D-13-09.1, in press

water mixing ratio (Tompkins 2008). In this study the scaling behaviour of total-water variance and its representation in a state of the art parameterization is investigated.

Currently, parameterizations are challenged by a new generation of global climate models (GCMs), which include the possibility to use local grid refinement (e.g. ICON (Wan et al. 2013), LMDZ (Hourdin et al. 2006)). With this it is no longer feasible to tune parameterizations to certain resolutions. The aim has to be to develop parameterizations which adjust naturally to different grid sizes. Those parameterizations should be able to manage a consistent transition from today's GCM resolution ($O(100\,\mathrm{km})$) down to cloud resolving scales ($O(1\,\mathrm{km})$) or even smaller.

According to Arakawa et al. (2011), there are two different approaches to reach this goal. The first approach is to develop parameterizations for a conventional climate model, which are flexible enough to allow for convergence with increasing resolution towards a global cloud resolving model. An alternative approach is to include a cloud resolving model as a parameterization in the grid of the global climate model, a so called "multi-scale modeling framework (MMF)".

One promising approach for the first and conventional concept is to develop scale aware statistical parameterizations. Statistical approaches are based on a representation of the higher moments of the subgrid-scale probability density function (PDF) so as to provide a distribution of the considered quantity, for instance total water mixing ratio. Typically in such approaches a moment expansion is taken and assumptions are required to truncate the moments (for instance by assuming a given family of PDFs) (e.g., André et al. 1976; Larson and Golaz 2005). Although it is generally well appreciated that the variance should be treated prognostically, the ability to treat higher order moments is a matter of some debate (e.g., Klein et al. 2005). This motivates the present, as well as other studies, that attempt to understand controls on the subgrid variance, particularly as a function of scale.

Variance as a function of scale can often be described by a power law and with this by a single scaling exponent. By extrapolating the resolved saturation variance with a power law exponent of $-\frac{5}{3}$ and introducing the resulting subgrid-scale variability, Cusack et al. (1999) found an improvement in cloud amount. Since then, a few additional studies have explored how different scales contribute to the water vapor variance. Using aircraft measurements Cho et al. (2000) found an exponent of -1.46 ± 0.04 for a wavenumber range of approximately 50 m - 100 km in the boundary layer; in the free troposphere a higher exponent of -1.63 ± 0.05 for tropical regions and -1.79 ± 0.05 for extra-tropical regions was estimated. Similar results were found by Kahn and Teixeira (2009), who used data from the Atmospheric Infrared Sounder (AIRS) (approx. 50 km resolution) to produce a global climatology of scaling exponents for water vapor and temperature. The estimated exponents for water vapor varied between -1.4 and -2.2. Nastrom et al. (1986) also reported evidence of power law scaling for water vapor, with a scaling exponent of $-\frac{5}{3}$ for the range of approximately 150-500 km and -2 for

500-1500 km. The height dependency of the exponents is investigated by Fischer et al. (2012), which analyzed a range of 10-100 km and found exponents of $-\frac{5}{3}$ for the lower troposphere and -2 for the upper level. All these results together imply that there is not a spectral gap between today's resolved ($O(100\,\mathrm{km})$) and parameterized (less than approx. 100 km) GCM scales and that formulations of the subgrid variance must incorporate information about the scales being parameterized.

Whether or not this scaling continues to the finest scales of variability is more unclear. There is some evidence of a change in scaling, or a scale break, at fine scales. Based on an analysis of numerical weather prediction and climate models, as well as available observational data, Kahn et al. (2011) reported evidence of such a break on scales of order 10 km, with a steeper gradient (less than -1.8) emerging at smaller scales.

All cited studies investigated more details and dependencies on different heights, meteorological conditions, or regions for the scaling of water-vapor variance. Here, they are cited in a way to generate a context for the discussion of the results on a more generalized scaling behaviour of total-water variance. As the differences in the scaling behaviour for water-vapor and total-water variance are expected to be small, at least for the large scales, a comparison between the previous and the new results can still be useful. The importance of more detailed investigations of the scaling behaviour of water vapor for the development of GCM parameterizations was also discussed by Pressel and Collins (2012), who analyzed first-order structure functions in the AIRS-Observed water vapor field.

In this study the scaling behaviour of total water variance in the warm cloudy boundary layer is analyzed in a hierarchy of models stretching from scales of tens of meters to the global scale. So doing permits the analysis of variance as a function of all relevant scales. The contribution of variance at different lengthscales is changing across several orders of magnitude. Because the construction of a single composited spectrum spanning all the scales can be sensitive to how the various scales are matched to one another, a detailed analysis is done for each dataset separately and the scaling behaviour is analyzed across the individual range of scales spanned by the individual data sets, instead of estimating an universal law for all scales. To further decrease the resulting uncertainty and to provide more background for the discussion of scaling exponents, in this study three different approaches are used for the estimation of the scaling exponent. The question of a scale break is additionally investigated by including data with a resolution of some millimeters from Direct Numerical Simulations (DNS). The scaling behaviour identified in this analysis is discussed in the context of the previous studies on water vapor scaling. Furthermore a state of the art parameterization of subgrid-scale variance developed for use in global climate models is validated against the results obtained in this study.

The chapter is organized as follows: Section 3.2 is a short overview of the data and methods used. In section 3.3 the three different approaches to estimate scaling of total

water mixing ratio variance and the respective results are presented. The description of a statistical cloud cover parameterization and its evaluation with regard to the scaling of variance is presented in section 3.4. Concluding remarks and perspectives for future research are given in section 3.5.

3.2 Background

3.2.1 Data

A continuous analysis of scales ranging from those sufficiently small to resolve ordinary cumulus clouds, to the planetary scales, would require a data set with very high resolution over very large domains. Calculations with this many degrees of freedom (e.g., Satoh et al. 2008) are only just becoming possible, and could be applied to explore these questions using a unified modeling framework, but even these do not reach into the scales relevant for boundary layer clouds. For this reason the present study is based on data from several different model types whose domain size and resolution differ, but which collectively span the desired range of scales.

The UCLA Large-Eddy Simulation (LES) model (Stevens et al. 1999, 2005; Stevens and Seifert 2008) is used to investigate the scale dependency of total water mixing ratio variance at cloud resolving scales. Four different cases with differing grid spacings and domain sizes are investigated. From the CFMIP-GCSS Intercomparison of Large-Eddy and Single-Column Models (CGILS) (Blossey et al. 2013) the trade-cumulus case (s6), simulated with a 100 m grid spacing, 96×96 points and 128 vertical levels, and the stratocumulus case (s12), simulated with a 25 m grid spacing, 128×128 points and 180 vertical levels, were analyzed. For both cases eight of the ten simulated days with hourly output were included. In addition two further 30 hours simulations of trade cumulus with hourly output using a grid mesh with a 25 m spacing, 1024×1024 points and 160 vertical levels, were analyzed. The trade cumulus simulations are based on observations made during the Rain in Cumulus over the Ocean field campaign (RICO) (Rauber et al. 2007), and differ in the specification of free tropospheric humidity following the set up described by Stevens and Seifert (2008). The moister simulation more readily simulates precipitation, which leads to a growth of variance of total water mixing ratio at large scales. More details on the organization and the different distribution of variance can be found in Seifert and Heus (2013).

The scale dependency at the mesoscales (10-100 km) is assessed using a numerical weather prediction model developed and maintained by the German weather service (Deutscher Wetterdienst). Two different setups of this model were explored: The local model COSMO-DE with a 2.8 km grid spacing and the European version COSMO-EU with a 7 km grid spacing (see e.g. Baldauf et al. 2011). To account for the effects of different physical situations and seasons, several periods of 6 hrs forecast, each with a

length of 4 days, from varying months of 2011 have been analyzed. The two periods (January and June) showing the largest differences were chosen for further study so as to bound the range of behaviour evident in the more extensive analysis (not shown).

With simulations using the ECHAM6 general circulation model (GCM) (Stevens et al. 2013) larger, through global, scales are analyzed. ECHAM6 is used in two different resolutions, the T63 (approx. 200 km resolution at the equator) and the T127 (approx. 100 km resolution at the equator) spectral truncations. Because the area of each gridbox of the latitude/longitude grid corresponding to the GCM spectral resolution converges towards the poles, the analysis is limited to the tropics, defined as the region between 30 °N and 30 °S so as to have gridboxes of approximately equal size. Within the analysed region the distance between two longitudes varies between 111 km and 96 km for the T127 grid, or twice that for the coarser resolution version of ECHAM6. Hence, the transform (physical space) grid is relatively uniform. In the analysis that follows the wavenumber spectrum is not corrected for the remaining small inhomogeneities in the grid relative to a fixed mesh with a spacing of 100 km (respectively 200 km). One month of data (June) with instantaneous output every 6 hours is analyzed.

In addition to the three types of models used for the main analysis, data from DNS are included to investigate the question of a scale break at finest scales. The DNS data were obtained from a $(1024)^3$ simulation of a 3 m wide mixed layer configuration that mimics a stratocumulus-top solely driven by evaporative cooling (Mellado 2010). The power density spectra from four different heights are included. As those domain sizes and resolutions are still negligible for global parameterizations this data is not included in the main analysis but provides information on the issue of a possible scale break.

To further simplify matters, analysis is restricted to grid levels where warm clouds can be found. This facilitates a comparison of models that span a wide range of resolutions, as fine scale simulations incorporating processes related to ice-clouds are not available to us. Because of the diversity of models used, it was necessary to define a general condition as to decide which model levels are related to warm clouds, and thus should be incorporated into the analysis. A good indicator for warm clouds is the presence of liquid water. Hence the vertical profiles (average over time and space) of liquid cloud water mixing ratio was used to identify levels relevant to warm clouds, and those levels where the liquid water was within 10% of the value at the level containing the maximum liquid water were analyzed (as an example see Fig. 3.1).

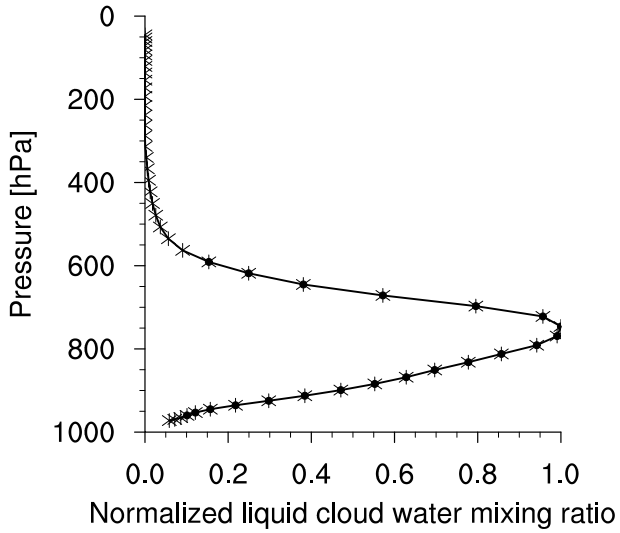

Figure 3.1: Temporal- and domain-average vertical profile of cloud liquid water mixing ratio for the COSMO-DE June dataset, normalized by its maximum value. Asterisks represent the mean values for the model levels and dots the levels selected, i.e., those with a value larger than the threshold of 0.1.

3.2.2 Method

Fourier transformation

The Fourier transformation requires periodic input data. If this requirement is not fulfilled the spectrum may show some artefacts associated with mismatches at the end points. As the COSMO-DE, the COSMO-EU, and the ECHAM6 datasets are not doubly periodic, it is necessary to preprocess the data by removing any linear trends, and tapering the data records to remove end point effects. For the tapering, a split-cosine-bell tapering is applied, following the implementation in the NCAR Command Language (2012). For consistency tapering was also applied to the datasets with periodic boundary conditions (LES, GCM in longitude direction).

The two-dimensional discrete Fourier transform is defined as

$$\mathcal{F}(k,l) = \frac{1}{MN} \sum_{m=0}^{M-1} \sum_{n=0}^{N-1} f(m,n)\ e^{-i2\pi \frac{mk}{M}}\ e^{-i2\pi \frac{nl}{N}} \tag{3.1}$$

$$= \frac{1}{MN} \sum_{m=0}^{M-1} \sum_{n=0}^{N-1} f(m,n)\ e^{-i2\pi (\frac{mk}{M} + \frac{nl}{N})} \quad , \tag{3.2}$$

with the wavenumbers $k = 0, \ldots, M-1$, $l = 0, \ldots, N-1$, the wavenumber-dependent

Fourier coefficients $f(m,n)$, and

$$e^{-i2\pi(\frac{mk}{M}+\frac{nl}{N})} = \cos\left[2\pi\left(\frac{mk}{M}+\frac{nl}{N}\right)\right] - i\sin\left[2\pi\left(\frac{mk}{M}+\frac{nl}{N}\right)\right] \quad .$$

The two-dimensional discrete Fourier transform can also be rewritten and calculated as a twice implemented one-dimensional Fourier transform:

$$\mathcal{F}(k,l) = \frac{1}{N}\sum_{n=0}^{N-1}\left[\frac{1}{M}\sum_{m=0}^{M-1} f(m,n)e^{-i2\pi\frac{mk}{M}}\right]e^{-i2\pi\frac{nl}{N}} \quad . \tag{3.3}$$

The resulting two-dimensional discrete Fourier transform is symmetric around the origin, that means $|\mathcal{F}(k,l)| = |\mathcal{F}(-k,-l)|$. Due to this it is common to describe the two-dimensional Fourier transform centered around the mean value, with wavenumbers $-\lfloor\frac{M}{2}\rfloor \leq k \leq \lfloor\frac{M-1}{2}\rfloor$, $-\lfloor\frac{N}{2}\rfloor \leq l \leq \lfloor\frac{N-1}{2}\rfloor$.

The effective frequency of the two-dimensional discrete Fourier transform is defined as

$$\hat{f}_{(k,l)} = \frac{1}{\Delta}\sqrt{\left(\frac{k}{M}\right)^2 + \left(\frac{l}{N}\right)^2} \quad , \tag{3.4}$$

where Δ is the spatial resolution. For this definition it is assumed that the spatial resolution is the same in both directions, this means $\Delta x = \Delta y = \Delta$. This is true for the LES and NWP datasets and, as discussed previously, can also be assumed for the analyzed ECHAM6 region. To avoid aliasing and artefacts, the effective frequency has to be constrained to: $\hat{f}_{k,l} \leq \frac{1}{2\Delta}$ for all k and l.

Power density spectrum

The power density spectrum of the two-dimensional Fourier transform provides scale-by-scale information about the variance, the variance scaling. It is defined as the product of the Fourier transform and its complex conjugate. For instance if $\mathcal{F}$ is the discrete Fourier transform, the power spectrum $\mathcal{P}$ is defined by

$$\mathcal{P} = \mathcal{F}\mathcal{F}^* = (\Re(\mathcal{F})^2 + \Im(\mathcal{F})^2) \quad , \tag{3.5}$$

where $\mathcal{F}^*$ is the complex conjugate, $\Re(\mathcal{F})$ the real and $\Im(\mathcal{F})$ the imaginary part of $\mathcal{F}$.

The power density at each point includes the information about the variance at a certain effective frequency or wavenumber. If the spectrum is isotropic then it is possible to reduce the two-dimensional (k,l) power spectrum into a one-dimensional spectrum by integrating over annuli which define an effective frequency. In the present study this is accomplished by binning the data by effective frequency. The number of bins can also be used to smooth the resulting spectrum. In the following results $\lfloor\frac{3}{4}\cdot n_p\rfloor$ bins were chosen, where n_p is the minimum of the number of discrete wavenumbers

in both spectral directions. With this the range of bins is defined as $[0, \Delta k, \ldots, \frac{1}{2\Delta}]$, where Δ is the gridspacing of the original data and

$$\Delta k := \frac{1}{3/4 \cdot n_p \cdot \Delta} \quad . \tag{3.6}$$

To get a quantity which is independent of the bin width (Δk), the density is calculated by dividing by Δk.

In the following analysis the focus will be placed on the scaling behaviour and not the amount of variance. For this the normalized power density spectrum is of interest and is defined by:

$$p(k_i) = \frac{\mathcal{P}(k_i)}{\Delta k} \frac{1}{\sum_{k_j \in K} \mathcal{P}(k_j)} \quad , \tag{3.7}$$

where K includes all considered wavenumbers and $k_i \in K$.

By Parseval's theorem the integral over the whole power spectrum is equal to the total resolved variance. In the discrete sense this means

$$\sigma^2 = \sum_{k_j \in K} \mathcal{P}(k_j) \quad , \tag{3.8}$$

where σ is the standard deviation.

To calculate the variance which is resolved with a certain range of wavenumbers $k_1 \leq k \leq k_2$, it is necessary to integrate the discrete spectrum between the minimum wavenumber k_1 and the maximum wavenumber k_2:

$$\sigma^2(k_1, k_2) = \sum_{k=k_1}^{k_2} \mathcal{P}(k) \quad . \tag{3.9}$$

Least-square fit

To estimate the slope of the power spectrum a least square algorithm is applied. If the data follows a power law, it fulfills the following equation:

$$\mathcal{P}(k_i) \approx \beta k_i^{\alpha} \quad , i = 1, 2 \ldots \tag{3.10}$$

$$\ln(\mathcal{P}(k_i)) \approx \ln(\beta) + \alpha \ln k_i \quad , i = 1, 2 \ldots \quad . \tag{3.11}$$

The coefficients α and β, which fit the data with respect to the least-square constraint, are defined implicitly by minimizing the function

$$F(\alpha, b) = \sum_{i=1}^{n} (y_i - b - \alpha x_i)^2 \quad , \tag{3.12}$$

where n is the number of considered points, $y_i = \ln(\mathcal{P}(k_i))$, $b = \ln(\beta)$ and $x_i = \ln(k_i)$.

3.3 Scaling of variance

3.3.1 Estimation of a valid range

The power density spectra for the whole wavenumber space is calculated, but only an intermediate range is considered robust because of numerical and subgrid parameterization effects at small scales (high wavenumbers) and domain size constraints, which influence the largest scales, or lowest wavenumbers. For this reason focus is placed on the calculation of power law exponents for an intermediate range of wavenumbers for each model. But also in this intermediate range there might be some fluctuations or a transition between different power law exponents. To address this issue an attempt is made to identify if there is an intermediate range of wavenumbers over which a power law scaling is evident. Ideally, within this range the estimated exponent is not sensitive to the exact start and end point of the chosen range. When power law scaling is not evident the estimated exponent will depend on the start and end points of the analyzed range and it will not be reasonable to estimate a single exponent.

Data	$\mathbf{k_{max}^{-1}}$ m	$\mathbf{k_{min}^{-1}}$ m	**timesteps**	**levels**
LES (CGILS s12)	59.38	237.50	191	56
LES (CGILS s6)	236.67	946.67	191	61
LES (RICO moist low k)	255.67	2556.67	26	74
LES (RICO moist high k)	63.92	153.40	26	74
NWP (COSMO-DE January)	13526.15	175840.00	33	20
NWP (COSMO-DE June)	13526.15	175840.00	33	21
NWP (COSMO-EU January)	27496.00	343699.97	33	15
NWP (COSMO-EU June)	27496.00	343699.97	33	14
GCM (ECHAM6 T63)	460000.00	2300000.00	120	13
GCM (ECHAM6 T127)	235000.02	2350000.00	120	13

Table 3.1: The investigated intermediate range, number of timesteps and number of levels for each dataset.

A procedure as described below helps to find a good estimate for a robust intermediate range, by revealing dependencies of the exponent on the exact start and end points more clearly. Nevertheless, the method is not purely objective and for each dataset a decision about acceptable deviations and uncertainties has to be made. The intermediate range for each dataset chosen for this study, as well as the number of levels and timesteps investigated, can be found in Table 3.1.

For a particular model the power density spectrum over the whole wavenumber space

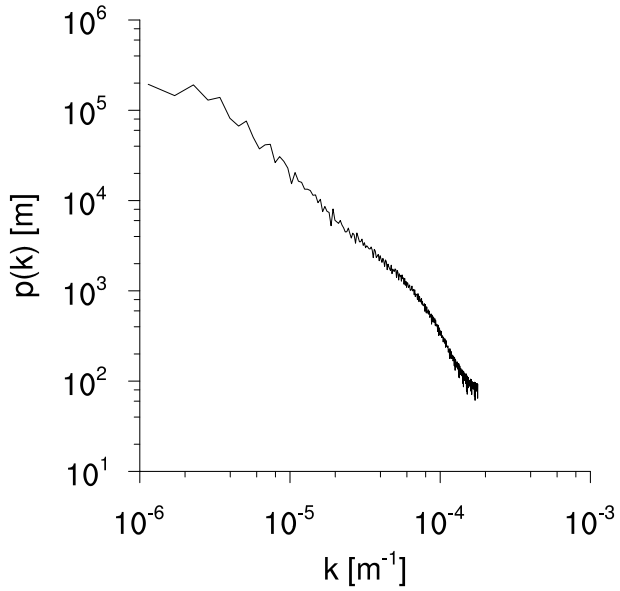

Figure 3.2: Normalized power density spectrum of total water mixing ratio for the COSMO-DE June dataset, averaged over time and height.

at each time and at each level is first normalized to unit variance and then averaged across all the levels and time periods analyzed to produce a mean spectrum. An example of such a spectrum is shown in Fig. 3.2 for the case of the COSMO-DE model. By eye the spectrum shows evidence of three regimes. The power density spectrum is relatively flat at very low wavenumbers, has apparent power law scaling in an intermediate range, and then the spectrum falls off increasingly sharply at high wavenumbers. The following procedure aims at identifying a minimum and maximum wavenumber, which sets limits to the intermediate range that shows a robust power law scaling.

The identification of the minimum and maximum wavenumber is outlined using the example of the COSMO-DE June dataset, which is shown in Fig. 3.3. To determine the minimum wavenumber, a wavenumber in the middle of the possible range for each model domain (e.g. $k_{\text{end}} \approx \frac{1}{7\Delta}$) is chosen as a fixed end point and the start wavenumber (k_{start}) is increased from k_1 until k_{end}. For each k_{start} a least square fit between k_{start} and k_{end} is performed, which gives an estimate for the exponent. The dependence of the estimated exponents on the choice of k_{start} is shown in Fig. 3.3 (a). At high wavenumbers clear fluctuations can be seen, as the number of points used for the least-square fit is decreasing with increasing k_{start}. Where the line in Fig. 3.3 (a) is approximating a straight line, the calculated exponent becomes less dependent on the exact starting point (k_{start}) and with this a good estimate for the start of a robust power law is reached. To find the maximum wavenumber the procedure is repeated the other way around, a start wavenumber is fixed and from this on k_{end} is increased until

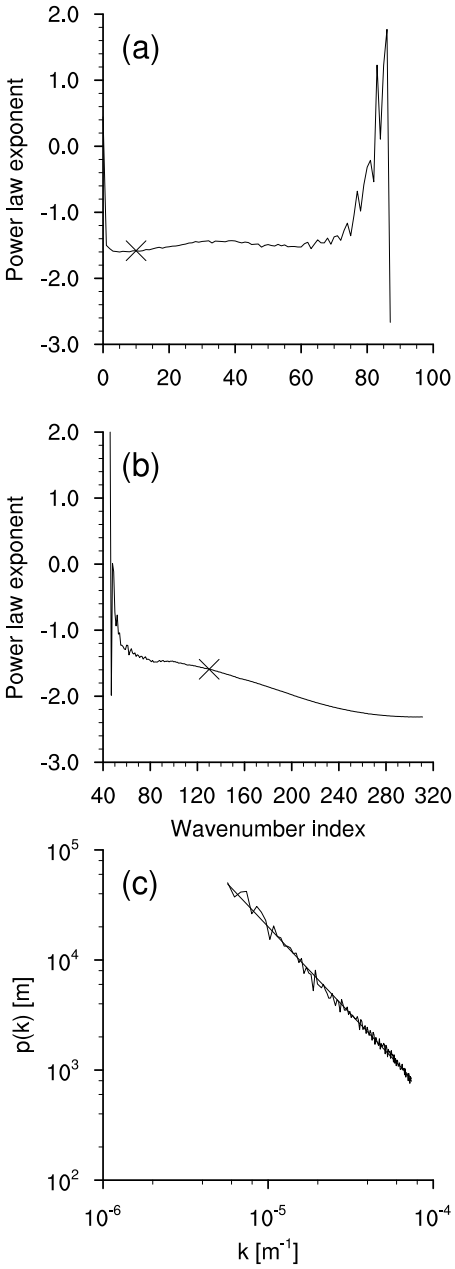

Figure 3.3: Estimation of the robust range for a power law for the COSMO-DE June dataset by approximating the power density spectrum of total water mixing ratio. Figure (a) and (b) show the variability of the power law exponent due to a change in the minimum and maximum wavenumber of the fitted wavenumber range, respectively. Small changes represent the beginning (or end) of a stable power law range. The chosen wavenumber index is marked with a cross. In figure (c) a least square fit (with a slope of $\alpha \approx -1.6$) to the selected range can be seen.

the highest possible value is reached (Fig. 3.3 (b)). Here the fluctuations due to a too small number of points can be seen at low wavenumbers, as the number of points used for the least-square fit is increasing by increasing k_{end}.

In this procedure there are two choices, which have to be made empirically. First, the fixed start and end point and second the threshold for a robust behaviour. The fixed start and end point should already be in the stable range but for a reasonable estimate with a least-square fit as many points as possible are needed. Due to these constraints the choice for the exact start and end points are made depending on the model and the respective stable range. The exponents calculated by changing the start or end point of the least-square fit, should approximate a straight line for a robust power law behaviour. But there will always remain some fluctuations and a threshold for robust behaviour has to be defined for each model independently. The made choices can be tested by looking at the resulting fit for an intermediate range. For the COSMO-DE June dataset this fit is shown in Fig. 3.3 (c).

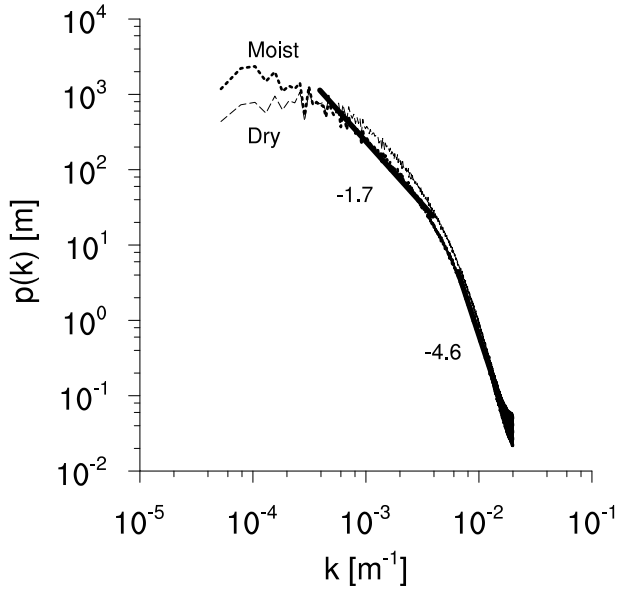

Figure 3.4: Normalized power density spectrum of total water mixing ratio for the two RICO datasets, averaged over time and height for the a moist (dotted, thick) and dry (dashed, thin) cases of the trade cumulus case simulated at 25 m resolution. Two fits to the moist RICO case are shown, one for the high wavenumbers (-4.6) and one for the low wavenumbers (-1.7).

For the two RICO cases, the procedure has been slightly extended. Both RICO cases show a similar behaviour for the high, but differ for the low wavenumbers. Figure 3.4 shows the normalized and averaged power density spectrum for both RICO cases. For the high wavenumbers both show a steep gradient with a scaling exponent around -4.6.

But for the large scales (low wavenumbers) the moist RICO case shows a growth in variance while the dry RICO case is already flat. As both cases have a similar scaling behaviour at high wavenumbers, but only the moist RICO case shows a scaling at low wavenumbers, only this case will be used for a more detailed estimation of the scaling exponent. To evaluate both scaling gradients the data set is split up into two parts, one part consisting of the range of high wavenumbers and one part consisting of the range of low wavenumbers.

3.3.2 Power density spectra of total water mixing ratio

Figure 3.5 shows datasets from all three kinds of models (GCM, NWP, LES), simulated for different regions and different seasons. This figure, showing the whole wavenumber range, demonstrates how well the datasets connect to each other and gives the impression of a continuous scaling. As the lines for each model are quite parallel and only shifted on the Y-Axis, there is no evidence for a height dependency of the scaling exponents but for the total amount of variance. Even though some variability in the slopes of differing models can be seen, there is a continuous distribution of variance from the large scales of GCMs ($O(100-1000\,\mathrm{km})$) until small scales of a LES simulation ($O(100\,\mathrm{m}-10\,\mathrm{km})$) without evidence for a spectral gap.

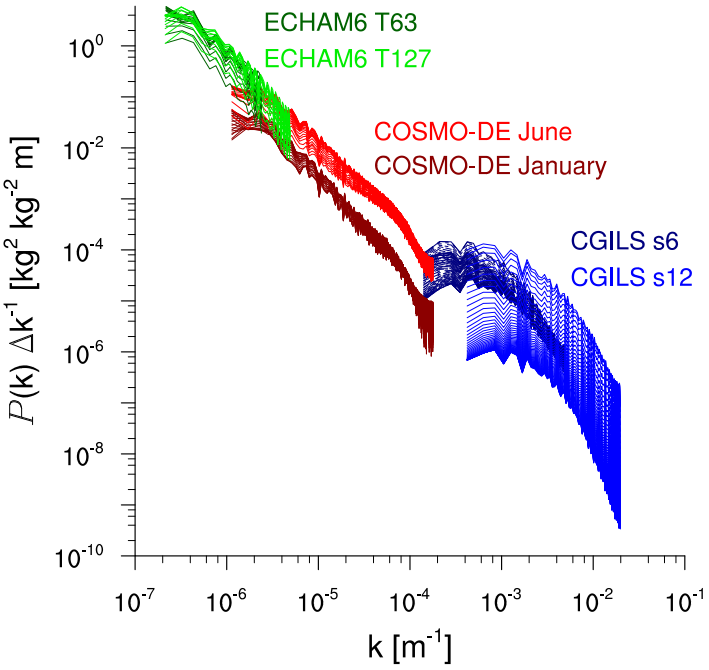

Figure 3.5: Power density spectra of total water mixing ratio for the GCM-, NWP- and CGILS LES simulations. Different lines of the same color represent different height levels. The spectra are temporally averaged.

Having ruled out the possibility of a spectral gap, i.e., a range of scales with greatly diminished variance, focus is placed on the scaling, i.e., the slopes of the individual spectra in Fig. 3.5. For a close look on the consistent scaling the mean variance (integral over the intermediate wavenumber space) of each model is adjusted to the variance of a k^{-2} slope (see Fig. 3.6). This calculation only affects the height of each line, not the slope. Especially the large scale models (GCM and NWP) show a similar slope and a scaling close to -2. This finding holds down to the range of the s6 CGILS case and the larger scales of the RICO dataset. For the small LES scales the gradient becomes steeper. This change may hint at a scale break around 1 km. This result would be in a similar range like the finding of Kahn et al. (2011) for water vapor. To investigate the question of a possible scale break in more detail, in this part of the evaluation also some data from Direct Numerical Simulations (DNS) is included. As this data also shows a scaling around -2, a strong break in the scaling, with a change in the exponent of 50% or more, is not evident. The steeper gradient at the high wavenumbers (approx. $k > 4 \cdot 10^{-3}\,\mathrm{m}^{-1}$) for the LES might also be due to too much dissipation at the small scales in the model. But because of the variability a weak scale break is certainly possible.

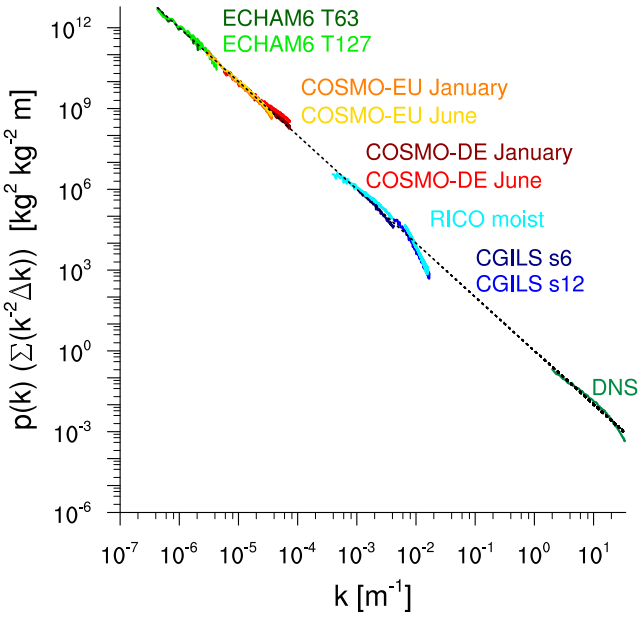

Figure 3.6: Power density spectra of the intermediate wavenumber space of total water mixing ratio. The integral over the spectra of each model is adjusted to the integral of a k^{-2} slope. The adjusted spectra are averaged over time and height.

To explore these issues in more depth Fig. 3.7 shows the compensated spectrum. The compensated spectrum is calculated by adjusting the mean variance to the k^{-2} slope

and an additional scaling by k^{-2}. Over a large range of scales, a consistent scaling can be seen, but also some deviations are obvious. There are some fluctuations for the large scale models around a scaling of -2 and this variability increases with the wavenumber. Especially the LES and DNS data tend to show a $-\frac{5}{3}$ scaling at the lower bound of their wavenumber range and an increasing exponent at the higher bound. By this analysis a weak scale break towards a $-\frac{5}{3}$ or also a $-\frac{7}{3}$ scaling at the meso and smaller scales, i.e. $O(1-10\,\mathrm{km})$ or smaller, can not be ruled out.

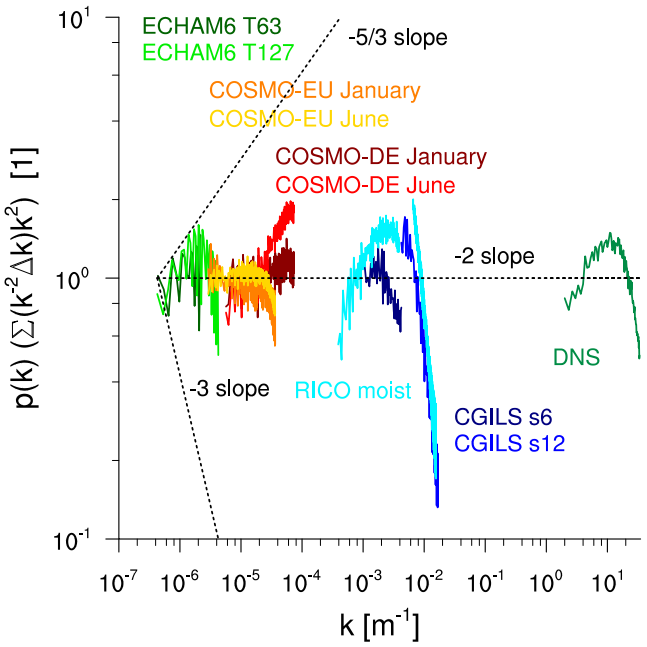

Figure 3.7: As Fig. 3.6 but the whole spectrum is additionally scaled by k^{-2} (compensated power density spectrum).

This first evaluation of the power density spectra shows a broadly consistent scaling among the different models and gives a first estimate for the power law exponent ($\alpha \approx -2$). Additionally there is no clear evidence of a strong break of scales in the spectrum, although a weak change with a transition to a slightly flatter ($-\frac{5}{3}$) or steeper ($-\frac{7}{3}$) spectra is difficult to rule out. In the following sections a more detailed estimation for the power law exponent is presented.

3.3.3 Estimation of the power law exponents based on least-square fit

To describe the scaling of the variance of total water mixing ratio in more detail, a good estimate for the power law exponent is necessary. One possibility to get an estimate is to use the least square fitting algorithm, described in section 3.2.2. With this not only a general estimate for the mean power density spectrum (as in section 3.3.2) is

possible, but also an estimate for every level and every timestep can be calculated. The resulting histograms of power law exponents (see Fig. 3.8) also describe the spread in the estimates and show the variability within the different datasets. A narrow histogram (e.g. COSMO-DE/EU or ECHAM6) provides evidence of a robust power law and only small variability, while a broad histogram (e.g. CGILS s12) hints at deviations from a robust power law scaling or at a high variability.

The impression of a robust estimate for the large scale models is supported by calculation of the mean exponents (see Table 3.2). The NWP and GCM datasets have similar mean values with a small standard deviation of about 10% of the average. The overall mean value for the large scale models $\alpha = -1.94 \pm 0.24$ is close to the first estimate of -2 from the previous section. Also in this evaluation the LES datasets show a differing behaviour for the high wavenumbers. The gradients are steeper and also the spread is increasing in absolute terms. The increasing variability in the estimate provides further evidence for the previous conclusion, that the steeper gradient for the high-resolved LES is likely not a signature of a scale break, but rather is associated with numerical issues (e.g. too much dissipation).

Data	**Mean exponent (α)**	**Standard deviation**
LES (CGILS s12)	-3.85	± 0.40
LES (CGILS s6)	-2.38	± 0.33
LES (RICO moist low k)	-1.72	± 0.28
LES (RICO moist high k)	-4.52	± 0.55
NWP (COSMO-DE January)	-1.92	± 0.16
NWP (COSMO-DE June)	-1.65	± 0.26
NWP (COSMO-EU January)	-2.11	± 0.12
NWP (COSMO-EU June)	-2.10	± 0.21
GCM (ECHAM6 T63)	-1.89	± 0.19
GCM (ECHAM6 T127)	-2.04	± 0.18

Table 3.2: Power law exponents estimated by a least square fit, as mean values and standard deviation for all time steps and levels considered.

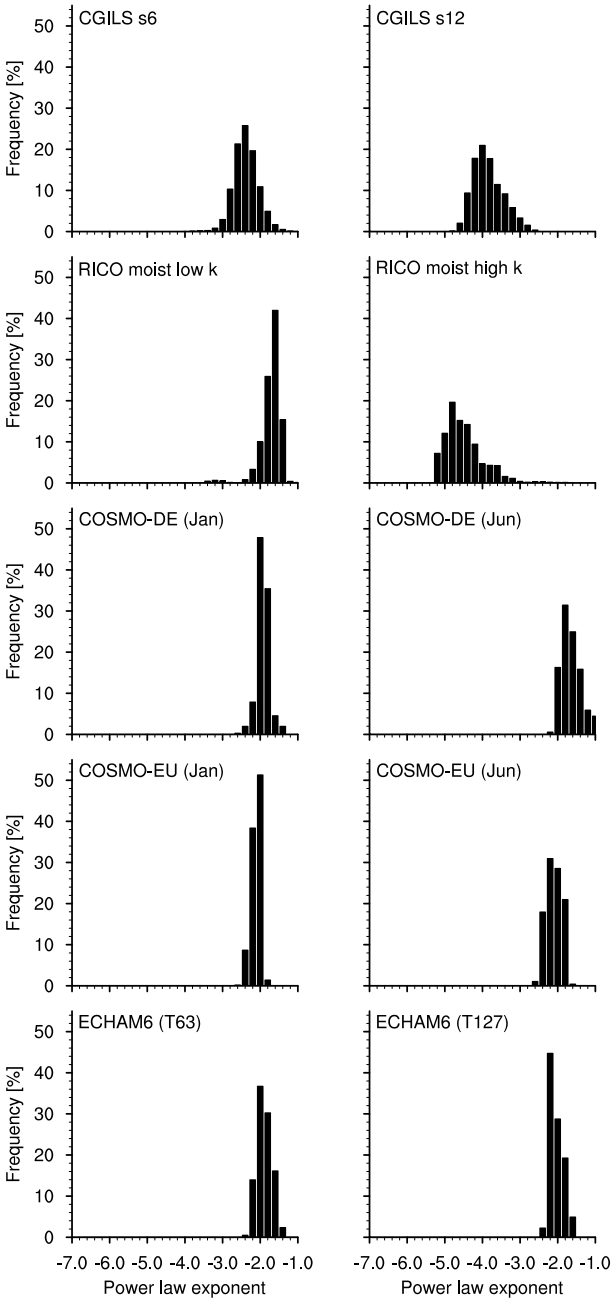

Figure 3.8: Histograms of power law exponents estimated by least square fitting done individually for each height level and time step of the model simulations.

3.3.4 Estimation of the power law exponents based on extrapolation

The approach for estimating the power law exponents used in this section is based on a method described by Cusack et al. (1999), where it was used to estimate the amount of unresolved variance by assuming a certain power law and extrapolating. Some modifications to the original method are necessary, in order to use it for the estimation of a power-law exponent.

First, the wavenumber space is divided into two subsets of wavenumbers higher and lower than a chosen threshold, the so called unresolved $\{k_{\text{unres}}\}$ and resolved $\{k_{\text{res}}\}$ part. Analogously the total variance can be divided into two parts with contributions from the resolved (low wavenumbers) and unresolved (high wavenumbers) wavenumber range:

$$\sigma^2_{\text{tot}} = \sigma^2_{\text{res}} + \sigma^2_{\text{unres}} \tag{3.13}$$

$$\Longleftrightarrow \sum_{k_x \in k_{\text{tot}}} \sum_{k_y \in k_{\text{tot}}} \mathcal{P}(k_x, k_y) = \sum_{k_x \in k_{\text{res}}} \sum_{k_y \in k_{\text{res}}} \mathcal{P}(k_x, k_y) + \sum_{k_x \in k_{\text{unres}}} \sum_{k_y \in k_{\text{unres}}} \mathcal{P}(k_x, k_y) \quad . \tag{3.14}$$

Now the assumption of having a power law is used. In the first approach (section 3.3.3), where the power law exponent α has been introduced, the data was integrated over annuli defined by effective frequency. This time every combination of (k_x, k_y) is allowed to contribute to the calculated variance. As the number of modes (k_x, k_y) in one annulus scales with the radius $\left(k = \sqrt{k_x^2 + k_y^2}\right)$, an exponent of $\alpha - 1$ is used in the following equations. For details see Cusack et al. (1999).

The ratio of total and resolved variance can then be written as:

$$\frac{\sigma^2_{\text{tot}}}{\sigma^2_{\text{res}}} \approx \frac{\sum_{k_x \in k_{\text{tot}}} \sum_{k_y \in k_{\text{tot}}} \psi \left(\sqrt{k_x^2 + k_y^2}\right)^{\alpha-1}}{\sum_{k_x \in k_{\text{res}}} \sum_{k_y \in k_{\text{res}}} \psi \left(\sqrt{k_x^2 + k_y^2}\right)^{\alpha-1}} = \frac{\sum_{k_x \in k_{\text{tot}}} \sum_{k_y \in k_{\text{tot}}} \left(\sqrt{k_x^2 + k_y^2}\right)^{\alpha-1}}{\sum_{k_x \in k_{\text{res}}} \sum_{k_y \in k_{\text{res}}} \left(\sqrt{k_x^2 + k_y^2}\right)^{\alpha-1}} \quad , \psi \in R\,. \tag{3.15}$$

With this an estimate for the unresolved part of the variance due to lower wavenumbers depending on the assumed exponent α can be obtained:

$$\left(\sigma^2_{\text{unres}}(\alpha)\right)^{\text{est}} := \frac{\sum_{k_x \in k_{\text{tot}}} \sum_{k_y \in k_{\text{tot}}} \left(\sqrt{k_x^2 + k_y^2}\right)^{\alpha-1}}{\sum_{k_x \in k_{\text{res}}} \sum_{k_y \in k_{\text{res}}} \left(\sqrt{k_x^2 + k_y^2}\right)^{\alpha-1}} \sigma^2_{\text{res}} - \sigma^2_{\text{res}} \quad . \tag{3.16}$$

The exponent α which minimizes the following difference of the correct unresolved variance, which can be calculated by integrating over the respective wavenumbers, and

the one estimated by extrapolation, is the resulting best estimate for the exponent of the approximated power law:

$$\left(\sigma^2_{\text{unres}}(\alpha)\right)^{\text{est}} - \sigma^2_{\text{unres}} = \left(\sigma^2_{\text{unres}}(\alpha)\right)^{\text{est}} - \sum_{k_x \in k_{\text{unres}}} \sum_{k_y \in k_{\text{unres}}} \mathcal{P}(k_x, k_y) \quad . \tag{3.17}$$

Data	**Mean exponent (α)**	**Standard deviation**
LES (CGILS s12)	-5.18	± 0.54
LES (CGILS s6)	-2.92	± 0.50
LES (RICO moist low k)	-2.04	± 0.26
LES (RICO moist high k)	-5.93	± 0.67
NWP (COSMO-DE January)	-2.00	± 0.21
NWP (COSMO-DE June)	-1.73	± 0.29
NWP (COSMO-EU January)	-2.29	± 0.16
NWP (COSMO-EU June)	-2.33	± 0.24
GCM (ECHAM6 T63)	-2.47	± 0.17
GCM (ECHAM6 T127)	-2.51	± 0.13

Table 3.3: As Table 3.2, but using the approach based on extrapolation.

In this evaluation three fourths of the intermediate wavenumber space is defined as "resolved" and the remaining one fourth is defined as "unresolved". The result of this evaluation can be seen in Fig. 3.9 and Table 3.3.

The results for the large scale models (GCM and NWP) from section 3.3.3 are broadly confirmed. There are small variations but these are likely attributable to different methods. The mean values and the shape of the histograms still show a consistent scaling for all large scale models. Here, the respective mean exponent for the large-scale models is $\alpha = -2.3 \pm 0.33$, which is well within the range of uncertainty of the exponent derived from the previous approach. The LES cases instead show again a lot more variability and higher mean values, than in section 3.3.3. Again this high uncertainty might be difficult to be explained by physical reasons and caused by other issues. As increasingly large domain and fine grid resolution simulations become available these issues should become easier to resolve.

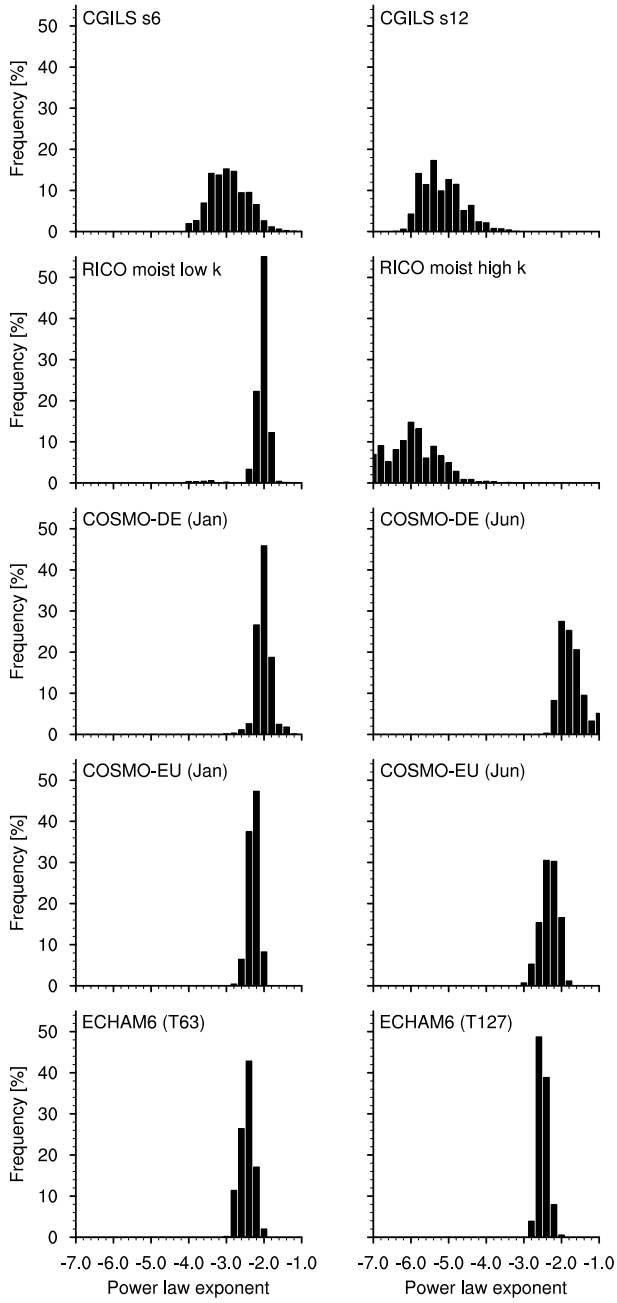

Figure 3.9: As Fig. 3.8, but estimating the power law exponents using the extrapolation approach.

3.4 Parameterizations of variance

3.4.1 Statistical cloud cover scheme

One example of a statistical cloud cover scheme is the one from Tompkins (2002), that is part of the ECHAM6 GCM. In this scheme, the total water mixing ratio is assumed to be described by a beta distribution. The upper and lower bounds of the distribution are described by two parameters (a, b). Two additional parameters (p, q) define the skewness. Instead of using prognostic equations for the moments of the distribution directly, Tompkins (2002) used the distribution width $(b - a)$ and the skewness parameter q as prognostic equations and for simplicity, assumed p to be constant ($p = 2$). The two prognostic equations are described by source and sink terms due to turbulence (turb), convection (cconv) and microphysics (micro):

$$\frac{\partial(b-a)}{\partial t} = \left(\frac{\partial(b-a)}{\partial t}\right)_{\text{turb}} + \left(\frac{\partial(b-a)}{\partial t}\right)_{\text{conv}} \quad , \tag{3.18}$$

$$\frac{\partial q}{\partial t} = \left(\frac{\partial q}{\partial t}\right)_{\text{turb}} + \left(\frac{\partial q}{\partial t}\right)_{\text{conv}} + \left(\frac{\partial q}{\partial t}\right)_{\text{micro}} \quad . \tag{3.19}$$

To calculate the three free parameters a, b and q three equations are needed. For partial cloudiness the mean values of total water and cloud water mixing ratio and the prognostic equation for q are used. In the case of cloud fraction zero (clear sky) or one (overcast sky), the prognostic distribution width $(b - a)$ is used instead of the mean cloud water mixing ratio.

Ideally, either through the coupling to other parameterizations, or by direct specification, the cloud cover scheme would get information about the resolution and be adapted to different grid sizes. As seen in the previous sections this should lead to a scaling behaviour of the variance of total water mixing ratio. Variance is not a prognostic variable in the original formulation of Tompkins (2002), but can be calculated by using the distribution width $(b - a)$ and the shape parameters (p, q) as follows:

$$\overline{r_t'^2} = \frac{(b-a)^2}{(p+q)^2}\frac{pq}{p+q+1} \quad . \tag{3.20}$$

For the evaluation of the statistical cloud cover scheme in the following section, Eq. (3.20) is used to calculate the parameterized subgrid-scale variance of total water mixing ratio. With this not only the prognostic equation for the distribution width (Eq. (3.18)) is evaluated, but errors and problems caused by both prognostic equations Eq. (3.18) and Eq. (3.19) are included in the evaluation of the variance (Eq. (3.20)).

3.4.2 Evaluation of the parameterized variance of total water mixing ratio

In this section the parameterized subgrid-scale variance of total water mixing ratio, which is predicted by the statistical cloud scheme of Tompkins (2002), is evaluated with regard to scale dependency. For this evaluation the output of the ECHAM6 setup as described in section 3.2.1 is used and the parameterized subgrid-scale variance is calculated by Eq. (3.20) using the prognostic distribution width, the prognostic shape parameter q, and the fixed shape parameter $p = 2$. For comparison, another subgrid-scale variance is calculated by extrapolating the resolved T63 variance with a power-law exponent of $\alpha = 2.1$, which is the mean value of the exponents estimated for the large scale models (GCM and NWP) with both methods. The extrapolation is done with the method described in section 3.3.4 up to a maximum wavenumber of $k_{\max} = 10^{-4}\,\mathrm{m}^{-1}$, which corresponds to a resolution of 10 km. Because of the already mentioned numerical constraints, only the intermediate wavenumber range can be used for the extrapolation. This leads to an uncertainty in the comparison of the different variances, as actually more variance is resolved by the model than used for the extrapolation. But the main results are not affected by this uncertainty.

	T63	**T127**	**T127-T63**
resolved $(\mathrm{kg/kg})^2$	$2.92 \cdot 10^{-7}$	$4.89 \cdot 10^{-7}$	$+1.97 \cdot 10^{-7}$
extrapolated $(\mathrm{kg/kg})^2$	$1.58 \cdot 10^{-7}$	$9.76 \cdot 10^{-8}$	$-6.01 \cdot 10^{-8}$
parameterized $(\mathrm{kg/kg})^2$	$7.74 \cdot 10^{-8}$	$7.58 \cdot 10^{-8}$	$-1.59 \cdot 10^{-9}$

Table 3.4: Mean values of resolved, extrapolated unresolved and parameterized unresolved variance in simulations of the ECHAM6 GCM at T63 ($\approx$ 190 km) and T127 ($\approx$ 100 km) horizontal resolutions. The term "resolved" refers to the amount of variance resolved by the mentioned resolution. The "extrapolated" part is the amount of unresolved variance extrapolated under the assumption of a power law of $\alpha = -2.1$. The parameterization of the subgrid-scale variability ("parameterized") is the one by Tompkins (2002).

In Table 3.4 the mean values of the resolved, the extrapolated subgrid-scale and the parameterized subgrid-scale variance for the two different ECHAM6 resolutions T63 and T127 are shown. The total variance – the sum of resolved variance and the mean subgrid-scale variance – should not change with changing resolutions. This means, that with an increasing resolved variance – T127 compared to T63 – the subgrid-scale variance should decrease. As shown in table 3.4, neither the sum of resolved variance and parameterized subgrid-scale variance nor the sum of resolved variance and extrapolated subgrid-scale variance is really constant. But the differences are remarkable higher for the parameterized subgrid-scale variance. Table 3.4 shows also

for the absolute values that the amount of parameterized subgrid-scale variance is smaller than the one calculated by extrapolating. This is consistent with earlier results of e.g. Quaas (2012) and Weber et al. (2011), which stated that the parameterized subgrid-scale variance of total water mixing ratio in the scheme of Tompkins (2002) is underestimated.

More remarkable is the missing scale dependency of the parameterized subgrid-scale variance. The amount of parameterized subgrid-scale variance should decrease with increasing resolution, but while this effect can be seen for the extrapolated variance, the parameterized variance does not decrease significantly. More details on the changes are provided by the histograms (Fig. 3.10) of the differences for the resolved, the extrapolated subgrid-scale and the parameterized subgrid-scale variances. For the resolved variance, the values are all positive, as with the higher T127 resolution more variance is resolved than with the coarser T63 (Fig. 3.10(a)). Respectively, the difference values for the extrapolated subgrid-scale variances are negative (Fig. 3.10 (b)), as the subgrid-scale variance should decrease with increasing resolution. But the values for the parameterized subgrid-scale variances are smaller in magnitude and have both signs, negative and positive (Fig. 3.10 (c)). Both, the smaller magnitude and the mix of signs, show clearly that the variance parameterized by the Tompkins scheme is missing a significant scale dependency. This explains why the mean difference between both resolutions of the parameterized variance (see Tab. 3.4) is two orders of magnitude smaller than expected.

The vertical structure of the three different types of variances is shown in Fig. 3.11. This time the mean exponents for the large-scale models from both approaches and their standard deviations ($\alpha = -2.3 \pm 0.33$ and $\alpha = -1.94 \pm 0.24$) are used for the extrapolation. This produces some estimate for the spread in the variance which is caused by the uncertainty in the exponents. The vertical profiles confirm the underestimation of the amount (Fig. 3.11 (a) and Fig. 3.11 (b)) and scale dependency (Fig. 3.11 (c)) of the parameterized subgrid-scale variability by the Tompkins scheme. Additionally the vertical profile of the parameterized subgrid-scale variance shows a strong decrease in the lower troposphere, in contrast to the constant or slightly increasing profile of the resolved variance. This gives some evidence on an unphysical behaviour of the parameterized subgrid-scale variance, which depends on the parameterized distribution width (Eq. (3.18)) and shape parameter q (Eq. (3.19)).

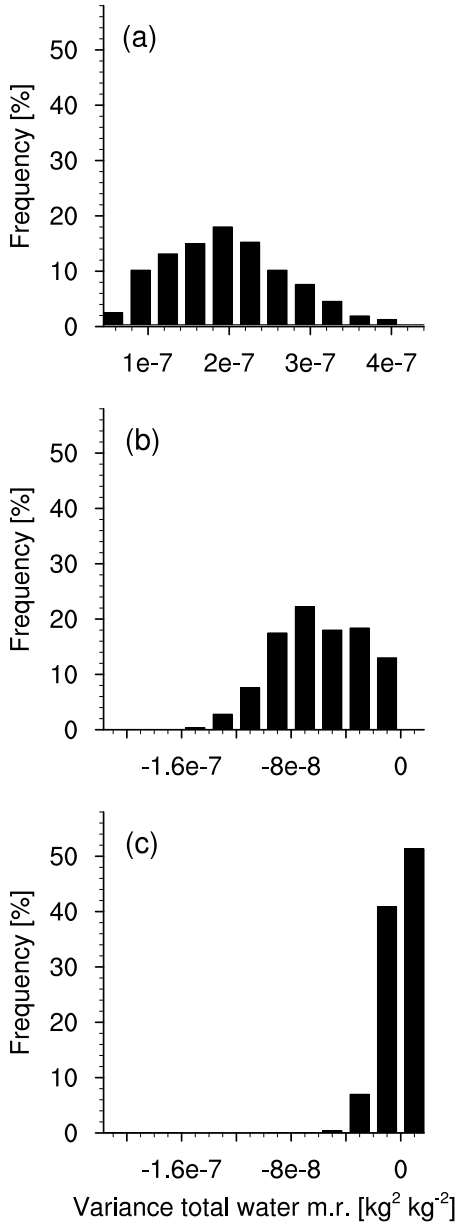

Figure 3.10: Histograms of the difference (T127-T63) for the resolved (a), the extrapolated subgrid-scale (b) and the parameterized subgrid-scale (c) variance, one value for each timestep and each height.

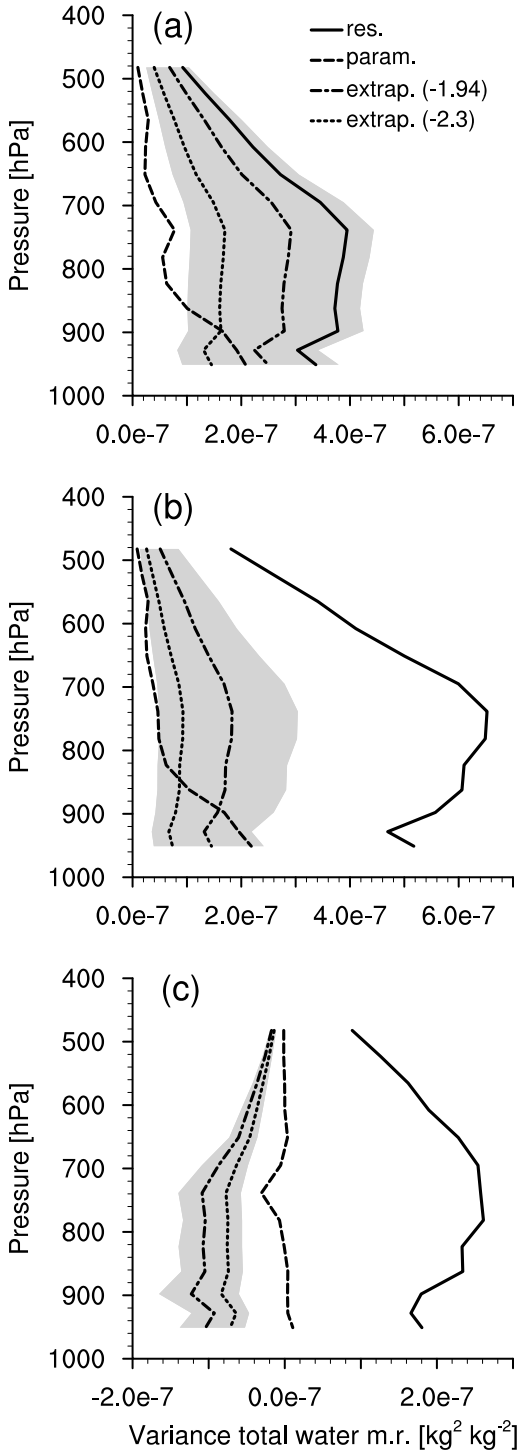

Figure 3.11: Vertical profiles of resolved (solid), extrapolated subgrid-scale (dotted, dash-dotted) and parameterized subgrid-scale (dashed) variance of the T63 (a), the T127 resolution (b) and the difference (T127-T63) (c). The grey shaded area represents the standard deviations for both estimated exponents.

3.5 Conclusions

Three different kinds of models (GCM, NWP and LES) covering a broad range of scales were analyzed to estimate the scale dependency of variance of total water mixing ratio. The combined power density spectrum showed a consistent and continuous scaling from global scales down to the small LES scales. The analysis provides no evidence for a spectral gap, nor is there a clear signal of a strong break in the scaling of the spectra. However, because of an increased variability of the estimated power-law exponent at small scales, a weak scale break towards $-\frac{5}{3}$ or $-\frac{7}{3}$, cannot be ruled out by our analysis. The existence of a clear scaling at all investigated scales, implies the necessity to include a scale dependency in future cloud process parameterizations.

For the large scale models (GCM and NWP) a common scaling exponent of $\alpha \approx -2$ could be estimated. As the NWP is covering the scales mainly contributing to the unresolved variance in a current GCM, this estimate provides a sufficiently good approximation for the evaluation of subgrid-scale parameterizations. The exponent -2 also lies in the range of earlier estimates of a scaling exponent of water vapor. As for the large scales the influence of cloud water and ice on the scaling is rather small, the estimates of previous studies on water vapor and the result of this study show a relatively good agreement.

For the smaller scales (less than approx. 1 km) more variability and a decreasing exponent at the higher wavenumbers was discovered. The change of scaling during the scales of a typical LES model, could hint at a scale break. But as a scaling exponent of $\alpha \approx -2$ was also found in DNS data this change in the scaling is likely due to excessive dissipation in individual models, rather than evidence of a strong break in scaling. Looking from a global modelling perspective the variance produced at scales less than 1 km is still rather negligible. Nevertheless, the discovered variability merits more attention, as does the possibility of a slight change in scaling at small scales.

The evaluation of the parameterized variance in the statistical scheme of Tompkins (2002) showed an underestimation of the amount of subgrid-scale variance in the current formulation. But more remarkable is the non existing scale dependency of the parameterized subgrid-scale variance of total water mixing ratio. As a follow up the explored scale dependency should be included in the parameterized variance to receive an improved representation of subgrid-scale variability at different resolutions. The common scaling behaviour of total water variance at a broad range of scales explored in this study, underlines the importance of the development of scale aware parameterizations also for current GCMs.

Short summary of chapter 3:

- The combined power density spectrum of total water variance showed a consistent and continuous scaling from global scales down to small LES scales.
- No evidence for a spectral gap or a strong break in the scaling was found.
- For the global and mesoscale model a common scaling exponent of approximately -2 could be estimated.
- The statistical cloud scheme by Tompkins (2002) produced almost no scale dependency of parameterized total-water variance.
- The development of scale aware, or scale dependent, cloud parameterizations is important also for current GCMs.

Chapter 4

Beyond Tompkins – Improving the representation of subgrid-scale variability of total water in GCMs

In this chapter several aspects of the development of a statistical cloud scheme are investigated. A common approach in the formulation of statistical cloud schemes is the reduction of degrees of freedom. Two different closures for the reduction of the parameters of a beta distribution and the resulting sensitivities of the scheme are discussed. This theoretical prerequisite is followed by three development steps in order to improve the representation of subgrid-scale variability of humidity by the statistical scheme of Tompkins. The first step is the introduction of a new approach to deal with negative distribution minima and the comparison with the previous approach and alternative ideas. As a second step prognostic equations for the higher moments skewness and variance are introduced. The parameterizations of the source and sink terms follow the original motivation of Tompkins (2002). The third development step is a new parameterization for the source terms representing the contribution by convection. The three development steps are followed by an analysis investigating the dependency of the calculated cloud fraction on the input parameter cloud water and skewness. This enables a better understanding of the expected behaviour of the statistical scheme and its response to changes of the environment.

4.1 Introduction

The method of assumed probability density functions (PDFs) provides a great potential to represent the subgrid-scale variability of total water (sum of water vapor, liquid and ice) and cloud water (liquid plus ice) within a grid box. The information about these subgrid-scale variabilities could be included in other parameterizations and improve the representation of physical processes in the model. In the ECHAM6 GCM the statistical scheme of Tompkins (2002) is implemented. This scheme uses the assumption of an underlying beta distribution and adds two additional prognostic equations to describe

the shape and the distribution width of the PDF (for details on the Tompkins scheme, see section 2.1.1). Weber et al. (2011) and Quaas (2012) used different methods to evaluate the scheme. Both studies showed, that the subgrid-scale variability of total water is underestimated. This underestimation was also seen in the previous chapter (chapter 3) during the evaluation of the statistical scheme. Besides all the possibilities and the great potential of coupling to different parameterizations, a good representation of the subgrid-scale variability of humidity should be the zeroth order task for statistical cloud schemes. In this chapter, three development steps to improve the representation of subgrid-scale variability of total water in the statistical scheme by Tompkins (2002) will be presented.

The general beta distribution, that is assumed in the statistical scheme by Tompkins (2002), is described by four parameters: two shape parameter p and q, a minimum a and a maximum b. This means, that four input variables are needed to determine a specific member of the PDF family of general beta distributions. But our physical understanding of the higher moments of a PDF of humidity, especially if it comes to kurtosis or higher, is limited and decreasing with increasing order of the moment. It is a common approach in the development of statistical schemes to reduce the degrees of freedom in order to avoid equations for moments with an order higher than three. For instance, Tompkins (2002) reduced the four needed input variables for the general beta distribution to three by introducing a closure equation, while Larson et al. (2001) and Naumann et al. (2013) reduced the five input variables for a double gaussian to three variables. These closures are projecting a higher-dimensional space onto a lower-dimensional subspace. Thereby, they are placing strong restrictions on the sensitivity and the behaviour of the scheme. While some studies in the literature are comparing different PDF families and their fit to datasets (e.g. Perraud et al. 2011), a thorough discussion about the different approaches to determine the parameter from the higher moments and especially the influence of closures on the behaviour of the schemes is missing. For the beta distribution two different closures and their influence on the sensitivity and the behaviour of the scheme will be discussed in the following.

One big advantage of the beta distribution is the compact support. But without strong additional constraints, it is possible that combinations of total water mean, cloud water mean, skewness and the applied closure lead to a (partially) negative support. As this is unphysical, in the original formulation of the scheme the minimum was adjusted to zero which led to an additional evaporation of cloud water (see section 2.1.1). This approach will be evaluated and discussed first, followed by a presentation of alternative methods for dealing with a negative support. Afterwards, a new approach of approximating a truncated beta distribution by the general beta distribution will be introduced.

The next step is the introduction of prognostic equations for the higher moments skewness and variance. In the original version by Tompkins (2002) prognostic equations

for one shape parameter q and the distribution width $(b - a)$ were used. For physical reasons it would be much more desirable to formulate the scheme in terms of the higher moments variance and skewness. To my best knowledge, this study is the first approach to revise the scheme in this direction and to suggest equations for the variance and skewness of total water. In this step the source and sink terms, introduced for the prognostic equations are based on the original motivation and parameterization presented in Tompkins (2002). This facilitates a comparison between the original and the revised scheme.

The final development step presented in this chapter is a new parameterization for the convection source terms. The convection source terms obtained in the previous step have two major drawbacks. Their formulation is rather ad-hoc, which leads to a tunable constant to describe how efficiently the skewness is increased with detrained cloud water. In addition, the variance source term is strongly coupled to the specific distribution member as the shape parameters are used explicitely to describe the change in variance. Klein et al. (2005) suggested different convection source terms, which are more physically based and are formulated independent of the specific distribution member. In the following, a simple parameterization for these convection source terms is derived based on the diagnostics of three different LES cases.

The last part of the chapter is dedicated to a better understanding of the behaviour of the statistical scheme and especially its response to changes in the environment. The dependency of the most important output parameter, the cloud fraction, on two important input parameter, the cloud water and the skewness, is investigated by analyzing three different LES cases. This is followed by an evaluation of the representation of this dependency in the used setup of the statistical scheme. This type of sensitivity analysis lays the groundwork for the evaluation and the interpretation of the schemes influence on the simulation of the climate system by ECHAM6, as discussed for instance in chapter 5.

The chapter is organized in the following way: In section 4.2 the reduction of degrees of freedom and its consequences will be discussed using the Tompkins scheme as an example. This will be followed by the first development step, the treatment of cases with a negative distribution minimum in section 4.3. The presentation of the prognostic equations for the higher moments skewness and variance will be done in section 4.4. In section 4.5, the new parameterization for the convection source terms will be derived. Finally the dependency of the cloud fraction on the cloud water and the skewness will be discussed in section 4.6. This discussion will be followed by a summary and conclusion in section 4.7. In this chapter the PDF will always be used to describe the variability of total water mixing ratio, but for a better readability the specification of 'mixing ratio' will be dropped in the following.

4.2 Prerequisite: A new view on the common reduction of degrees of freedom

The skewness ζ of a beta distribution is described by two shape parameter p and q (see Eq. (2.15)). If p equals q the distribution is symmetric, for p less than q positively skewed and for p greater than q negatively skewed. Two beta distributions can have the same skewness but different parameters p and q (see Fig. 4.1).

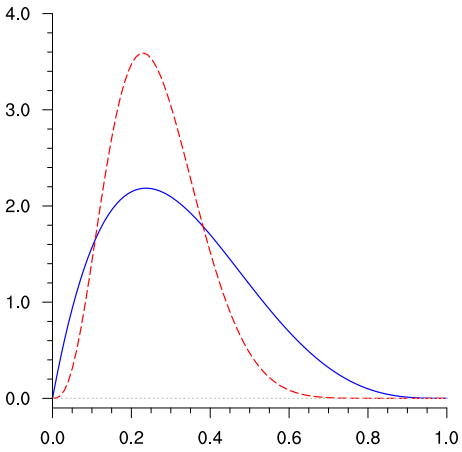

Figure 4.1: Two beta distributions, having the same skewness ($\zeta = 0.5$) and minimum and maximum ($a = 0.0$, $b = 1.0$), but different parameters p and q: blue line: $p = 2$, $q = 4.22$; red line: $p = 4$, $q = 11.1$

Figure 4.2 presents the skewness of a beta distribution as a two dimensional field with the dimensions p and q. As described in section 2.1.1, Tompkins (2002) introduced the constraint

$$p = 2 \quad . \tag{4.1}$$

This equals a projection of the skewness onto a one dimensional field, with the dimension q. This is shown in Fig. 4.2 as a blue line. A more flexible projection was suggested by Tompkins (2008) with

$$(p-1)(q-1) = 2 \quad . \tag{4.2}$$

This projection is also shown in Fig. 4.2, as a black line. Both closures will be discussed and compared in more detail in the following, and they will be refered to as T02 for $p = 2$ and as T08 for $(p-1)(q-1) = 2$.

The new closure (T08) is more flexible, and it allows negative skewness. However, the main reason is a pragmatic decision as the new closure simplifies the equations for skewness and variance, by:

$$(p-1)(q-1) = 2 \quad \Leftrightarrow \quad pq = p + q + 1 \quad . \tag{4.3}$$

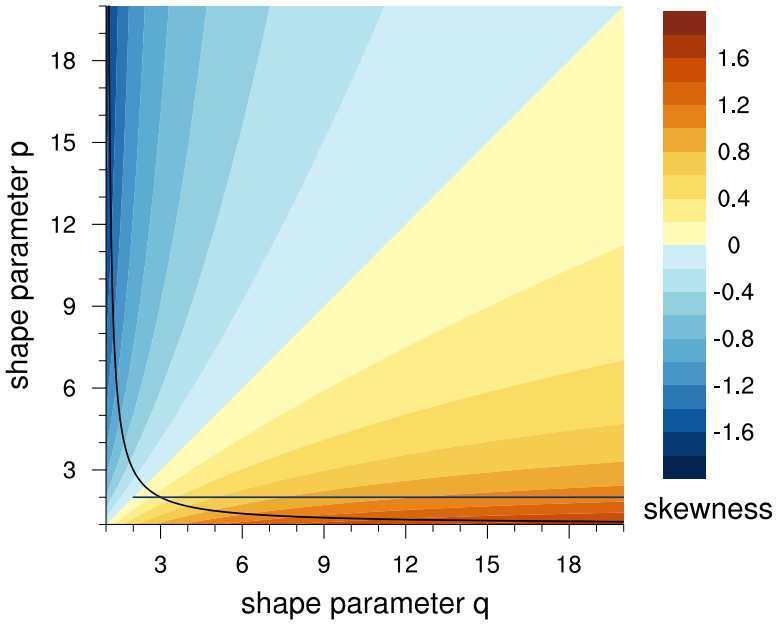

Figure 4.2: The skewness of a beta distribution can be described by two dimensions, the shape parameter p and the shape parameter q. Additionally, two approaches for a projection on a one dimensional line are shown: T02 defined by $p = 2$ (blue line) and T08 defined by $(p-1)(q-1) = 2$ (black line).

With the closure T08 the shape parameters q and p can be calculated from a skewness ζ by

$$\begin{aligned} q &= \frac{(\zeta+2)+\sqrt{2(\zeta^2+4)}}{(2-\zeta)} \\ p &= \frac{q+1}{q-1} \end{aligned} \tag{4.4}$$

For small values of p and q both closures lead to projections on a rather sensitive part of the two dimensional space (see Fig. 4.2).

To reduce the degrees of freedom by introducing a closure is a common approach in the development of statistical schemes (e.g. Larson et al. (2001), Naumann et al. (2013)). Often the closure is defined by more or less physically based assumptions or by defining fixed relations between variables. Nevertheless, the main reason is almost always a pragmatic decision as our understanding of the higher moments is limited. Even though, pragmatic decisions are necessary and useful for the development of parameterizations, it is essential to keep in mind that they influence the behaviour of the scheme. Introducing a closure is essentially selecting a subfamily of PDFs which defines the behaviour of the scheme and its sensitivity to perturbations. This changed sensitivity not only changes the robustness of the scheme, but also how the higher

moments would change based on the source terms. The correct strength of a source or sink term could lead to a wrong result if the sensitivity is under- or overestimated. This issue will be discussed in more detail in the following by discussing two examples. But a first impression is given by Fig. 4.2 where the two projections mentioned earlier are defined in the more sensitive part of the two dimensional space spanning the skewness, T08 even more than T02.

4.2.1 Sensitivity of skewness to a perturbed shape parameter

To estimate the effect of a change to the shape parameter q on the skewness with respect to the applied closure, initial values of $p = 2$ and $q = 3$ are used for both cases. Then the shape parameter q is increased and the effect of this perturbation on the skewness is calculated. Figure 4.3 shows the sensitivity of the skewness to changes of the shape parameter q. These perturbations to the shape parameter are simulating the effect of the microphysics tendency. Figure 4.3 shows that the sensitivity is different for the two closures. As already seen in Fig. 4.2, the closure T08 is in a more sensitive part for small values of q than T02. This explains the higher sensitivity of the skewness to a perturbed shape parameter q with the closure T08 compared to T02 (Fig. 4.3). The high sensitivity can especially be seen for small values of q, while for large values of q, the sensitivity is decreasing for both closures and the skewness is affected less by small perturbations in q.

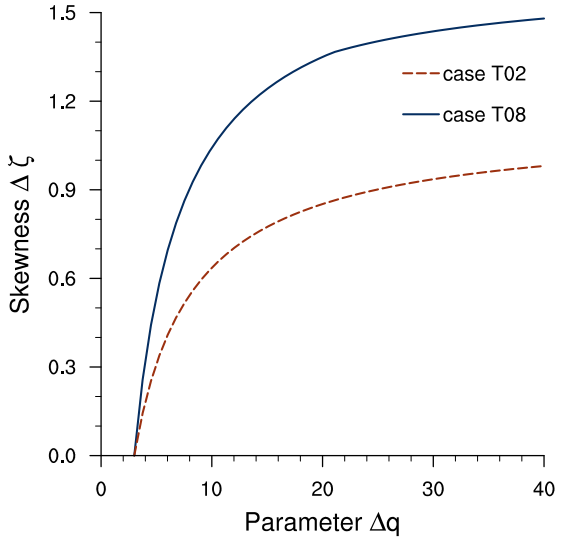

Figure 4.3: Sensitivity of skewness to a perturbed shape parameter q for the two closures: on the x-Axis the perturbations added to a start value q_0 is shown, while on the y-Axis the resulting change in skewness ($\Delta\zeta = \zeta(q_0 + \Delta q) - \zeta_0(q_0)$) is shown. The blue line shows results for the closure T08, the red line for the closure T02.

4.2.2 Sensitivity of cloud water to perturbed skewness

The second example is the sensitivity of the cloud water to small changes of the skewness. To analyze the effect of a changed skewness on the cloud water, the total water mean ($\bar{r}_t = 4\,\mathrm{g\,kg^{-1}}$), the saturation mixing ratio ($r_s = 4.5\,\mathrm{g\,kg^{-1}}$), and the distribution minimum ($a = 2\,\mathrm{g\,kg^{-1}}$) and maximum ($b = 6\,\mathrm{g\,kg^{-1}}$) are fixed. Only the skewness and with this the two shape parameters p and q are allowed to change. In Fig. 4.4a it can be seen that for a positive change of skewness the effect produced by the closure T02 is this time stronger than the one with the closure T08. The cloud water is more strongly reduced for a fixed value of p and a variable q, than for the closure combining both parameters. For a negative skewness tendency (Fig. 4.4b) the cloud water calculated with the closure T02 is not changing anymore, as the skewness cannot become smaller than zero. For the closure T08 which allows negative skewness, the cloud water is increasing further.

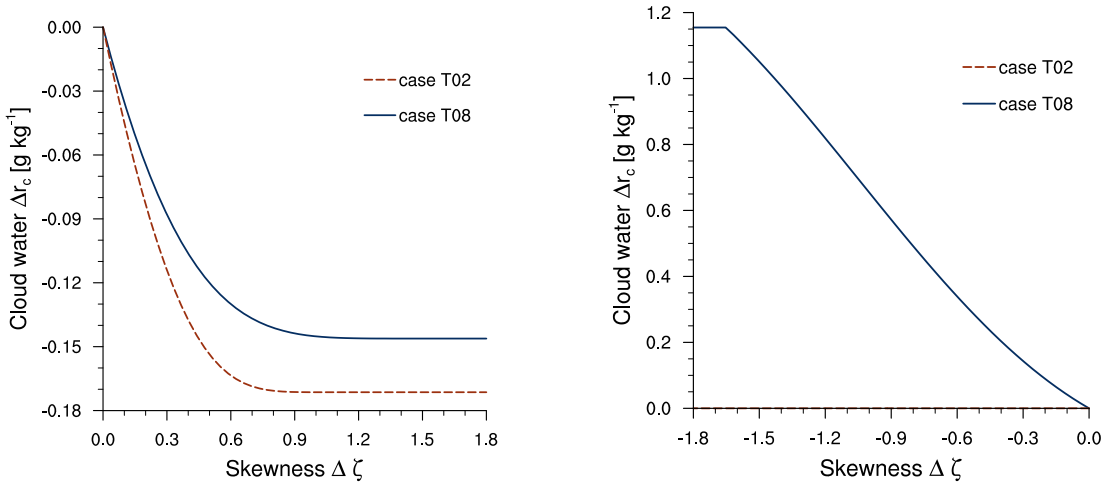

(a) Change to negative skewness

(b) Change to positive skewness

Figure 4.4: Effect of a changing skewness on the cloud water for the two different closures. On the x-Axis the change in skewness relative to a start value is shown, the y-Axis shows the resulting change in cloud water. For this the mean total water ($r_t = 4\,\mathrm{g\,kg^{-1}}$), the saturation mixing ratio ($r_s = 4.5\,\mathrm{g\,kg^{-1}}$), and the distribution minimum ($a = 2\,\mathrm{g\,kg^{-1}}$) and maximum ($b = 6\,\mathrm{g\,kg^{-1}}$) are fixed. In the right panel, the red line of the case T02 is lying exactly on the x-Axis, as the change of cloud water is zero due to the restrictions on the skewness.

4.2.3 Implications for the moments equation

As shown with the two previous examples, the sensitivity of certain quantities on perturbations varies markedly. This effect has to be taken into account when implementing the scheme and formulating equations for the moments. It would be desirable to formulate the prognostic equations only in the space of the moments and with this to separate them from the actual used distribution. For a successful separation it is also necessary to reduce the number of transformations between the moments and the parameters and to only apply it at necessary steps (e.g. the calculation of the cloud fraction). This would facilitate an easy exchange of the specific assumed PDF family or closure and ensure a more consistent and flexible scheme.

4.3 Step 1: Dealing with a negative distribution minimum

One big advantage of the beta distribution is the bounded interval $[a, b]$. But this also leads to an open issue. Without strong additional constraints, there is no way to avoid combinations of total water mean, cloud water mean, and skewness that lead to a negative distribution minimum a. As a negative distribution minimum is considered to be unphysical, these situations deserve a more detailed analysis. There are several options which can be applied in case of a negative distribution minimum.

In the following section, the closure T08 ($(p-1)(q-1) = 2$) will be used for the presented calculations. This closure provides more flexibility, especially as it allows negative skewness.

4.3.1 Previous approach: Assuming an incomplete beta function

One possibility is to change the assumed PDF family to the incomplete beta function in case of a negative distribution minimum. The incomplete beta function is described by:

$$B(b, p, q) = \int_0^b r_t^{p-1}(1 - r_t)^{q-1} dr_t \quad . \tag{4.5}$$

The incomplete beta function is defined by three parameters, which means that one of the four conditions mentioned in section 2.1.1 has to be dropped.

- **Total water mean:** The first constraint is the total water mean. In theory this constraint could be relaxed and an incomplete beta function could be picked, that fulfills the other constraints but has a different mean value. As it is essential to only use a PDF that has the same mean value as already in the model, this option will not be discussed further.
- **Cloud water mean:** A distribution could be picked, that has the same total water mean and skewness, but cannot be adjusted to the cloud water anymore.

This option was picked in the original formulation and will be discussed in more detail in the following.

- **Skewness:** Another possibility would be to adjust the shape parameter p and q in a way, that the total water and cloud water mean are contained in the PDF description. In this case the skewness will be updated. Also this approach will be discussed in more detail.

- **Closure:** Also the closure $(p-1)(q-1) = 2$ could be relaxed. But by picking this option, it becomes necessary to solve the problem iteratively in a two-dimensional space, and this more than once during one timestep in the GCM. Additionally, the switching between the full two-dimensional space and the trajectory defined by the closure could lead to discontinuities. Due to these reasons, this possibility will not be discussed in more detail.

The two options, to either relax the constraint on the cloud water mean or on the skewness, will be discussed in more detail in the following.

Cloud water mean

If the family of incomplete beta functions is used, and if the member is defined by the mean value, the skewness and the closure, then the contained cloud water becomes a diagnostic quantity. As a consequence of keeping the mean value and the skewness the same and shifting the minimum a to zero, the new value for the maximum b will be smaller (see Fig. 4.5). Interpreted in a physical sense, the new distribution contains less cloud water in its description, than the original amount of cloud water (see Fig. 4.5). This leads to an additional evaporation of cloud water (Tompkins 2002).

To investigate the effect of the additional evaporation in a less idealized setup, the two COSMO-DE datasets (see section 2.2.2) are analyzed. First, the distribution minima are calculated by using the total water mean, the cloud water mean, the skewness and the closure as input parameter. In case of a negative distribution minimum, the minimum is adjusted to zero and the respective distribution maximum is calculated. The original cloud water and the difference to the cloud water resulting from the shift of the distribution minimum are shown in Fig. 4.6. It can be seen that almost all the cloud water disappears in cases where the distribution minimum has been adjusted to zero. This additional evaporation of cloud water places a strong constraint on subgrid-scale variability of humidity and especially the conservation of small amounts of cloud water.

It is always mentioned as a big disadvantage of relative humidity schemes using a threshold of critical relative humidity, that in cases where the mean relative humidity is below the critical relative humidity cloud water detrained by convection is evaporated

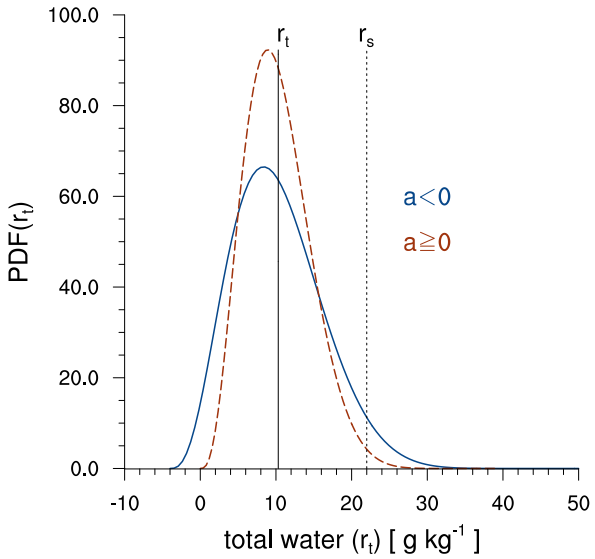

Figure 4.5: Two beta distribution, both having the same mean value (black line) and skewness. For one distribution (blue line) the minimum a is negative, for the other distribution (red line) the minimum is adjusted to 0.0. By keeping the mean value and the skewness the same the adjustment of the minimum a to zero leads to a smaller maximum b. For a fixed saturation value (black, dotted) the amount of cloud water would be less.

instantaneously. By using the incomplete beta function in this way, a similar problem is introduced in the assumed PDF method which should be avoided. The possibility to keep and include also small amounts of cloud water produced by the convection scheme is one big advantage of the assumed PDF method compared to the relative humidity schemes and should be retained.

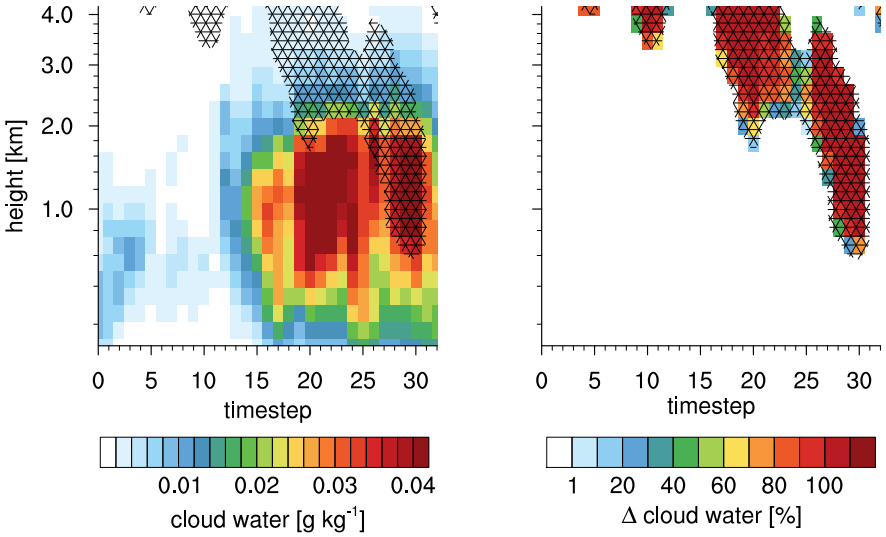

(a) COSMO-DE January dataset, cloud water

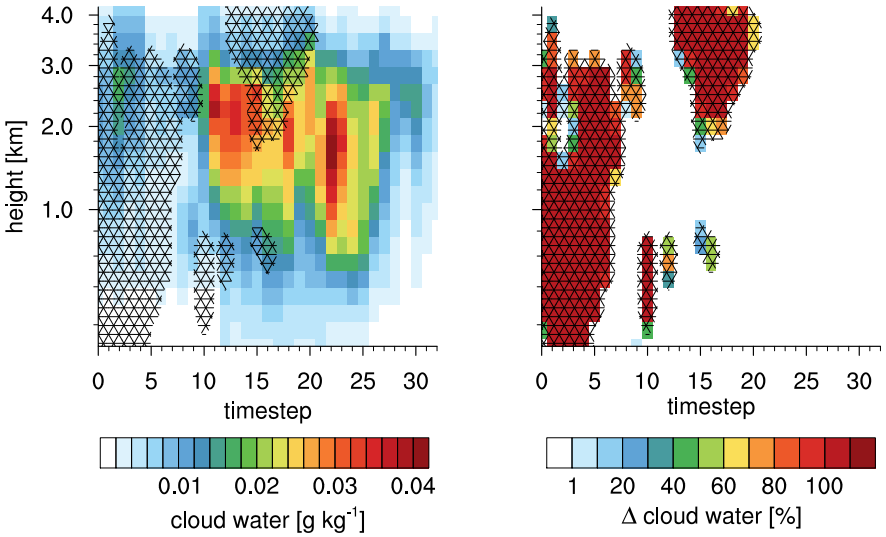

(b) COSMO-DE June dataset, cloud water

Figure 4.6: Left: Original profile of the cloud water (color, g kg^{-1}) for each timestep. The hatched part marks the cases with a negative distribution minimum ($a < 0$) of the general beta distribution. Right: Reduction of the cloud water (%) caused by adjusting the distribution minimum to $a \geq 0$.

Skewness

Another possibility is to use the total water mean, the cloud water mean and the closure as input variables and to accept the skewness to be a diagnostic quantity. In this case it is necessary to introduce a new iteration and adjust the skewness in order to obtain a consistent distribution with $a = 0$. This could be done in the following way: In the case of a negative distribution minimum, a is set to zero and the iteration for the cloud water is done again, but this time for the shape parameter p and q, coupled by $(p-1)(q-1) = 2$. That means, the following system is solved for q:

$$\begin{aligned} p &= \frac{q+1}{q-1} \\ 0 &= r_t I_x(p+1,q) - r_s I_x(p,q) + r_s - r_v \quad \text{, with} \\ x &= \frac{p r_s}{r_t(p+q)} \end{aligned} \tag{4.6}$$

The new iteration is tested for the same COSMO-DE datasets as in the previous section. The original cloud water as well as the difference before and after the additional iteration are shown in Fig. 4.7. If the iteration converges, it is possible to reproduce the original cloud water in the range of numerical uncertainty (see Fig. 4.7) and to achieve a distribution minimum of $a \geq 0$ by adjusting the skewness.

If the iteration led to strong changes in the skewness, this could result in discontinuities in the evolution of the PDF. To avoid these discontinuities it is desirable to find a member of the incomplete beta functions with a skewness close to the original one. In order to find such a solution, the original shape parameter q is used as a starting value for the iteration. In the current scheme the PDF is mainly used to describe properties of the saturated part of a grid box, as it is used to calculate the cloud fraction and changes to the cloud water. Therefore, the main interest is in the saturated part of the distribution and it is important to keep the right side of the distribution as consistent as possible. The differences in skewness and both shape parameters p and q are shown in Fig. 4.8. The skewness as well as the shape parameters are changed considerably for both datasets. But the change in the parameter p is stronger than for the parameter q that is describing the saturated part of the distribution. Especially for the January dataset the change of q is rather small.

Besides the considerable changes in the skewness, another drawback of this procedure is the need to introduce a second iteration and with this not only the computing time, but also the risk of not finding a solution is increasing.

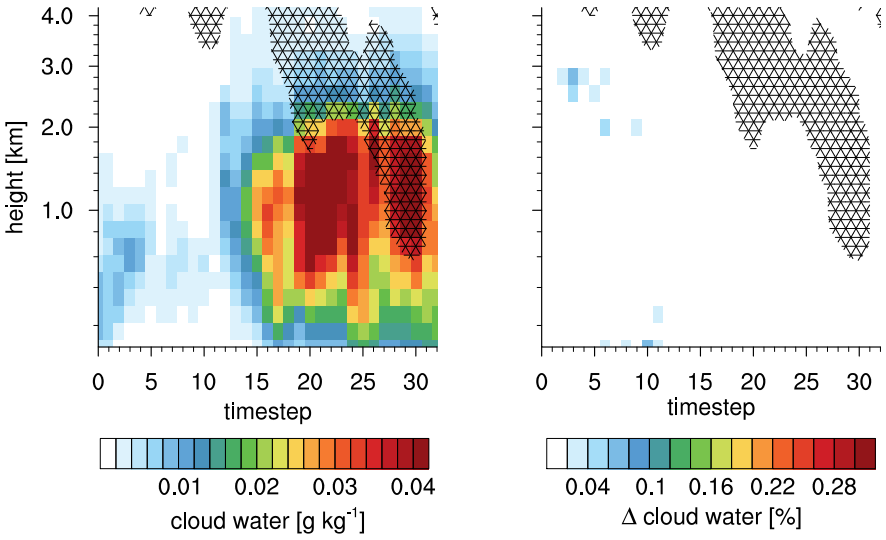

(a) COSMO-DE January dataset, cloud water

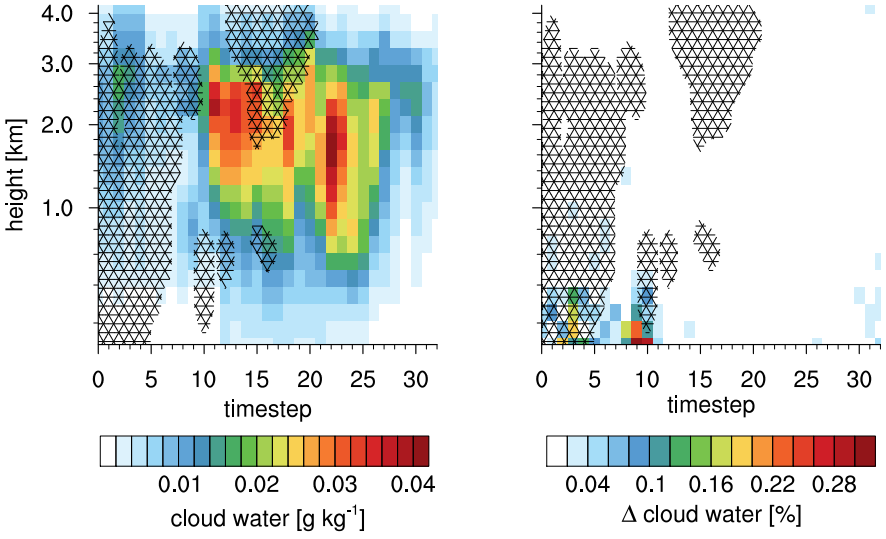

(b) COSMO-DE June dataset, cloud water

Figure 4.7: Left: Original profile of the cloud water (color, g kg^{-}1) for each timestep. The hatched part marks the cases with a negative distribution minimum ($a < 0$) of the general beta distribution. Right: Reduction (%) of the original cloud water by applying the additional iteration to find a solution with $a \geq 0$. Changes in parts of the space where no adjustment is necessary are due to numerical uncertainty introduced by the iterative calculation.

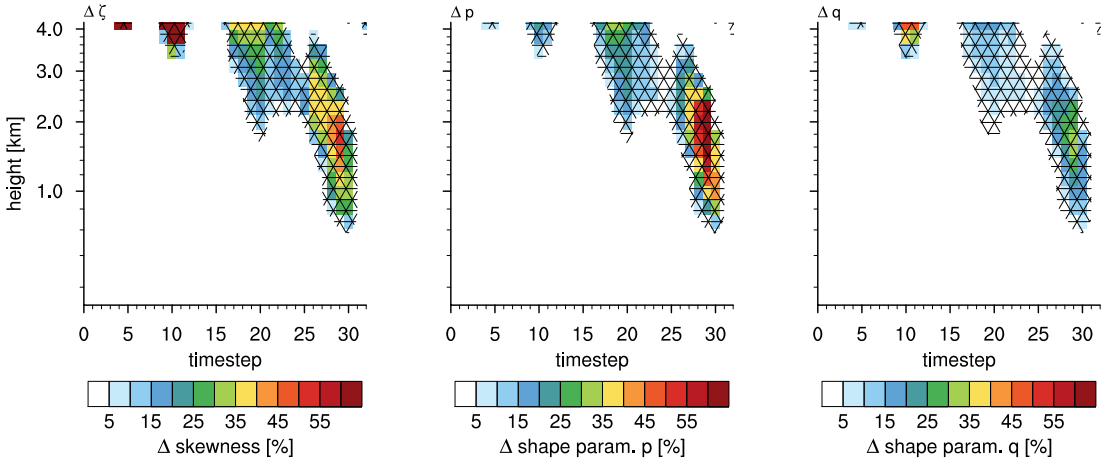

(a) COSMO-DE January dataset

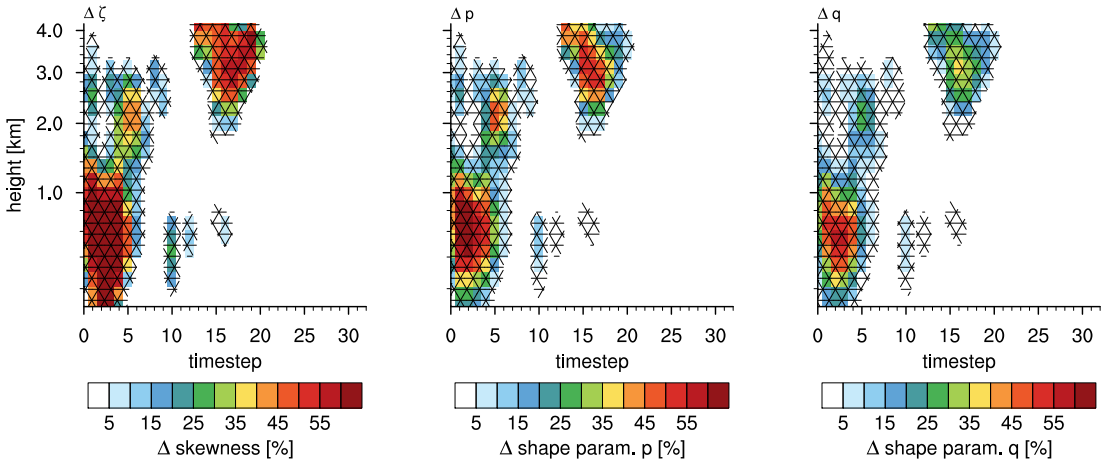

(b) COSMO-DE June dataset

Figure 4.8: Change (%) during the additional iteration for the skewness ζ (left), the shape parameter p (middle), and the shape parameter q (right) for each height and each timestep. The hatched part marks the cases with a negative distribution minimum ($a < 0$) of the beta distribution. In these cases the additional iteration is applied.

4.3.2 Discussion of alternative approaches

Iterative solution for the distribution maximum

One way to avoid using the distribution minimum explicitly and to also strengthen the connection to the cloud water could be to iterate for the maximum b and to use the cloud water instead of iterating for a and using the water vapor. This would lead to the following system of equations:

$$(b - r_t)\frac{p}{q}(1 - I_x(p+1, q)) + ((r_t - b)\frac{p}{q} + r_t - r_s)(1 - I_x(p, q)) - r_c = 0 \quad , \tag{4.7}$$

with

$$x = \frac{(r_s - r_t)q + (b - r_t)p}{(b - r_t)(q + p)} \quad . \tag{4.8}$$

The distribution minimum a could then be diagnosed by

$$a = (r_t - b)\frac{p}{q} + r_t \tag{4.9}$$

Also the calculation of the cloud water r_c could be done without using the minimum, a, explicitly:

$$r_c = (b - r_t)\frac{p}{q}\,(1 - I_x(p+1, q)) + (r_t - r_s + (r_t - b)\frac{p}{q})\,(1 - I_x(p, q)) \quad , \text{ with} \tag{4.10}$$

$$x = \frac{(r_s - r_t)q + (b - r_t)p}{(b - r_t)(p + q)} \tag{4.11}$$

This avoids using the distribution minimum a explicitly in most of the calculations. Nevertheless it is possible to get negative values for a when calculating it diagnostically. It might be easier to adjust the value to zero as it is calculated diagnostically. This change however would still lead to inconsistencies or changes in the mean value and the variance and with this also to changes of the cloud water and all other properties of the distribution.

Finding a completely iterative solution (no closure)

Instead of using a constraint to a trajectory through the parameter space spanned by p and q (see Fig. 4.2) another possibility is to use the prognostic variance ($\overline{r_t'^2}$) and skewness (ζ) and solve iteratively for p and q. Additionally to the iterative solution of the equation for a or b (see e.g. section 4.3.2) the following equations have then to be solved:

$$x = \frac{r_t - a}{\sqrt{r_t'^2}} \tag{4.12}$$

$$p = \frac{2x^2 + \zeta x - 1}{4 + \frac{\zeta}{x} - \zeta x} \tag{4.13}$$

$$q = \frac{(p^2 + 2p)\frac{\zeta}{x} + 2p}{2 - p\frac{\zeta}{x}} \tag{4.14}$$

This approach would avoid the use of a closure and be able to use the whole variability provided by the family of general beta distributions. Nevertheless, there are also some drawbacks. One is to find a stable, computationally efficient and converging algorithm to solve the system. Additionally, the system is not closed in case of clear sky or overcast conditions, and another constraint has to be introduced to replace the cloud-water mean as an input parameter.

4.3.3 New approach: Approximation by a general beta function

Assuming a truncated beta function

In the case of a negative distribution minimum, the family of truncated beta distributions, or more specific beta distributions truncated at zero, can be used. The distribution function for this family is defined as:

$$\begin{aligned} f_t(t) &= \frac{\frac{\Gamma(p+q)}{\Gamma(p)\Gamma(q)}}{1 - I_{\frac{0-a}{b-a}}(p,q)} \frac{(t-a)^{p-1}(b-t)^{q-1}}{(b-a)^{p+q-1}} \quad \text{, with} \\ I_x(p,q) &= \frac{1}{B(p,q)} \int_0^x t^{p-1}(1-t)^{q-1} dt \end{aligned} \tag{4.15}$$

This leads to different equations for the mean value

$$\bar{r}_t = \frac{p}{p+q}(b-a) + a + \frac{1}{p+q}(0-a)(b-a) f_t(0) \quad , \tag{4.16}$$

the cloud water

$$\begin{aligned} \bar{r}_c &= \int_{r_s}^{b} (r_t - r_s) f_t(r_t) dr_t \\ &= \bar{r}_t - r_s - \frac{1}{1 - I_{\frac{0-a}{b-a}}} \left((b-a) \frac{p}{p+q} \left(I_{\frac{r_s-a}{b-a}}(p+1,q) - I_{\frac{0-a}{b-a}}(p+1,q) \right) \right) \\ &\quad - (r_s - a) \left(I_{\frac{rs-a}{b-a}}(p,q) - I_{\frac{0-a}{b-a}}(p,q) \right) \quad , \end{aligned} \tag{4.17}$$

and the cloud fraction

$$f = \int_{r_s}^{b} f_t(r_t) dr_t = \frac{1 - I_{\frac{r_s - a}{b-a}}(p,q)}{1 - I_{\frac{0-a}{b-a}}(p,q)} \quad . \tag{4.18}$$

This option would be the desirable choice as it allows to keep the distribution consistent with all constraints and it is only defined on physically reasonable values. But from a computational point of view, the increased complexity of equations would lead to a highly increased computational effort and with this the advantage caused by the introduced closure will be lost.

Approximation by a general beta function

If the negative part of the distribution is small

$$I_{\frac{0-a}{b-a}}(p,q) << 1 \quad ,$$

then the truncated beta distribution might, for computational reasons, be approximated by the generalized beta function, that is already used for $a \geq 0$.

$$f_g(t) = \frac{\Gamma(p+q)}{\Gamma(p)\Gamma(q)} \frac{(t-a)^{p-1}(b-t)^{q-1}}{(b-a)^{p+q-1}} \quad . \tag{4.19}$$

This choice allows to keep the distribution consistent to all four input constraints, to keep the computational effort low and to use the advantage of the introduced closure. To correct for the approximation, the PDF has to be renormalized for the calculation of the cloud fraction:

$$f = \int_{r_s}^{b} f_t(r_t) dr_t = \frac{\int_{r_s}^{b} f_g(r_t) dr_t}{1 - I_{\frac{0-a}{b-a}}(p,q)} = \frac{1}{1 - I_{\frac{0-a}{b-a}}(p,q)} \int_{r_s}^{b} f_g(r_t) dr_t = \frac{1 - I_{\frac{r_s - a}{b-a}}(p,q)}{1 - I_{\frac{0-a}{b-a}}(p,q)} \quad . \tag{4.20}$$

Finding the best compromise

On a long-term perspective, an iterative solution for the truncated beta function (section 4.3.3) or the approach without any closure (section 4.3.2) will be desirable. For now, the approximation of the truncated beta function by a general beta function (section 4.3.3) provides the best compromise between computational effort, mathematical complexity, and consistency within the GCM. Especially the consistency of the prognostic cloud water of the GCM can be improved by applying the approximation by the general beta distribution and continuously using the cloud water as an input parameter. This avoids additional evaporation of cloud water and ensures that the statistical

scheme is able to represent situations as e.g. caused by detrainment of cloud water by convection into a dry environment. The previous approach shared the problem of critical relative humidity schemes, to tend to evaporate small amounts of detrained cloud water instantaneously within a dry environment.

4.4 Step 2: Prognostic equations for skewness and variance

The statistical cloud scheme by Tompkins (2002) uses prognostic equations for the shape parameter q and the distribution width $(b-a)$, while our physical understanding and interpretation of a PDF of total water is rather based on the higher moments skewness and variance. The use of prognostic equations for skewness and variance provides the possibility to include our physical understanding of the varying moments based on physical processes more directly. Additionally, such equations would highly improve the flexibility of the whole framework, as it would be possible to exchange the assumed distribution or the applied closure without rewriting the whole scheme. Another advantage would be the increased consistency with for instance the turbulence parameterization, which provides source terms for the variance of total water rather than the distribution width of a certain PDF. With this increased consistency, the interactions between different physical processes and parameterizations can also be investigated in an easier and more detailed way.

For these reasons, prognostic equations for the skewness and variance will be presented in the following. The motivation for the individual source terms and their concrete formulation is similar to Tompkins (2002). The original source terms formulated in q and $(b-a)$ are provided in A.1.

In the following the closure T08 (Eq. (4.2)) will be used. Introducing this closure in the skewness equation (Eq. (2.15)), it becomes possible to calculate the shape parameter from the skewness ζ as done in equation (4.47).

Similar to the original formulation of the Tompkins scheme (see section 2.1.1), the prognostic equations for skewness ζ and variance $\overline{r_t'^2}$ of total water (r_t) are based on source and sink terms due to convection (conv), turbulence (turb) and microphysics (micro):

$$\left(\frac{\partial \overline{r'^2}}{\partial t}\right) = \left(\frac{\partial \overline{r'^2}}{\partial t}\right)_{\text{conv}} + \left(\frac{\partial \overline{r'^2}}{\partial t}\right)_{\text{turb}} \tag{4.21}$$

$$\left(\frac{\partial \zeta}{\partial t}\right) = \left(\frac{\partial \zeta}{\partial t}\right)_{\text{conv}} + \left(\frac{\partial \zeta}{\partial t}\right)_{\text{turb}} + \left(\frac{\partial \zeta}{\partial t}\right)_{\text{micro}} \tag{4.22}$$

4.4.1 Convection source term

The influence of convection on the shape of the PDF is described by the values of total water, that are brought into the grid box by convection. Convective towers detrain high values of total water into the grid box and this is understood as a cause of positive skewness. Similarly the downdrafts, bringing dry air into a grid box, would lead to negative skewness. The effect of downdrafts is still neglected in the scheme. The increase of positive skewness due to convection is parameterized by relating the source term to the detrainment of cloud water:

$$\frac{\partial \zeta}{\partial t} = \frac{K}{\bar{\rho} r_s} \frac{\partial}{\partial z} (M^{\mathrm{cu}} r_c^{\mathrm{cu}}) \quad , \tag{4.23}$$

where M^{cu} is the updraft mass flux and r_c^{cu} the mean cloud water in the convective updraft, which is assumed to be greater than the mean cloud water in the grid box ($r_c^{\mathrm{cu}} \gg \overline{r_c}$). K is a dimensionless tunable constant, which describes how efficiently detrained cloud water increases the skewness. Based on tuning results, Tompkins (2002) suggested to use $K = 10$.

The variance is also understood as increase due to the detrainment of high values of total water. With this, the increase in variance can be associated with an increase in skewness that is affecting mainly the distribution maximum b, while the minimum a is assumed to stay almost unchanged. Here, the new value for skewness, $\zeta_{n+1}^{\mathrm{conv}}$, can be used to determine the resulting change of the shape parameters q and p and the distribution width $(b-a)$.

$$q_{n+1}^{\mathrm{conv}} = \frac{(\zeta_{n+1}^{\mathrm{conv}} + 2) + \sqrt{2((\zeta_{n+1}^{\mathrm{conv}})^2 + 4)}}{2 - \zeta_{n+1}^{\mathrm{conv}}} \tag{4.24}$$

$$p_{n+1}^{\mathrm{conv}} = \frac{q_{n+1}^{\mathrm{conv}} + 1}{q_{n+1}^{\mathrm{conv}} - 1} \tag{4.25}$$

$$(b-a)_{n+1}^{\mathrm{conv}} = \frac{(\bar{r}_t - a)(p_{n+1}^{\mathrm{conv}} + q_{n+1}^{\mathrm{conv}})}{p_{n+1}^{\mathrm{conv}}} \tag{4.26}$$

$$= (b-a)_n \frac{(p_{n+1}^{\mathrm{conv}} + q_{n+1}^{\mathrm{conv}})}{p+q} \frac{p}{p_{n+1}^{\mathrm{conv}}} \tag{4.27}$$

Now these new terms can be used to determine the new value of the variance due to convection:

$$\overline{r'^2}_{n+1}^{\mathrm{conv}} = \frac{\left((b-a)_{n+1}^{\mathrm{conv}}\right)^2}{(p_{n+1}^{\mathrm{conv}} + q_{n+1}^{\mathrm{conv}})^2} \tag{4.28}$$

Certainly, this strong coupling of the convective source term for the variance to changes in the distribution parameter is not desirable. Additionally, the approach to assume a scaling to the detrainment of cloud water for the skewness source term and

to tune the efficiency is rather ad-hoc. For these two reasons, a new parameterization for the source terms due to convection will be presented in the next development step (section 4.5).

4.4.2 Turbulence source term

Tompkins (2002) assumed subgrid-scale vertical turbulent motions to be dynamically isotropic, and therefore to have no production effect on the skewness budget. Additionally, the effect of vertical transport of skewness by vertical turbulence was neglected, based on the limited vertical gradients of skewness. Those two assumptions will also be used in this approach. And with them, the effect of turbulence on the skewness budget is only the mixing inside one grid box and this is described by a dissipation term, which relaxes the skewness to symmetry:

$$\frac{\partial \zeta}{\partial t} = (\zeta_0 - \zeta)\left(\frac{1}{\tau_v} + \frac{1}{\tau_h}\right) \quad , \tag{4.29}$$

with $\zeta_0 = 0$. This dissipation term is based on two different timescales, one representing the dissipation due to 3D turbulence in the planetary boundary layer (PBL) and in the neighborhood of deep convection (τ_v), and one representing the dissipation by larger-scale 2D horizontal eddies caused by horizontal wind shear instabilities (τ_h).

For the influence of the turbulence on the variance, a more complete approach is taken. The variance source term includes the production of variance in the presence of a vertical moisture gradient, the vertical transport of moisture variance and a dissipation term.

$$\frac{\partial r_t'^2}{\partial t} = -2\overline{w'r_t'}\frac{\partial \bar{r}_t}{\partial z} - \frac{\partial \overline{(w'r_t'^2)}}{\partial z} - r_t'^2\left(\frac{1}{\tau_v} + \frac{1}{\tau_h}\right) \tag{4.30}$$

with $\overline{w'r_t'^2} = \Lambda\sqrt{e}\frac{\partial \overline{r_t'^2}}{\partial z}$, $\overline{w'r_t'}$ being the turbulence moisture flux, e the turbulent kinetic energy and Λ a mixing length-scale. The parameterization of the three different terms, should be consistent with the turbulence scheme of the GCM. More details on the timescales and the chosen approaches can be found in the original publication by Tompkins (2002).

4.4.3 Microphysics source term

The several microphysical processes (e.g. precipitation) are assumed to reduce the skewness and the variance of the distribution as they are mainly affecting the saturated part and the high values of total water. For the variance this effect is only taken into account implicitly, as the variance is calculated diagnostically in partially cloudy cases. Theoretically, it would be desirable to calculate the change in skewness, by solving for the new values of cloud water and water vapor. But as this would need an iterative

solution, instead, an approximation based on a linear increase of the maximum b is taken. As mainly the saturated part should be affected, the distribution minimum is assumed to stay constant ($\Delta a = 0$), while the change is projected onto the distribution maximum b. If the whole cloud would be removed, the change of the distribution maximum should be $\Delta b_{\max} = (r_s - b)$ and with this $b_{n+1} = b + \Delta b_{\max} = r_s$. Therefore, the change of the distribution maximum is related to the relative change of cloud water, bounded by $(b - r_s)$:

$$\Delta b = \frac{\Delta \bar{r}_c^{\text{micro}}}{\bar{r}_c}(b - \bar{r}_s) \quad . \tag{4.31}$$

The change of cloud water ($\Delta \bar{r}_c$) is calculated by taking the following processes into account: effect of convection, autoconversion of cloud water to rain, accretion of cloud droplets by falling rain, accretion of ice and cloud droplets by falling snow, large-scale condensation and deposition, generation of liquid water and ice by the turbulence tendency (section 4.4.2).

As the change due to microphysics should mainly change the saturated part of the distribution, and with this the right shape parameter q, the change in b is translated into a change in q by assuming $\Delta a = 0$ and introducing the closure T08 into the equation for the mean value $\bar{r}_t = (b - a)\frac{p}{p+q} + a$.

$$q^2 - q\frac{b_{n+1} - a}{r_t - a} - \frac{b_{n+1} - a}{r_t - a} + 1 = 0 \tag{4.32}$$

Two possible solutions exist for this quadratic equation:

$$q_{1,2} = \frac{1}{2}\frac{b_{n+1} - a}{r_t - a} \pm \sqrt{\frac{1}{4}\left(\frac{b_{n+1} - a}{r_t - a}\right)^2 + \frac{b_{n+1} - a}{r_t - a} - 1} \quad . \tag{4.33}$$

The two solutions can be constrained by the following relations:

$$\frac{1}{2}\frac{b_{n+1} - a}{r_t - a} < \sqrt{\frac{1}{4}\left(\frac{b_{n+1} - a}{r_t - a}\right)^2 + \frac{b_{n+1} - a}{r_t - a} - 1}\,, \quad \text{and} \quad 0 < q \tag{4.34}$$

Based on this, the solution for the new value for q has to be:

$$q_{n+1}^{\text{micro}} = \frac{1}{2}\frac{b_{n+1} - a}{r_t - a} + \sqrt{\frac{1}{4}\left(\frac{b_{n+1} - a}{r_t - a}\right)^2 + \frac{b_{n+1} - a}{r_t - a} - 1} \tag{4.35}$$

As p and q are coupled by the closure T08, the desired behaviour, that the unsaturated part of the distribution stays unchanged has to be violated:

$$p_{n+1}^{\text{micro}} = \frac{q_{n+1}^{\text{micro}} + 1}{q_{n+1}^{\text{micro}} - 1} \quad . \tag{4.36}$$

With the new values for the two shape parameters, finally the new skewness can be calculated:

$$\zeta_{n+1}^{\text{micro}} = \frac{2(q_{n+1}^{\text{micro}} - p_{n+1}^{\text{micro}})}{p_{n+1}^{\text{micro}} + q_{n+1}^{\text{micro}} + 2} \sqrt{\frac{p_{n+1}^{\text{micro}} + q_{n+1}^{\text{micro}} + 1}{p_{n+1}^{\text{micro}} q_{n+1}^{\text{micro}}}} \tag{4.37}$$

$$\frac{\Delta\zeta_{n+1}^{\text{micro}}}{\Delta t} = \frac{\zeta_{n+1}^{\text{micro}} - \zeta_n}{\Delta t} \quad . \tag{4.38}$$

Even though this linear approach is also rather simple and ad-hoc, it is also convincing in its way of including our understanding and expectations of how the PDF should change with microphysics. Nevertheless, it is ignoring any more detailed process dependency. Theoretically, the shape of the PDF would be expected to change differently for a process as precipitation, where liquid water is removed, compared to a process as condensation, where a phase change appears. In the future it would be desirable to represent these varying effects, as they also lead to different changes in the cloud fraction. For precipitation the cloud fraction is not necessarily expected to change, while condensation certainly should lead to an increase in cloud fraction. A more thorough parameterization of the microphyiscal effects, that is independent of the specific distribution parameters and is taking into account the varying effects of microphysical processes, could lead to a great improvement of the representation of physical processes within the statistical scheme.

4.5 Step 3: Parameterization of new convection source terms

The convection source term presented in the previous section has two major drawbacks: the source term for the skewness is formulated rather ad-hoc and needs additional tuning, and the source term for the variance is strongly coupled to the distribution parameters. In this section, an alternative parameterization for the convection source terms will be presented. Especially, as the convection source terms are considered as the main source for skewness and variance, it is important to test different parameterizations. The idea for a new convection source term presented in the following was published in Klein et al. (2005). Due to the limited availability of higher moments in the convection parameterization, a direct implementation of the suggested source terms into the ECHAM6 GCM, and most current GCMs, is not possible. Here, a simple parameterization derived from LES diagnostics, will be presented and discussed. With this simple parameterization, the issues of the tunable constant and the strong coupling between source term and distribution parameters will be solved, but the rather simple parameterization might be refined at a later time.

4.5.1 New convection source terms for skewness and variance

The suggestion of Klein et al. (2005) for new convection source terms uses a common approximation for convection in coarse models: it is assumed, that the convective towers cover only a small area compared to the environmental part. Even though the process of detrainment and entrainment is highly complex (see e.g. de Rooy et al. (2013)), here a simplification is used: Detrainment and entrainment are rather understood as a certain mass package, that is transported from the convective tower into the environment (detrainment) or from the environment into the convective tower (entrainment). Further, this mass package is assumed to have its own statistics: $(\bar{r}_t)_{\text{detr}}$, $(\overline{r_t'^2})_{\text{detr}}$, $(\overline{r_t'^3})_{\text{detr}}$ for detrainment, and $(\bar{r}_t)_{\text{entr}}$, $(\overline{r_t'^2})_{\text{entr}}$, $(\overline{r_t'^3})_{\text{entr}}$ for entrainment. These values are expected to be different from the values in the environment $\bar{r}_t$, $\overline{r_t'^2}$, $\overline{r_t'^3}$. In this approach the third moment $\overline{r_t'^3}$ will be used, which is connected to the skewness ζ by

$$\zeta = \frac{\overline{r_t'^3}}{(\overline{r_t'^2})^{\frac{3}{2}}} \quad . \tag{4.39}$$

With these different statistics, and the assumption, that the fraction of the detrained (entrained) mass over the sum of the detrained (entrained) mass and the mass of the environment will be small, source terms can be obtained for the variance

$$\begin{aligned}\left(\frac{\partial \overline{r'^2}_t}{\partial t}\right)_{\text{conv}} =& D((\bar{r}_t)_{\text{detr}} - \bar{r}_t)^2 + D((\overline{r_t'^2})_{\text{detr}} - \overline{r_t'^2}) \\ &- E((\bar{r}_t)_{\text{entr}} - \bar{r}_t)^2 - E((\overline{r_t'^2})_{\text{entr}} - \overline{r_t'^2}) - M_c \frac{\partial \overline{r_t'^2}}{\partial p} \quad ,\end{aligned} \tag{4.40}$$

and the third moment

$$\begin{aligned}\left(\frac{\partial \overline{r'^3}_t}{\partial t}\right)_{\text{conv}} =& D((\bar{r}_t)_{\text{detr}} - \bar{r}_t)^3 + D((\overline{r_t'^3})_{\text{detr}} - \overline{r_t'^3}) + 3D((\bar{r}_t)_{\text{detr}} - \bar{r}_t)((\overline{r_t'^2})_{\text{detr}} - \overline{r_t'^2}) \\ &- E((\bar{r}_t)_{\text{entr}} - \bar{r}_t)^3 - E((\overline{r_t'^3})_{\text{entr}} - \overline{r_t'^3}) - 3E((\bar{r}_t)_{\text{entr}} - \bar{r}_t)((\overline{r_t'^2})_{\text{entr}} - \overline{r_t'^2}) \\ &- M_c \frac{\partial \overline{r_t'^3}}{\partial p} \quad .\end{aligned} \tag{4.41}$$

Here, M_c is the convective mass flux, D the mass detrainment rate from convection and E the entrainment rate, both in units of inverse seconds.

Physically, these source terms are describing the fact, that the higher moments in the environment are changed by convection through the differences of the mean values and moments. The more formal derivation of the equations can be found in Klein et al. (2005).

It is not trivial to introduce these source terms into a common GCM. The first problem is that the variance ($(\overline{r_t'^2})_{\mathrm{detr}}$, $(\overline{r_t'^2})_{\mathrm{entr}}$) and the third order moment ($(\overline{r_t'^3})_{\mathrm{detr}}$, $(\overline{r_t'^3})_{\mathrm{entr}}$) of detrained (resp. entrained) total water are usually not known. It is a common approach for GCMs to assume that the statistics of entrained air equals the statistics of environmental air (e.g. Tiedtke (1989)). With this assumption, the differences in Eq. (4.40) and Eq. (4.41) connected to entrainment are zero. In addition, Klein et al. (2005) showed, that the mass flux terms (the last terms on the right hand side) are negligible compared to the other contributions. For the first approach to implement the new source terms presented in this study, these two terms are therefore neglected.

4.5.2 Characterizing the convective source terms from LES data

The original source terms to describe the influence of convection on the skewness and variance of the PDF, Eq. (4.40) and Eq. (4.41), have been reduced by neglecting entrainment and the contribution of the mass flux. Now, the source terms are only describing the contribution by detrainment, but there is still the need to find parameterizations for the higher order moments of detrained total water. In this part, high resolution LES datasets will be used to investigate the magnitude and properties of the specific detrainment terms in order to parameterize or neglect the higher order differences in the following reduced form of the source terms:

$$\left(\frac{\Delta\overline{r'^2}_t}{\Delta t}\right)_{\mathrm{conv}} = D((\bar{r}_t)_{\mathrm{detr}} - \bar{r}_t)^2 + D((\overline{r_t'^2})_{\mathrm{detr}} - \overline{r_t'^2}) \tag{4.42}$$

$$\left(\frac{\Delta\overline{r'^3}_t}{\Delta t}\right)_{\mathrm{conv}} = D((\bar{r}_t)_{\mathrm{detr}} - \bar{r}_t)^3 + D((\overline{r_t'^3})_{\mathrm{detr}} - \overline{r_t'^3}) + 3D((\bar{r}_t)_{\mathrm{detr}} - \bar{r}_t)((\overline{r_t'^2})_{\mathrm{detr}} - \overline{r_t'^2}) \tag{4.43}$$

Three different LES cases will be analyzed, the CGILS shallow cumulus (s6) and the stratocumulus (s12) case, and a deep convective case (for more details, see section 2.2.3). As it is difficult to determine the actually detrained water it is assumed that the statistics of the detrained water equals the statistics inside the updraft. To calculate the higher order moments of the total water in the updraft it is necessary to define convective and stratiform parts. Following Xu (1995), a column is defined as convective, if the maximum vertical velocity below the melting level is twice as high as in the 4 neighboring grid-boxes (in the two horizontal directions), or if it is higher than a threshold updraft velocity w_t. To test the sensitivity to these assumptions, two different thresholds are used: $w_t = 0.5\,\mathrm{m\,s^{-1}}$ and $w_t = 1\,\mathrm{m\,s^{-1}}$. The statistics are computed at each timestep.

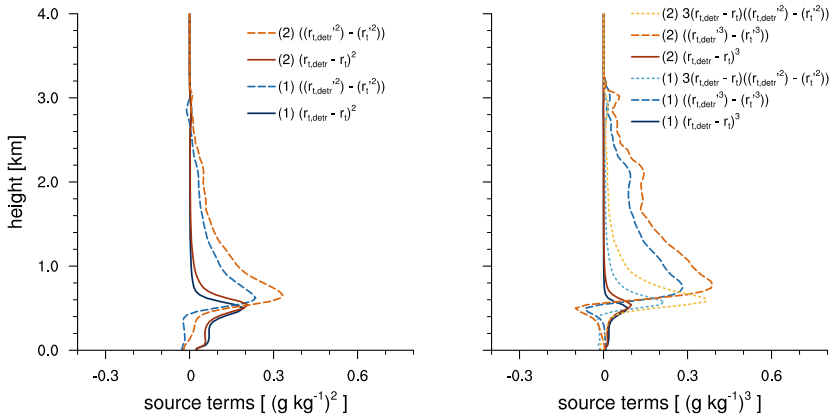

(a) trade-cumulus (s6)

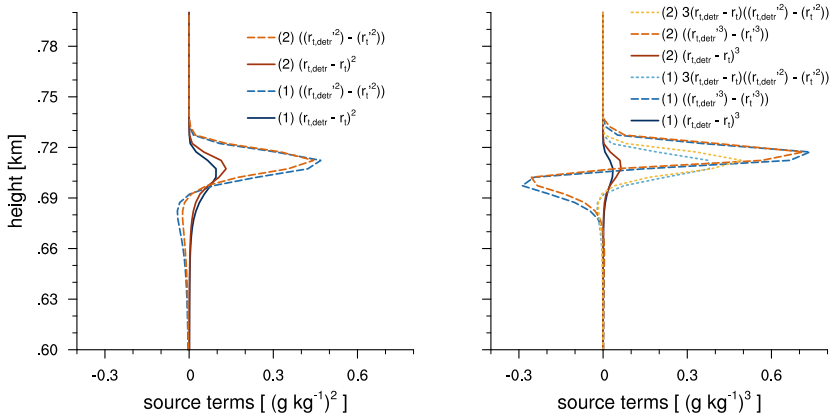

(b) stratocumulus (s12)

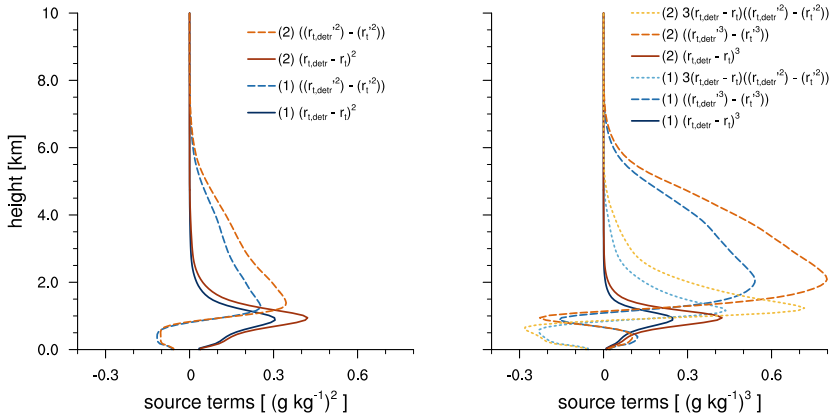

(c) deep convection

Figure 4.9: Convection source terms due to detrainment (see Eq. (4.40) and Eq. (4.41)) for the variance (left column) and the skewness (right column) for the different LES cases, (a) the CGILS trade-cumulus case, (b) the CGILS stratocumulus case and (c) a deep convective case. To determine the convective areas two different thresholds for the vertical velocity are chosen: (1) a threshold of $w_t = 0.5\,\mathrm{m\,s^{-1}}$ (blue) and (2) $w_t = 1\,\mathrm{m\,s^{-1}}$ (red). The source terms are calculated with the assumption of similar statistics for total water in the updrafts and the detrained total water.

In Fig. 4.9 the terms from Eq. 4.42 and Eq. 4.43 estimated for the three different LES cases and for the two thresholds are shown. As the main interest is to find an estimate for the magnitude and mean sensitivity to the thresholds, the terms are averaged over time and shown as vertical profiles. The difference of the mean values shows the most robust but also smallest signal. The sensitivity, as well as the magnitude of contribution is increasing for the higher order moments. For the stratocumulus case, mainly the inversion can be seen, while the shallow cumulus and the deep convective case show a similar profile, only differing in the height. It is clear, that the higher order terms cannot be neglected in a reasonable way, but that it is necessary to find a parameterization to include them. Nevertheless, the high sensitivity also poses a challenge to the parameterization.

4.5.3 Parameterization of skewness and variance of detrained total water

In order to include the higher order moments of the detrained total water (used in Eq. (4.42) and Eq. (4.43)) it is important to parameterize them, as they are not included in a typical GCM. Here, the parameterization is kept as simple as possible to provide a starting point, but it can definitely be refined in the future. As a first step, it is assumed again, that the properties of the detrained total water are the same as in the updraft. To keep the parameterization simple, it is aimed on using a simple scaling relation between a known variable and the two unknown variables. Klein et al. (2005) suggested to parameterize the updraft total water variance in terms of the updraft total water mean. Additionally to this suggestion, also the correlation between the unknown variables and the higher moments of total water in the environment is analyzed. The correlations for these three known variables, the mean in the updraft and the second and third moment in the environment, to the two unknown variables, the second and third moment of total water in the updraft, are shown in Fig. 4.10. As a threshold for the vertical velocity to determine convective points $w_t = 0.5\,\mathrm{m\,s^{-1}}$ is used.

The suggested correlation between the mean and the variance of total water in the updraft (Klein et al. 2005), is not found in the three LES cases used in this analysis. The best scaling can be seen between the variance of total water in the environment and in the updraft. Less convincing, but still somehow plausible is the scaling between the third order moment of total water in the environment and in the updraft. For both correlations, the stratocumulus case shows a nice relation between the higher order moments in the environment and in the updraft. The shallow cumulus case shows in both cases a broad spread and no distinct line or direction. The deep convection case on the other side, seems to include specific breaking points, where the relation is changing. But in all cases a positive correlation can be seen, and by taking the average of these three diverse cases a certain mean behaviour should be represented that can be used in this first parameterization approach. The specific regression coefficients for

the three types of correlation and the three simulations can be found in table 4.1. Two types of regression are done, a normal regression producing a y-Axis intercept, and one regression that is forced to go through the origin. For the parameterization in the GCM the mean correlation coefficients of the regressions going through the origin are used, 1.27 for the second order term and 1.53 for the third order term. These two coefficients could also be interpreted as tunable constants, but they are certainly more physically based and restricted as the former tunable constant K (see section 5.3.4).

With this a simple parameterization of the source terms for the higher order moments of total water mixing ratio due to convection can be derived:

$$\left(\frac{\Delta\overline{r_t'^2}}{\Delta t}\right)_{\text{conv}} = D(\bar{r}_{t,\text{detr}} - \bar{r}_t)^2 + D(1.27 \cdot \overline{r_t'^2} - \overline{r_t'^2}) \tag{4.44}$$

$$\left(\frac{\Delta\overline{r_t'^3}}{\Delta t}\right)_{\text{conv}} = D(\bar{r}_{t,\text{detr}} - \bar{r}_t)^3 + 3D(\bar{r}_{t,\text{detr}} - \bar{r}_t)(1.27 \cdot \overline{r_t'^2} - \overline{r'^2}_t) + D(1.53 \cdot \overline{r_t'^3} - \overline{r_t'^3}) \tag{4.45}$$

Data	**deep conv.**		**shallow (s6)**		**strato (s12)**		**Mean**
	Intercept	Origin	Intercept	Origin	Intercept	Origin	Origin
$\bar{r}_t^2$ and $(\overline{r_t'^2})_{\text{detr}}$	0.0055	0.0060	0.00082	0.00087	-2.8·10^{-5}	0.00032	
$\overline{r_t'^2}$ and $(\overline{r_t'^2})_{\text{detr}}$	1.04	1.08	1.34	1.38	1.35	1.35	1.27
$\overline{r_t'^3}$ and $(\overline{r_t'^3})_{\text{detr}}$	1.97	1.97	1.05	1.13	1.48	1.48	1.53

Table 4.1: Regression coefficients for the three datasets (deep convection, shallow cumulus, stratocumulus) calculated in two different ways: one with allowing a y-Axis intercept and one that is forced through the origin. The last column shows the mean values over the regression coefficients through the origins, which are used for the parameterizations. For clarity reasons standard deviations and units are omitted. The first data row shows the regression coefficients for the correlation between the square of the mean total water in the updraft and the variance of total water in the updraft, with the unit $(\text{g kg}^{-1})^2$. The second row shows the coefficients for the correlation between the variance of total water in the environment and the variance of total water in the updraft, again with the unit $(\text{g kg}^{-1})^2$. The third row shows the coefficients for the correlation between the third moment of total water in the environment and the third moment of total water in the updraft, these values are having the unit $(\text{g kg}^{-1})^3$.

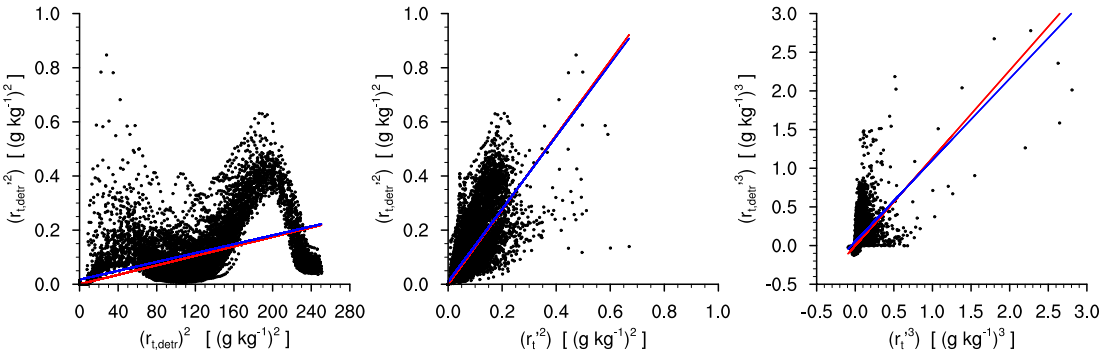

(a) trade-cumulus (s6)

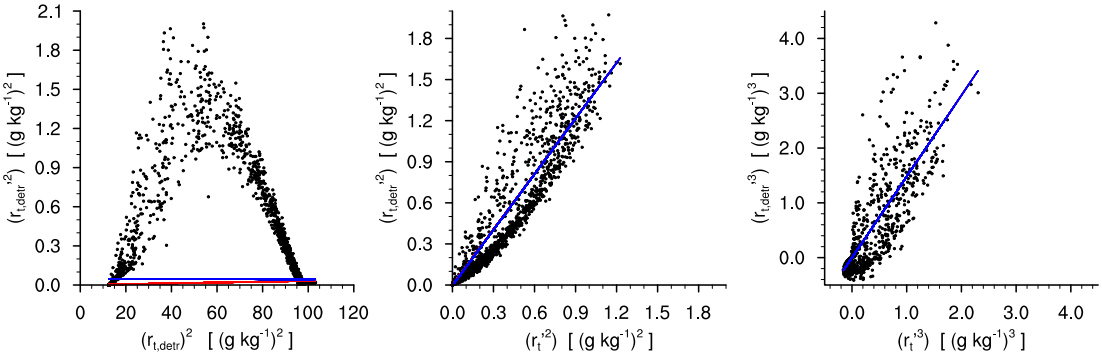

(b) stratocumulus (s12)

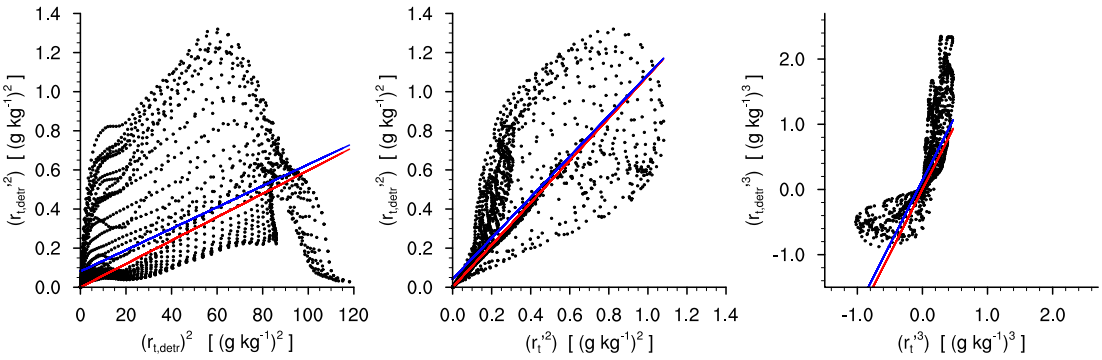

(c) deep convection

Figure 4.10: Correlation of the second and third order moment of the detrained total water to known quantities: the second moment in the updraft to the square of the mean in the updraft (first column), the second order moment in the updraft to the second order moment in the environment (second column), and the third order moment in the updraft to the third order moment in the environment (third column) – all moments are shown for total water. Convective points are determined using a threshold for the vertical velocity of $w_t = 0.5\,\mathrm{m\,s^{-1}}$. The same analysis is presented for three different LES cases, and for each correlation two regression lines are calculated, one having a y-Axis intercept (blue) and one forced to go through the origin (red).

The new source terms are solving two clear drawbacks of the earlier source terms, as they do not include an additional tuning constant and are independent of the distribution parameters. Nevertheless, the analysis and parameterization presented above is rather simple and the new terms should be understood as a starting point, that can be used without introducing more additional equations. Of course, there are many possibilities to refine the presented analysis and parameterization, and it is also still desirable to include downdrafts and entrainment. Convection is still understood as a major source for positive skewness, but depending on the timescale, it could also turn into a negative source term. The positive tendency is based on the interpretation of convection adding high total water values to a comparably dry environment (grid box), but convection could also lead to a general shift of the environment (grid box) to moister values. This general shift should then go along with a negative skewness tendency. In the non-parameterized source terms (Eq. (4.40) and Eq. (4.41)) at least some saturation of the increase in skewness can be imagined by the differences of the detrained skewness and the skewness in the environment. Unfortunately, this relation is lost in the parameterized equations, which are leading more to a self amplification of the skewness. Maybe it will be necessary, to include an additional equation for the skewness of detrained total water. And for sure, a more detailed investigation of the timescales on which convection is acting on the skewness could greatly contribute to our understanding and ability to parameterize the effect of convection on the PDF.

4.6 Understanding the dependency of the PDF on the input parameters

4.6.1 Dependency of cloud fraction on cloud water and skewness

There are many different possibilities to calculate the needed parameters from the moments, to define closures or use varying input variables even for one PDF family. For the evaluation of different approaches, but also for improving our understanding of the distributions and how they should change in certain situations, it is essential to develop theoretical expectations on the sensitivity to the input parameters. Here, the focus is on the dependency of the distribution, more specifically the cloud fraction, on the skewness and cloud water. For the cloud water, clearly a positive correlation is expected. If the skewness is kept constant and the cloud water is increasing, the cloud fraction should increase as well, and the other way around. The more open question is: How should the cloud fraction change, if the skewness is changed but the cloud water stays the same? The skewness is a measure for the heterogeneity of the distribution of total water. For a positively skewed distribution, there is a specific probability for some clearly higher total water values than the mean value. A similar argument can be made for the cloud water: for a distribution containing a certain amount of cloud

water, positive skewness would lead to a specific probability for points with a high cloud water. This means, that the amount of cloud water that is present, would be clustered at a small area, in a relatively seen drier environment. If the skewness is decreased, these clusters of high cloud water would disappear and in order to keep the same cloud water mean, the cloud water has to be distributed over a larger area. This would lead to a more homogeneous distribution over a larger area, and with this to a higher cloud fraction. The hypothesis based on these arguments is: Assuming the mean cloud water stays constant, the cloud fraction is expected to increase with decreasing skewness, and the other way around.

This hypothesis will be tested by analyzing high-resolution model output. Afterwards, the representation of this behaviour in the statistical schemes assuming a beta distribution will be evaluated for both closures (T02 and T08).

4.6.2 Evaluation of the expected dependency using LES data

For the evaluation of the dependency of cloud fraction on cloud water and skewness, three different LES simulations are used: the two shallow cumulus cases (s6 and RICO), and a deep convective case (for more details see section 2.2.3). Those simulations are expected to vary in cloud water amount and skewness and with this provide a good impression of the dependencies. To separate the effects of the input parameter, the cloud fraction is sorted in terms of cloud water and skewness.

The cloud fraction for LES simulations is calculated based on the all-or-nothing approach: a point with a cloud water greater zero is defined as cloudy. In Fig. 4.11 the colors show the average cloud fraction for a specific combination of cloud water and skewness for the LES simulations. The variability in horizontal direction represents the dependency on the skewness while the variability in vertical direction represents the dependency on the cloud water. It can nicely be seen, that the cloud fraction increases for increasing cloud water as well as for decreasing skewness. These idealized cases confirm our hypothesis, that for a constant cloud water content a decrease in skewness should lead to an increase in cloud fraction. Parameterizations of cloud fraction using the higher moment skewness should be able to represent this effect.

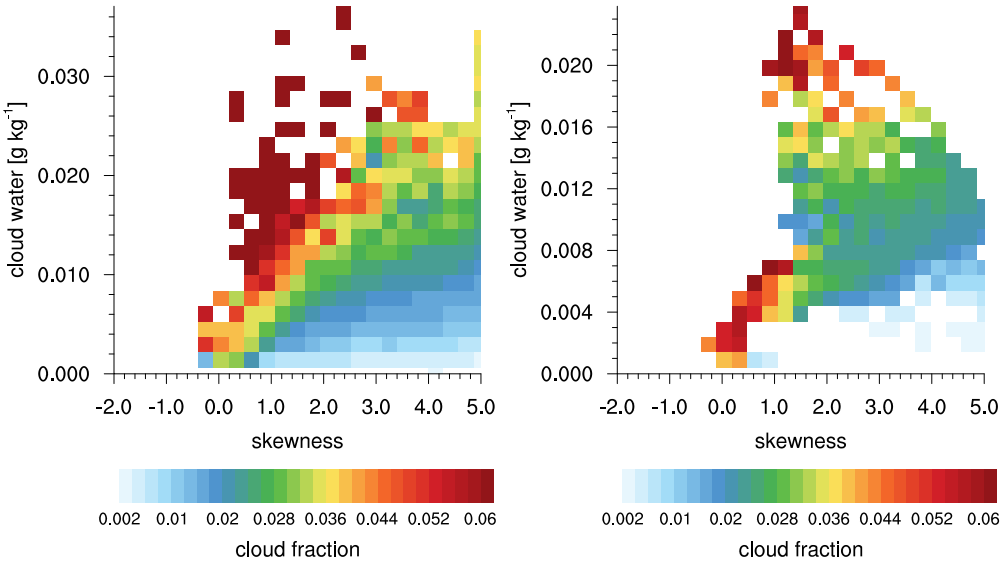

(a) CGILS shallow cumulus case (s6)

(b) RICO shallow cumulus case

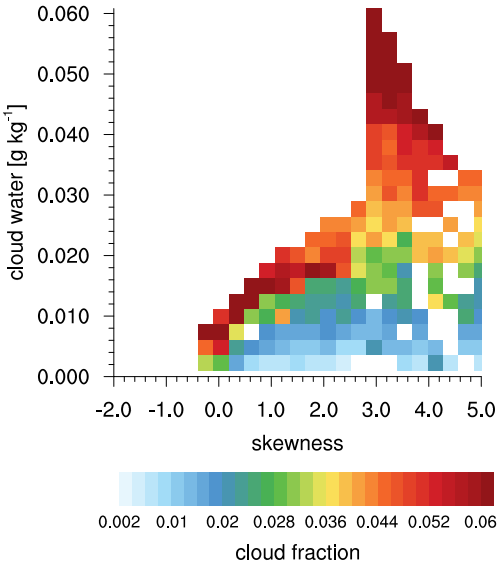

(c) Deep convection

Figure 4.11: Average cloud fraction for a specific combination of cloud water and skewness: a change parallel to the x-Axis represents the dependency of cloud fraction on perturbations in skewness, a change parallel to the y-Axis represents the dependency of cloud fraction on cloud water. The analysis is shown for three different LES datasets: two shallow cumulus cases and one deep convective.

4.6.3 Evaluation of the representation of the dependency

The dependency of cloud fraction on cloud water and skewness seen in the previous section, should also be represented by cloud fraction parameterizations. The effect of changes in cloud water and skewness will be tested for two different setups using the two different closures (T02 and T08).

- **Case T02** Given: Skewness ζ, total water r_t, cloud water r_c, $p = 2$

$$\begin{aligned} & p = 2 \\ & \zeta = \frac{2(q-p)}{p+q+2}\sqrt{\frac{p+q+1}{pq}} \quad \Rightarrow \quad q \\ & q \geq 2 \end{aligned} \tag{4.46}$$

- **Case T08** Given: Skewness ζ, total water r_t, cloud water r_c, $(p-1)(q-1) = 2$

$$\begin{aligned} q &= \frac{(\zeta+2)+\sqrt{2(s^2+4)}}{2-\zeta} \\ q &\geq 1.1 \\ p &= \frac{q+1}{q-1} \\ p &\geq 1.1 \end{aligned} \tag{4.47}$$

The case T02 is formulated in the same way as the original setup in the Tompkins scheme. This means, that it also neglects negative skewness. For the case T08 only the restriction to bell shape ($(p > 1) \wedge (q > 1)$)is introduced, but negative skewness is allowed.

For the test-experiment fixed values for the total water mean ($\bar{r}_t = 4\,\mathrm{gkg}^{-1}$) and the saturation mean ($\bar{r}_s = 4.5\,\mathrm{gkg}^{-1}$) are used. Then the cloud water and skewness are varied and the respective cloud fraction is calculated. Figure 4.12 shows the cloud fraction for both cases calculated for this test-experiment sorted by skewness and cloud water. It can be seen that the expected dependencies are represented. The cloud fraction increases for increasing cloud water and decreasing skewness. For the case T02 the strong limitations on the skewness can be seen (Fig. 4.12a). This leads to both an over- and an underestimation of the cloud fraction compared to the case T08 (Fig. 4.12b) with the more flexible skewness. By comparing the range of skewness between the LES datasets (Fig. 4.11) and the parameterizations (Fig. 4.12) it can be seen, that also the more flexible closure T08 might still be too restrictive on the skewness, as a skewness higher than $\zeta = 1.8$ is not allowed.

By using the cloud water as an input parameter, the influence of the skewness can be represented in a reasonable way. This could allow the representation of the effects of physical processes (e.g. precipitation) which are affecting either the cloud water or the cloud fraction but not both in the same way.

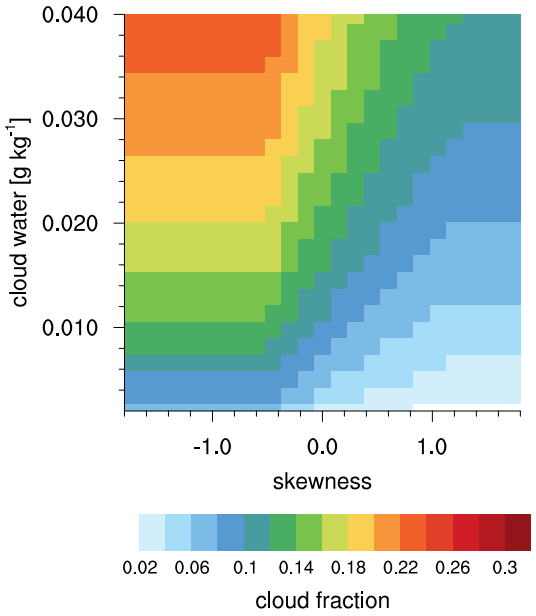

(a) Case T02

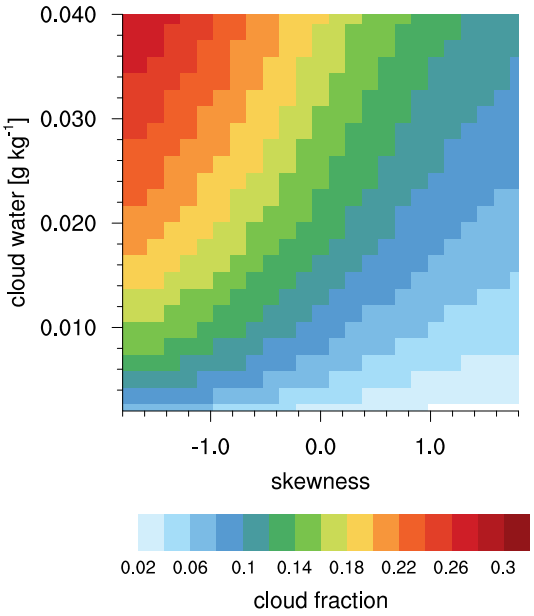

(b) Case T08

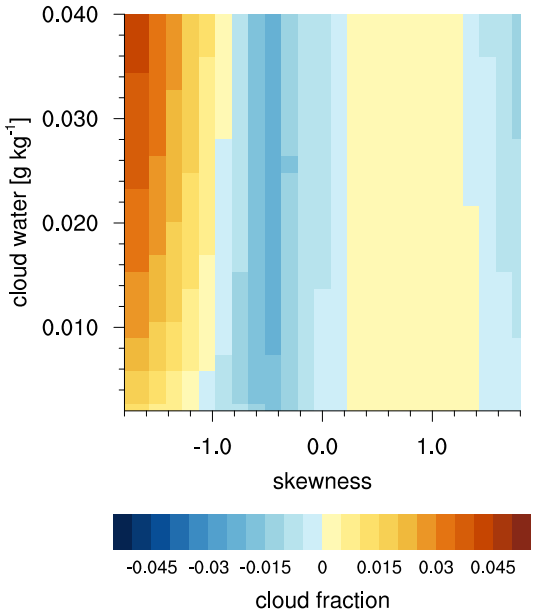

(c) Difference: case T08 - case T02

Figure 4.12: Dependency of cloud fraction on skewness and cloud water for the two different constraints T02 and T08: a change parallel to the x-Axis represents the dependency of cloud fraction on perturbations in skewness, a change parallel to the y-Axis represents the dependency of cloud fraction on cloud water. The experiments use a fixed total water mean $\bar{r}_t = 4\,\mathrm{g\,kg^{-1}}$ and saturation mixing ratio of $\bar{r}_s = 4.5\,\mathrm{g\,kg^{-1}}$. The third plot is showing the difference between the two cases.

4.7 Summary and Conclusions

Besides assuming a PDF family and choosing the best possible distribution, statistical schemes also face the challenge of selecting a member of the PDF family based on the information about the moments or other input parameter. One common approach to simplify this process is to reduce the dimension of the parameter space needed to define one member of an assumed PDF family. This reduction changes the behaviour of the scheme and especially the sensitivity to perturbations. This sensitivity due to different ways to determine one specific distribution and the use of varying input parameters, is only rarely discussed, but of a similar importance as the question which PDF family to assume. It is also especially important for the development of equations for the higher moments, as a perfect source term could lead to too strong or weak forcing due to an over- or underestimated sensitivity. In this study differences in sensitivity have been discussed using the example of two different closures for the beta distribution suggested by Tompkins (2002, 2008).

One big advantage of the general beta distribution is the compact support, but this can also lead to the unphysical existence of a negative distribution minimum. Without introducing additional constraints, it is not excluded, that certain combinations of total water, cloud water and skewness are leading to such a negative distribution minimum. Several options to deal with this situation have been discussed and evaluated using high-resolution model output. In the original scheme by Tompkins (2002) an additional evaporation of cloud water was used to ensure a distribution minimum greater or equal to zero. Based on the presented analysis, a better compromise between physical correctness and computational effort is to keep the general beta distribution as an approximation to the truncated beta distribution and correct for this approximation by renormalization for the cloud fraction.

Our physical understanding how the PDF of humidity should change and evolve in time is based on the evolution of the higher moments variance and skewness. In the original version Tompkins (2002) introduced prognostic equations for one shape parameter and the distribution width of the PDF. In order to prepare the scheme for the introduction of new source terms and to improve the representation of subgrid-scale variability, the original prognostic equations have been revised to be formulated in terms of skewness and variance.

With the introduction of prognostic equations for skewness and variance, it became easier to exchange the source terms and introduce new parameterizations. Especially the old convection source term was formulated in an ad-hoc way by using a tunable constant and was also strongly coupled to a specific distribution. These two issues could be solved by presenting a new parameterization of the convection source terms. Klein et al. (2005) suggested more physically based source terms for the contribution by convection, but these terms were based on the differences between the moments of

the total water in the environment and in the updraft (or detrained quantities). As the higher order moments of detrained total water are not available in a typical GCM, large eddy simulations have been analyzed to provide a first simple parameterization of the source terms, that can be implemented in a common GCM without the need to introduce new variables.

The most important output parameter of a statistical cloud scheme is still the cloud fraction itself. The dependency of the cloud fraction on perturbations in the input variables cloud water and skewness has been analyzed using high-resolution model data. As expected, an increasing cloud water content led to an increasing cloud fraction, if the rest of the environment stayed relatively similar. If the cloud water content is not changed, an increase in cloud fraction can also be obtained by a decrease in skewness. This can be explained by understanding the skewness as a measure of heterogeneity for the distribution of cloud water. The condensed cloud water could be clustered with high values at a small area (strong positive skewness) or it could be distributed rather homogeneously covering a larger area (small skewness). The two correlations can be reproduced by assuming a beta distribution and using the total water mean, the cloud water mean, the skewness and one of two closures suggested by Tompkins (2002) and Tompkins (2008). In theory, the connection between the skewness and the cloud fraction could be used to provide a better representation of microphysical processes. Some processes, for instance precipitation, are influencing the amount of cloud water but not the actual cloud fraction. This could be obtained by compensating the effect of a change in cloud water by a change in skewness. A step into that direction is certainly made by the simple linear approach presented in section 4.4.3, but for a more thorough representation of the influence on the distribution by microphysical processes, a more sophisticated parameterization would be necessary.

Three major development steps have been suggested to the statistical scheme of Tompkins (2002) in order to improve the representation of subgrid-scale variability of total water. Even though the formulation of a completely consistent PDF approach is a big challenge, this also shows its great potential. There are many options to couple the PDF to other approaches, besides the ones earlier mentioned, also the optical thickness, the radiation or the autoconversion could benefit from a more detailed description of the subgrid-scale variability as it is provided by a PDF. All those couplings will cause new challenges for the consistency, but in the end a good interaction between the parameterizations could greatly improve the overall performance of the model.

Short summary of chapter 4:

- Different closures used to reduce the degrees of freedom for the determination of a specific PDF lead to different sensitivities to perturbations. This has to be taken into account for the prognostic (or diagnostic) equations for the moments.
- The approximation of a truncated beta distribution by the general beta distribution in case of a negative distribution minimum provides a consistent treatment of the prognostic cloud water. Avoiding the previous additional evaporation leads to an improved representation of subgrid-scale variability of total water.
- Prognostic equations for the higher order moments variance and skewness of total water have been suggested.
- A new parameterization for the convection source terms has been introduced. This parameterization is formulated independent of the specific distribution parameters, and does not contain an additional tunable constant.
- If the cloud water is increased or the skewness is decreased, the cloud fraction should increase, assuming the rest of the environment stays unchanged. This behaviour can be represented by the statistical cloud scheme (based on Tompkins (2002)) irrespective of the closure.

Chapter 5

Evaluating the revised statistical cloud schemes in the ECHAM6 GCM

In chapter 4, three major development steps for the statistical cloud scheme by Tompkins to improve the representation of subgrid-scale variability of total water were presented. In this chapter, the development steps are evaluated by comparing the resulting critical relative humidity with observational datasets. As reference experiments a relative humidity scheme and the original implementation of the statistical cloud scheme by Tompkins are used. The differences in the representation of the critical relative humidity obtained by the implementation of the three development steps, are explained based on a detailed analysis of: the changes in the source terms of the prognostic equations for skewness and variance, the resulting mean skewness, and the coupling between the statistical scheme and the cloud physics. This study emphasizes the potential of the statistical cloud scheme to produce a reasonable subgrid-scale variability of total water, but it also points out the importance of a detailed investigation and understanding of the coupling between the cloud cover scheme and the cloud physics.

5.1 Introduction

The varying representations of clouds in general circulation models (GCM) remain one major driver for uncertainties in climate change simulations (e.g., Bony and Dufresne 2005; Randall et al. 2007). As today's general circulation models' (GCM) resolution of $\mathcal{O}(100\,\mathrm{km})$ is still too coarse to resolve clouds, a parameterization for cloud processes and fractional cloud cover is needed. In this chapter, three development steps taken to improve the representation of the subgrid-scale variability of total water (sum of water vapor, liquid and ice water) by a statistical cloud scheme (Tompkins 2002) will be evaluated applying the metric of critical relative humidity.

All cloud cover parameterizations used in current GCMs assume a certain distribution of subgrid-scale variability of humidity. Two main categories of cloud cover parameterizations are Relative Humidity (RH) schemes and statistical schemes, which are also known as assumed PDF schemes. RH schemes (e.g. Sundqvist (1978), Sundqvist et al.

(1989)) assume a distribution of relative humidity with a fixed distribution width. In these schemes, a critical relative humidity is defined as a threshold for the relative humidity to allow cloud fraction to grow. Beyond this threshold, cloud fraction increases monotonically with relative humidity, until a 100% relative humidity leads to a cloud fraction of 1. In these schemes, the critical relative humidity defines the point where the subgrid-scale variability of humidity is strong enough to cause fractional cloud cover in an environment that is – on average – still unsaturated. Quaas (2012) used observational data of cloud fraction and relative humidity to calculate an observed value of critical relative humidity by assuming a uniform distribution of relative humidity. With this, the critical relative humidity can be understood as a measure for the strength of subgrid-scale variability of humidity and can be applied for the evaluation of cloud fraction parameterizations.

Statistical cloud schemes are defined by the assumption of a specific underlying probability density function (PDF) of humidity. Some approaches also assume joint PDFs of humidity and temperature, and some even of vertical velocity (e.g. Larson et al. (2002)). If the distribution width of the assumed PDFs is fixed, they can be associated with a RH scheme (see e.g. Smith (1990)). Tompkins (2002) introduced a statistical scheme assuming a beta distribution of total water and using two additional prognostic equations to determine the shape and the distribution width of the PDF. In the previous chapter (chapter 4), possible extensions and modifications of this scheme have been presented in order to improve the representation of subgrid-scale variability of humidity.

The representation of subgrid-scale variability of humidity is the zeroth order task of every cloud fraction parameterization. In this chapter, a comparison to observed values of critical relative humidity will be used to evaluate the possible extensions of the statistical scheme by Tompkins (2002). As reference experiments, a RH scheme based on Sundqvist et al. (1989) and the original statistical scheme by Tompkins (2002) will be used. Both schemes are already implemented in the ECHAM6 GCM. Three major development steps in order to improve the subgrid-scale variability of humidity by the statistical scheme and one minor change to an additional restriction on the cloud water (liquid plus ice) will be introduced stepwise. This facilitates an analysis of the effects of each step of the development. To solely analyze the differences caused by the development steps to the statistical cloud scheme, all changes have been implemented without any retuning of the ECHAM6 GCM. Furthermore, the evaluation of the experiments is performed for model levels without any height interpolation in order to avoid the consequential effects on the results.

The study is organized in the following way: In section 5.2, some remarks on the method and observational data are made. Section 5.3 provides a short review of the RH scheme by Sundqvist et al. (1989) and the statistical scheme by Tompkins (2002) as well as the development steps applied to the statistical scheme. The results of the

evaluation based on critical relative humidity and a detailed analysis of the differences in the statistical schemes are shown in section 5.4, followed by summary and conclusions in section 5.5. The PDF used in the statistical schemes presented here, is a PDF of total water mixing ratio, but for a better readability the specification 'mixing ratio' will be dropped in the rest of the study.

5.2 Method, Model and Data

5.2.1 Metric of critical relative humidity

One measure to evaluate the representation of subgrid-scale variability of humidity is to use the metric of critical relative humidity. This quantity describes the relative humidity threshold (less than 100% of the grid box mean relative humidity) where clouds start to form. If a uniform PDF with a width related to the saturation is assumed, the critical relative humidity can be obtained by

$$\mathrm{RH}_{\mathrm{crit}} = 1 - \frac{1 - \overline{\mathrm{RH}}}{(1-f)^2} \quad , \tag{5.1}$$

where f with $0 < f < 1$ describes the cloud fraction, $\overline{\mathrm{RH}}$ the mean relative humidity and $\mathrm{RH}_{\mathrm{crit}}$ the critical relative humidity. With this the measure of critical relative humidity has become an observable and the model output can be compared to observational datasets and it is possible to evaluate the strength of subgrid-scale variability of humidity (Quaas 2012).

5.2.2 Model and Data

For the model development and global climate runs, the general circulation model (GCM) ECHAM6 (Stevens et al. 2013) is used. The presented version of the model contains the bugfixes mentioned in Stevens et al. (2013) and a new radiation parameterization (see section 2.2.1). For the evaluation of the varying changes to the cloud scheme, 1 year (2008) of an AMIP Simulation (present-day conditions and fixed SSTs) with a 2 months spinup is analyzed.

As a reference for the critical relative humidity two different observational datasets (annual mean of 2007) are used. One dataset is a combination of relative humidity from the European Centre for Medium-Range Weather Forecasts Interim Re-Analysis (ERA) and cloud cover from the Cloud-Aerosol Lidar with Orthogonal Polarization satellite observations (CALIPSO), as summarized by the GCM-Oriented CALIPSO Cloud Product (CALIPSO-GOCCP) (Chepfer et al. 2010). The other dataset consists of observations from the Atmospheric Infrared Sounder (AIRS). Details about the observational data can be found in Quaas (2012).

5.3 The evaluated cloud cover schemes

5.3.1 Relative Humidity scheme - Sundqvist

In the control simulation, the relative humidity scheme of Sundqvist (1978) is used. This scheme is the default cloud cover parameterization in the current ECHAM6 (Stevens et al. 2013). If the relative humidity reaches a critical value $\mathrm{RH_{crit}}$ the cloud fraction is calculated as follows:

$$f = 1 - \sqrt{\frac{\mathrm{RH_{sat}} - \overline{\mathrm{RH}}}{\mathrm{RH_{sat}} - \mathrm{RH_{crit}}}} \quad , \tag{5.2}$$

where

$$\mathrm{RH_{crit}} = \mathrm{RH_{crit,top}} + (\mathrm{RH_{crit,surf}} - \mathrm{RH_{crit,top}}) \exp\left(1 - \left(\frac{P_{\mathrm{srf}}}{P}\right)^{\eta}\right) \quad . \tag{5.3}$$

with $\mathrm{RH_{sat}} = 1$, $\mathrm{RH_{crit,top}} = 0.75$, $\mathrm{RH_{crit,surf}} = 0.9$, $\eta = 1$, and a pressure P. The values of $\mathrm{RH_{crit,top}}$ and η are slightly different from the values mentioned in Stevens et al. (2013) of $\mathrm{RH_{crit,top}} = 0.7$ and $\eta = 4$. The changes result in a small shift to higher critical relative humidity values at the top and also a less steep gradient with height compared to the original profile.

5.3.2 Statistical cloud scheme - Tompkins plus modifications (Step 1)

The second reference cloud cover parameterization is the statistical cloud cover scheme by Tompkins (2002), which is also an optional cloud scheme of the ECHAM6 GCM (see section 2.1.1). For this scheme, the spatial subgrid-scale variability of total water is described by assuming a beta distribution as the underlying PDF. The beta distribution is characterized by a minimum and maximum value (a and b) and two shape parameters (p and q).

For partial cloudiness, the distribution is calculated using the mean values of total water and cloud water, the closure $p = 2$ and a prognostic equation for q (Tompkins 2002). In case of a cloud fraction of 0 (clear sky) or 1 (overcast sky), the problem is underdetermined. To still have a description of the subgrid-scale variability of total water and cloud water, an otherwise redundant prognostic equation for the distribution width ($b - a$) is used in these cases. Both prognostic equations are formulated with respect to sources and sinks due to turbulence and convection. For the shape parameter q an additional term due to microphysical changes is included. For the distribution width the microphysical changes are treated implicitly by diagnosing the distribution width in case of partial cloud cover.

The original implementation of the Tompkins scheme contains a condition for the case of partial cloud cover that forces the cloud fraction (f) to be $f \geq 0.01$. This condition is omitted for all statistical schemes in the presented study.

In this study the statistical scheme by Tompkins (2002) is changed in two ways. The first change relaxes a constraint on the minimal amount of cloud water that is needed for a cloud fraction greater zero. If neither the liquid water content nor the ice water content was larger than $\epsilon = 10^{-4}\,\mathrm{g\,kg^{-1}}$ the cloud fraction was set to zero. This was meant to be a consistency check to avoid empty or too small clouds, but the constraint of $\epsilon = 10^{-4}\,\mathrm{g\,kg^{-1}}$ was found to be too restrictive and is relaxed to $\epsilon = 10^{-15}\,\mathrm{g\,kg^{-1}}$. The second change is to use the approximation by the general beta distribution (section 4.3.3) instead of the incomplete beta distribution (section 4.3.1) in case of a negative distribution minimum.

5.3.3 Statistical cloud scheme - revised to use skewness and variance (Step 1+2)

The first development step is to change the scheme introduced by Tompkins (2002) to use prognostic equations for the higher order moments variance and skewness instead of the parameters of the beta function – the distribution width $(b-a)$ and the shape parameter q. The parameterizations for the temporal evolution of the source terms in terms of convection, turbulence and microphysics follow the ideas of Tompkins (2002) and are presented in section 4.4. The original closure of $p = 2$ is replaced by the closure $(p-1)(q-1) = 2$. This closure suggested by Tompkins (2008) provides more flexibility for the skewness – especially with respect to negative skewness – by allowing both shape parameters to change. The specific form of the closure is a pragmatic decision, as it simplifies the equations for skewness and variance. The beta distribution is still restricted to a bell-shaped distribution by ensuring $p > 1$ and $q > 1$.

One important difference of the revised scheme to the original scheme is the possibility to have negative skewness. Especially the microphysics source term, which reduces the skewness, can lead to negative skewness.

For the experiments with the revised statistical scheme, the reduced constraint $\epsilon = 10^{-15}\,\mathrm{g\,kg^{-1}}$ is applied, and in case of a negative distribution minimum, the approximation with a general beta distribution (see section 4.3.3) is used.

5.3.4 Statistical cloud scheme - fully revised, including new convection source terms (Step 1-3)

This implementation of the statistical scheme is based on the revised scheme using prognostic equations for the higher moments variance and skewness. Additionally the new parameterization of the convection source terms presented in section 4.5 has been implemented. With these source terms an additional tunable constant used in the original source terms could be avoided and the formulation of the convection source terms is now independent of the specific distribution parameters.

For the experiments with the revised statistical scheme with the new convection source terms, the reduced constraint $\epsilon = 10^{-15}\,\mathrm{g\,kg^{-1}}$ is applied, and in case of a negative distribution minimum, the approximation with a general beta distribution (see section 4.3.3) is used.

Details on the implementation

In the ECHAM6 GCM, the default convection scheme is based on the Tiedtke mass flux scheme (Tiedtke 1989) with modifications to the treatment of deep convection following Nordeng (1994). A review of the actual implementation in the ECHAM6 GCM can be found in Möbis and Stevens (2012).

The new source terms for the variance ($\overline{r_t'^2}$) and the third moment ($\overline{r_t'^3}$) of total water (r_t) due to convection (conv) are:

$$\left(\frac{\partial \overline{r_t'^2}}{\partial t}\right)_{\mathrm{conv}} = D((\bar{r}_t)_{\mathrm{detr}} - \bar{r}_t)^2 + D(0.27 \cdot \overline{r_t'^2}) \tag{5.4}$$

$$\left(\frac{\partial \overline{r_t'^3}}{\partial t}\right)_{\mathrm{conv}} = D((\bar{r}_t)_{\mathrm{detr}} - \bar{r}_t)^3 + 3D((\bar{r}_t)_{\mathrm{detr}} - \bar{r}_t)(0.27 \cdot \overline{r_t'^2}) + D(0.53 \cdot \overline{r_t'^3}) \quad , \tag{5.5}$$

where $(\bar{r}_t)_{\mathrm{detr}}$ is the detrained total water, D the detrainment rate in inverse seconds and 0.53 and 0.27 regression coefficients derived in section 4.5. In the convection parameterization detrained total water is typically understood as a fraction of the total water in the updraft. This is not consistent with the mean detrained total water, which is used for the source terms in Eq. (5.4) and Eq. (5.5). It is necessary to use the assumption that the mean detrained total water is the same as the mean total water in the updraft.

In the code, the variable connected to the detrainment rate is most of the time carried as a combination of the turbulent detrainment rate (δ_{turb}), the organized detrainment rate (δ_{org}), the mass flux (M) and a height dependency (Δz): $\delta_{\mathrm{turb}} M \Delta z + \delta_{\mathrm{org}} M \Delta z$. The detrainment rate for Eq. (5.4) and Eq. (5.5) is then:

$$D = \frac{(\delta_{\mathrm{turb}} M \Delta z + \delta_{\mathrm{org}} M \Delta z)}{(\Delta z \rho)} \quad , \tag{5.6}$$

where ρ is the density.

The parameterized tendency (Eq. (5.5)) is formulated in terms of the third order moment $\overline{r_t'^3}$, but the quantity needed for the parameterization is the skewness, the central third order moment:

$$\zeta = \frac{\overline{r_t'^3}}{(\overline{r_t'^2})^{\frac{3}{2}}} \quad . \tag{5.7}$$

To still use the original source term, first the skewness is changed to the third order moment by multiplication with the third power of the standard deviation, then the term

is updated and finally converted again to skewness by dividing by the third power of the updated standard deviation. For clarification this transformation between skewness (ζ) and the third order moment ($\overline{r_t'^3}$) is outlined below.

$$\begin{aligned}
(\overline{r_t'^3})_n &= \zeta_n \cdot ((\overline{r_t'^2})_n)^{\frac{3}{2}} \\
(\overline{r_t'^2})_{n+1} &= (\overline{r_t'^2})_n + \left(\frac{\partial(\overline{r_t'^2})_n}{\partial t}\right)_{\text{conv}} \cdot \Delta t \\
(\overline{r_t'^3})_{n+1} &= (\overline{r_t'^3})_n + \left(\frac{\partial(\overline{r_t'^3})_n}{\partial t}\right)_{\text{conv}} \cdot \Delta t \\
\zeta_{n+1} &= \frac{(\overline{r_t'^3})_{n+1}}{(\overline{r_t'^2})^{\frac{3}{2}}_{n+1}}
\end{aligned} \tag{5.8}$$

5.4 Evaluation of the revised implementations using the critical relative humidity metric

The different experiments with the varying cloud schemes are summarized in Tab. 5.1. The names introduced in the left column of Tab. 5.1 will be used in the following to identify a certain experiment. For all experiments with the statistical scheme the constraint to the cloud fraction of $f \geq 0.01$ in case of partial cloud fraction, has been omitted compared to the original implementation in the ECHAM6.

Model version	ϵ [g kg^{-1}]	$a < 0$	**comments**
Sundqvist			used as reference
Tompkins	$1.e^{-4}$	prohibited	used as reference
Tompkins +min	$1.e^{-15}$	prohibited	
Tompkins +min +step1	$1.e^{-15}$	allowed	
Skew & var	$1.e^{-15}$	allowed	prog. eq. for higher moments
New conv	$1.e^{-15}$	allowed	new convection source terms

Table 5.1: Summary of the varying model versions used in this study and the following comparison. In the result sections, the experiments will be identified by the names provided in the 'model version' column.

Further, as the total water mean value is always positive and it is expected that a negative distribution minimum (a) is always connected to a negative skewness with a long left tail, it is assumed that the area under the negative part of the PDF is small and the general beta distribution provides a good approximation to the truncated

beta distribution (section 4.3). To avoid numerical artifacts, a safety negative limit of $a \geq -50\,\mathrm{g\,kg^{-1}}$ has been implemented.

5.4.1 Critical relative humidity in comparison to observational datasets

In this section, the revised implementations and especially their representation of subgrid-scale variability of humidity are evaluated with the metric of critical relative humidity (section 5.2.1).

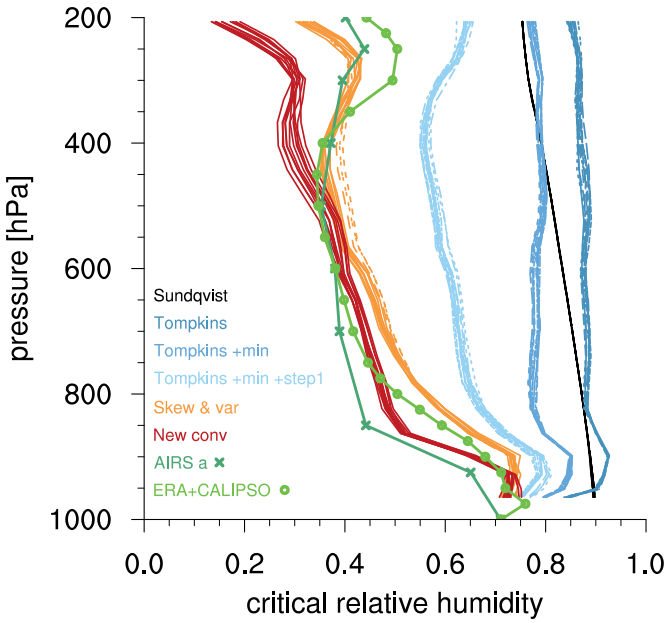

Figure 5.1: Vertical profile of critical relative humidity (global average). For the model runs each line of the same color is the time average of 1 month, for the observational datasets the annual mean is shown.

As a first evaluation step the vertical global mean profiles of critical relative humidity are calculated for the model experiments. Figure 5.1 shows the monthly mean profiles for the model experiments and the yearly profiles for the observational datasets as a reference. With each development step, the vertical profiles of critical relative humidity produced by the statistical scheme get closer to the profiles from observational data. For the Sundqvist scheme the fixed implemented profile is reproduced. Compared to Quaas (2012) the profile shows a slightly different gradient, due to the differences of the constants mentioned in section 5.3.1. The profile for the original Tompkins scheme shows a clear overestimation of the critical relative humidity compared to the observational profiles and is similar to the one in Quaas (2012). The relaxation of the constraint on a necessary minimal amount of cloud water for cloud formation (ϵ) already leads to an improvement for the Tompkins scheme with respect to critical relative humidity. If

additionally not the incomplete beta function is used, but the approximation by the general beta distribution is applied, this leads to a clearly better representation of the subgrid-scale variability of humidity than the original implementation. The two implementations of the revised scheme using prognostic equations for variance and skewness show a good agreement with the observational datasets. The implementation of the new parameterized source terms for the contribution due to convection gives an additional slight improvement compared to the revised scheme (Skew & var). But also for the two revised schemes, the relaxation of the constraint (ϵ) and the use of the general beta distribution instead of the incomplete beta function in case of a negative distribution minimum are essential to obtain such a good agreement with the observational datasets. The earlier constraint of $\epsilon = 10^{-4}\,\mathrm{g\,kg^{-1}}$ was too restrictive and led to a suppression of subgrid-scale variability of humidity. The use of the incomplete beta distribution in case of negative distribution minimum in the original implementation led to additional evaporation of cloud water. This evaporation also suppressed the subgrid-scale variability of humidity, as especially in rather dry areas small amounts of cloud water were evaporated instead of causing a small cloud fraction.

The differences seen in the global mean profiles are also obvious in the global distribution at one specific height level. For the analysis of the global distribution a height of approximately 700 hPa (no interpolation for the model data) has been chosen, as at this height the profiles already developed clear differences (Fig. 5.1), which need to be understood in more detail. But of course, at a height of 700 hPa some numerical artifacts over the continents due to high mountain chains will appear. The conclusions made in this study could also be drawn by only considering the ocean, but for completeness the whole distribution including land is shown in Fig. 5.2. The critical relative humidity profile implemented in the Sundqvist scheme is independent of longitude and latitude. This leads to an almost constant global distribution, which is considerably higher than the observed values. Also the overestimation by the original Tompkins scheme can clearly be seen in the global distribution. Almost no global variability is produced by this implementation. The improvement that has been obtained by the changes to the original implementation of the Tompkins scheme can also be seen in the global distribution. Especially the use of the approximation of the general beta distribution in case of a negative distribution minimum, leads to a global distribution which already shows a similar pattern as the observational data, but is still overestimating the magnitude. The two revised schemes are able to reproduce the global distribution of critical relative humidity shown by observational datasets at 700 hPa in both magnitude and structure. Again, the replacement of the source terms due to convection by the new parameterizations leads to a slight improvement compared to the first version of the revised scheme.

For the discussion about the representation of subgrid-scale variability, not only the mean values as shown in Fig. 5.1 and Fig. 5.2 are relevant, but also the variability of the

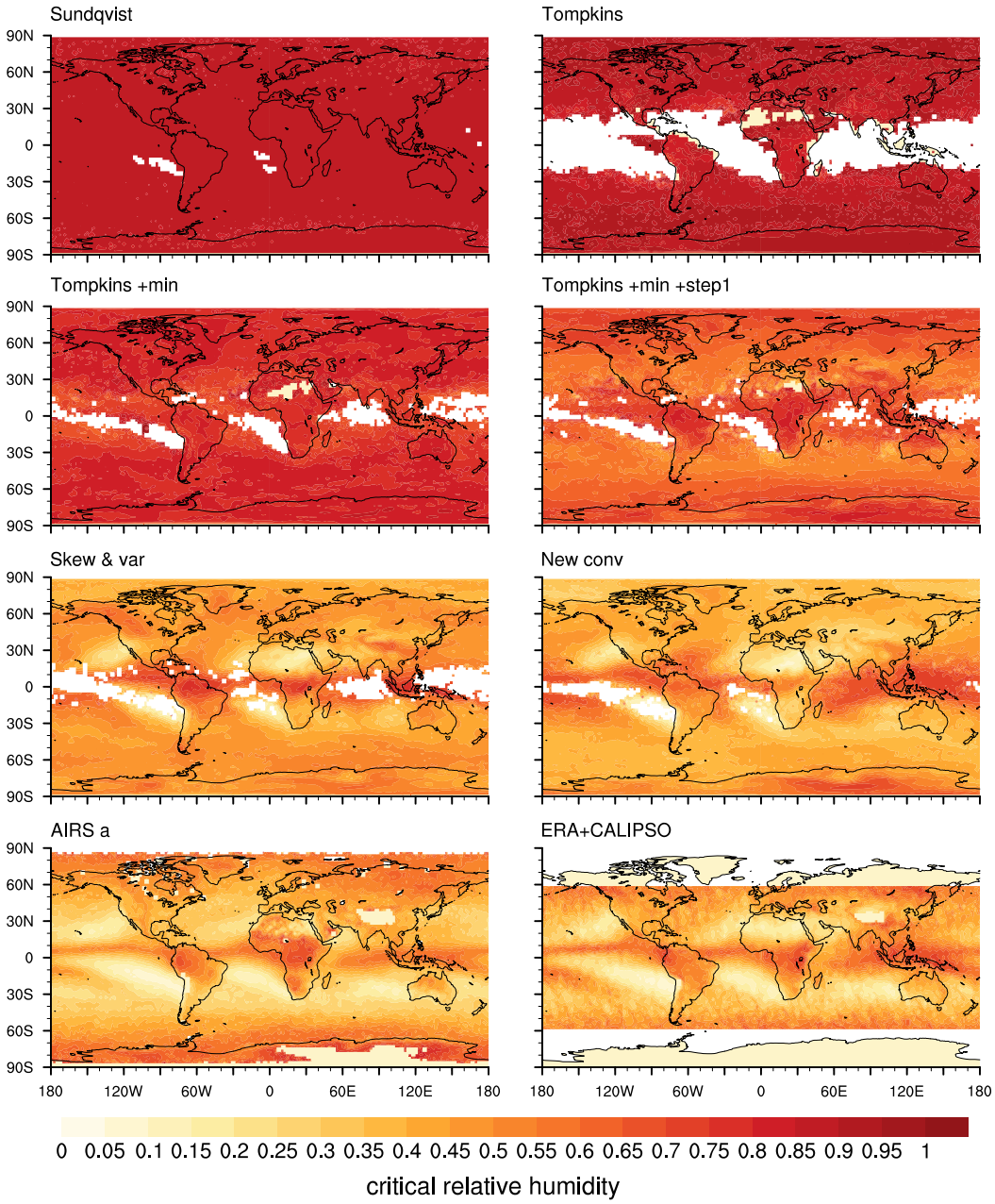

Figure 5.2: Global critical relative humidity at pressure level of approximately 700 hPa (no interpolation for the model data), annual mean for present day conditions, (a) for the Sundqvist scheme, (b) the original implementation of the Tompkins scheme, (c) the Tompkins scheme with $\epsilon = 10^{-15}\,\mathrm{g\,kg^{-1}}$, (d) the Tompkins scheme additionally modified by step 1, (e) the statistical scheme, revised to use prognostic variance and skewness, (f) the revised scheme using the new convective source terms, (g) observations from AIRS, and (h) a combination of relative humidity from ERA-Interim and cloud cover from CALISPSO-GOCCP. White points are missing values due to the restrictions of $0 < f < 1$ and of the critical relative humidity to be greater or equal to zero.

values that are averaged to obtain the mean profile or global distribution. To compare this variability, for one month (June) of data with instantaneous output every 6 hrs, a frequency density function of critical relative humidity is calculated for each height level. As the critical relative humidity is only calculated for partially cloudy cases ($0 < f < 1$), the number of these cases can also be seen as a measure for the variability. The frequency density function of critical relative humidity and the number of partially cloudy cases at each height level are shown for each implementation in Fig. 5.3. The frequency density functions show that the changes in the profile (Fig. 5.1) and the global distribution (Fig. 5.2) for the critical relative humidity are not due to averaging, but that also the internal variability of critical relative humidity is increasing with each development step. For the Sundqvist and original Tompkins scheme the number of partially cloudy cases is low and connected to high values of critical relative humidity. With both changes to the implementation of the Tompkins scheme, the variability of critical relative humidity and the number of partially cloudy cases is increased. The two revised schemes are covering almost the whole possible space, with a higher frequency close to the mean profile, and a high number of partially cloudy cases.

The variability of critical relative humidity is produced by a variability in relative humidity and cloud fraction. To understand the differences produced by the different schemes in more detail, the variability of relative humidity and cloud fraction will be analyzed in the next section.

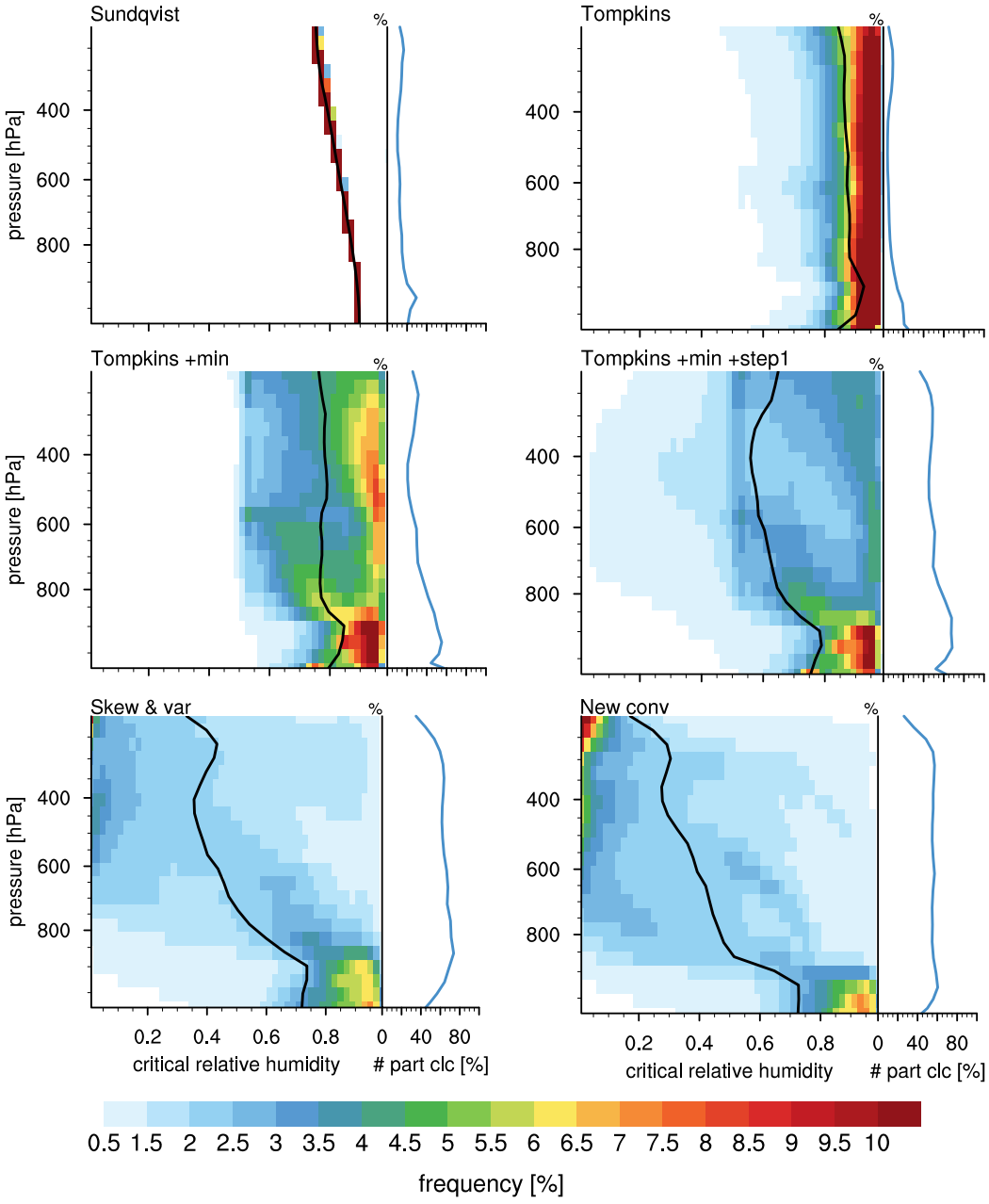

Figure 5.3: Left: Frequency density function of critical relative humidity, calculated for one month of data with instantaneous output every 6 hrs, including every longitude and latitude. No averaging is applied for the values included in the frequency density function. For completeness also the global mean profile is shown in black. Right: Number of partially cloudy cases, $0 < f < 1$, (%). Only for these cases the critical relative humidity is calculated.

5.4.2 Variability of relative humidity and cloud fraction

The variability of relative humidity and cloud fraction is investigated in the same way as the variability of critical relative humidity. For one month of data with instantaneous output every 6 hrs, a frequency density function is calculated at each height level.

The frequency density function of the cloud fraction is shown in Fig. 5.4. For the Sundqvist scheme and the original Tompkins scheme, the cloud fraction contains mainly values of $f = 0$ or $f = 1$. This is consistent with the small number of partially cloudy cases seen in Fig. 5.3. At all heights, the frequency of a cloud fraction with $0 < f < 1$ stays below 1 %. Again, an increase in variability can be seen for the two changes to the implementation of the Tompkins scheme. For the two revised schemes a high increase in variability can especially be seen for the small cloud fractions below 40 %. For the frequency of cloud fractions larger than 80 % a slight decrease appears at pressure levels around 300-200 hPa for the two revised schemes. For the new convection source terms, the frequency of overcast sky ($f = 1$) strongly decreases. Even though it is nontrivial to measure a frequency density function of cloud fraction at different heights, there is strong evidence (e.g. Illingworth and Coauthors (2007)) that a higher frequency of partial cloud cover than the one shown by the Sundqvist and the original Tompkins scheme is desirable.

Figure 5.5 shows the frequency density function of relative humidity. For the pressure level $P < 300$ hPa the frequency of values larger than 80 % is reduced. This tendency is similar to the one that can be seen for the cloud fraction (Fig. 5.4). Especially for the revised schemes, the frequency of high relative humidity values at the levels with $P < 300$ hPa is decreasing. This decrease could lead to the strong decrease in critical relative humidity (see Fig. 5.3) starting at the level around 300 hPa.

By analyzing the changes in the variability of cloud fraction and relative humidity, it seems that the changes in the critical relative humidity are mainly driven by the increased variability in the cloud fraction, especially the higher frequency of small cloud fractions. But also the decrease of relative humidity influences the critical relative humidity and enforces the development of lower critical relative humidity values by the revised schemes.

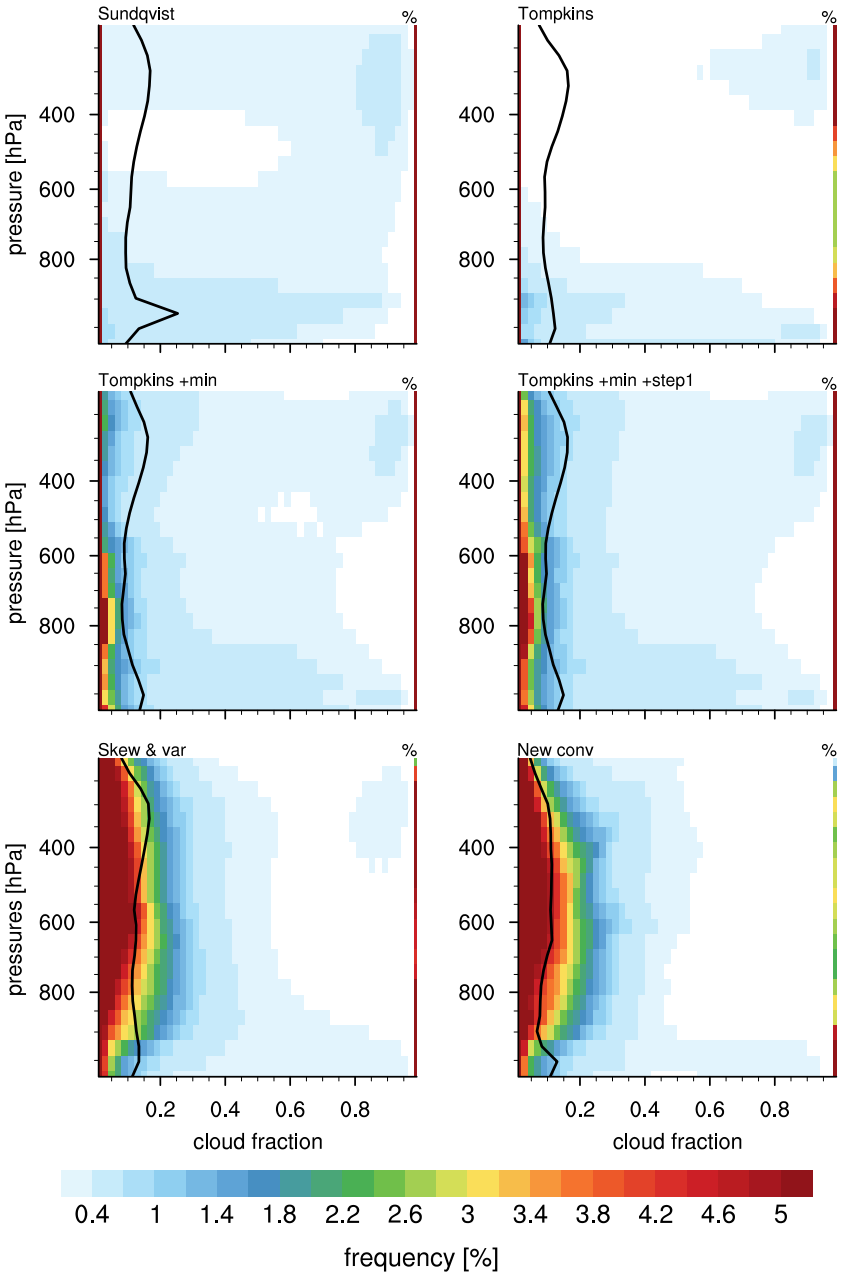

Figure 5.4: Frequency density function of cloud fraction for each height level (contours). The frequency density functions are calculated globally (every latitude and longitude is included) for one month of data with instantaneous output every 6 hrs. No averaging has been applied except for the global mean profile (black line). The colored bar at the right side of each figure shows the high frequency of cloud fraction $f = 1$.

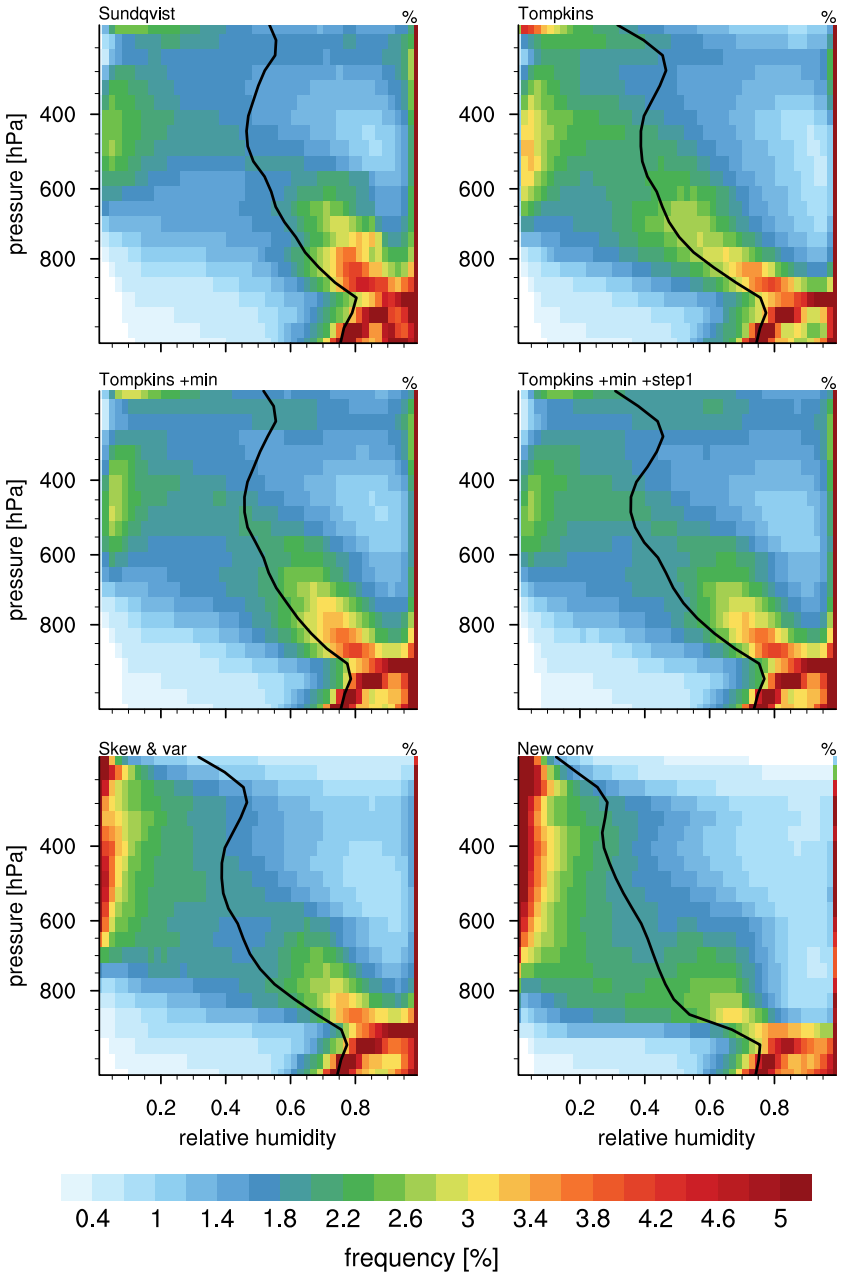

Figure 5.5: Frequency density function of relative humidity for each height level (contours). The frequency density functions are calculated globally (every latitude and longitude is included) for one month of data with instantaneous output every 6 hrs. No averaging has been applied except for the global mean profile (black line).

5.4.3 Differences caused by the changed prognostic equations

In this section, the differences in the representation of subgrid-scale variability of humidity between the three main development steps will be analyzed in detail. The focus will be on the influence of the changed prognostic equations and no longer on the changes introduced by the new treatment of the negative distribution minimum and the relaxation of the minimal threshold for cloud water. In the following analysis the Tompkins scheme using $\epsilon = 10^{-15}\,\mathrm{g\,kg^{-1}}$ and the general beta distribution in cases of a negative distribution minimum (Tompkins +min +step1) will be compared to the revised scheme using prognostic equations for skewness and variance (Skew & var) and the revised scheme using additionally new convective source terms (New conv). If possible also the observational reference datasets will be used.

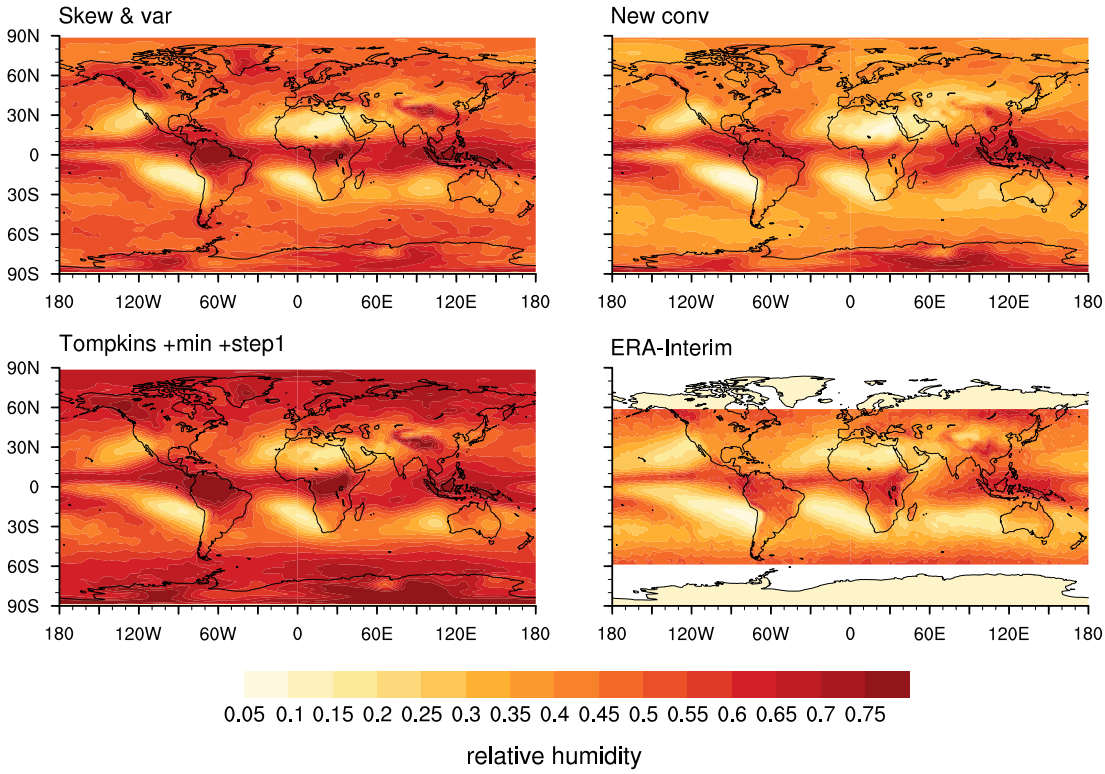

Figure 5.6: Global distribution of annual mean relative humidity at approximately 700 hPa for the revised scheme using skewness and variance, the revised scheme with new convection source terms, the modified Tompkins scheme (+min +step1) and the ERA-Interim reanalysis.

The following analysis will be restricted to the height level of approximately 700 hPa and will explain the differences that can be seen in the relative humidity and cloud fraction, which then finally lead to the differences in the critical relative humidity

(Fig. 5.2). The global distribution of relative humidity is shown in Fig. 5.6. Especially for the new convection source terms, the resulting relative humidity is clearly lower compared to the Tompkins scheme. The relative humidity of the revised scheme lies between the Tompkins scheme and the new convection source terms. For the cloud fraction in Fig. 5.7, the most remarkable change is the increased small cloud fraction in the tropical area for the new convection source terms. This can certainly be seen as one main reason for the improvement of the representation of critical relative humidity in the tropical area (see Fig. 5.2).

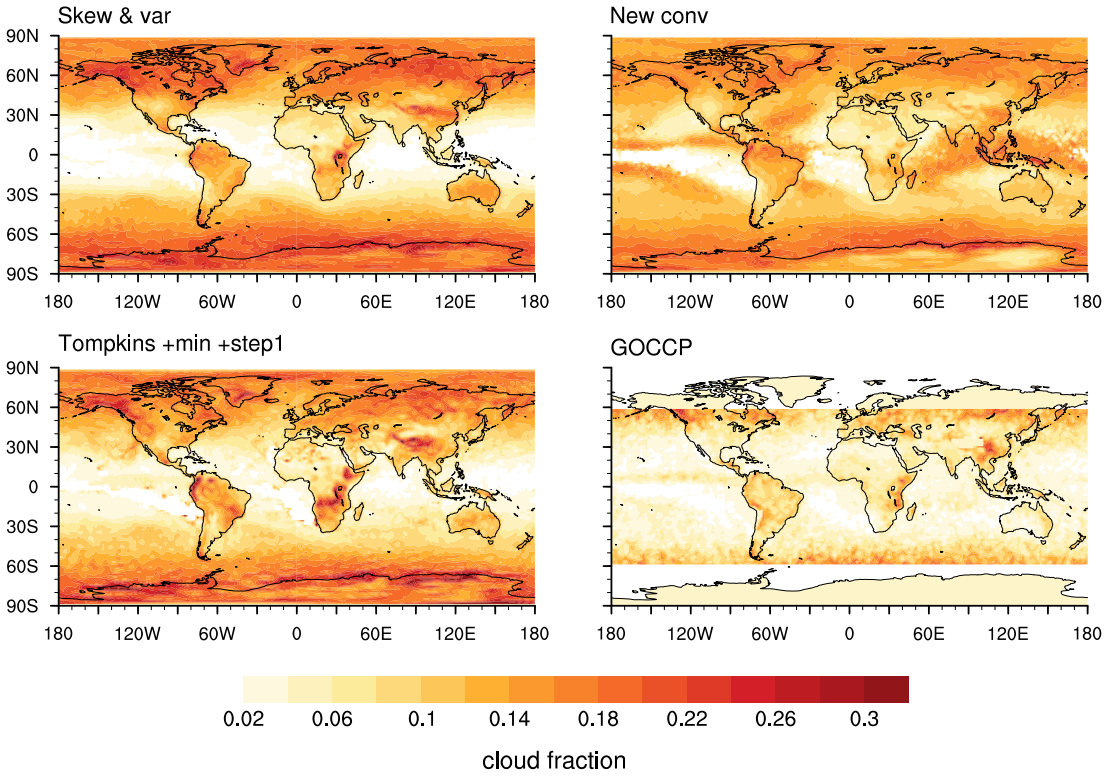

Figure 5.7: Global distribution of annual mean cloud fraction, with $0 < f < 1$, at approximately 700 hPa for the revised scheme using skewness and variance, the revised scheme with new convection source terms, the modified Tompkins scheme (+min +step1) and the GOCCP dataset.

Changes in cloud physics

A lower relative humidity hints at a drier atmosphere containing less water vapor. The comparison of the annual mean water vapor in the three model experiments (Fig. 5.8) shows that for the revised scheme at the height of approximately 700 hPa, less water vapor can indeed be found. The increase in partial cloud cover especially in the tropical

region hints at more cloud water in the atmosphere. And indeed, the comparison of the annual mean liquid water in the three model experiments (Fig. 5.9) shows an increase for the revised schemes compared to the Tompkins scheme. For the scheme using new convection source terms, a decrease in liquid water can be observed around 60° North and 60° South.

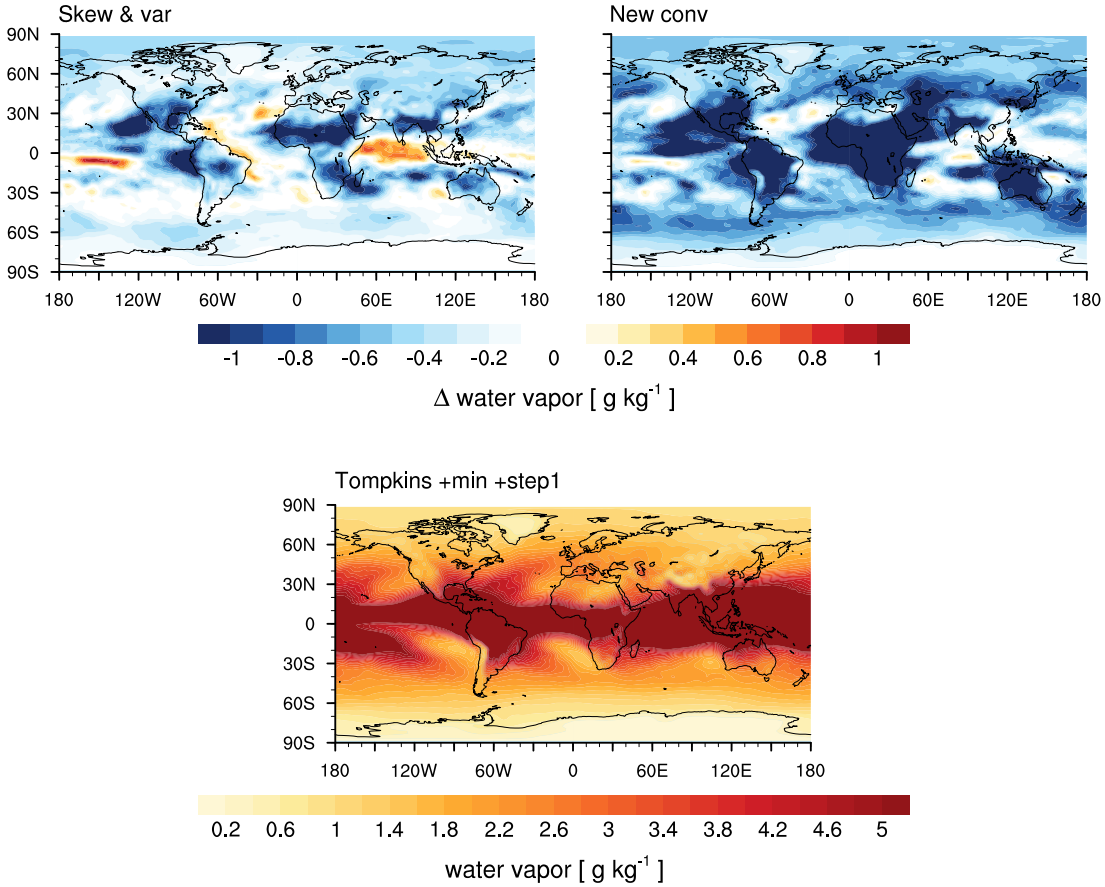

Figure 5.8: Top: Global distribution of the difference between the annual mean water vapor for the revised schemes (Skew & var, New conv) and the annual mean water vapor for the Tompkins scheme (+min +step1) at approximately 700 hPa. Bottom: Annual mean water vapor for the Tompkins scheme (+min +step1) at approximately 700 hPa.

This change to an atmosphere containing less water vapor but more liquid water could be produced by changes in the cloud physics (microphysics parameterization). There are several source and sink terms for the evolution of water vapor and liquid water. Here, as an example, one source and one sink term of liquid water will be investigated, as they are directly influenced by the changes applied to the statistical

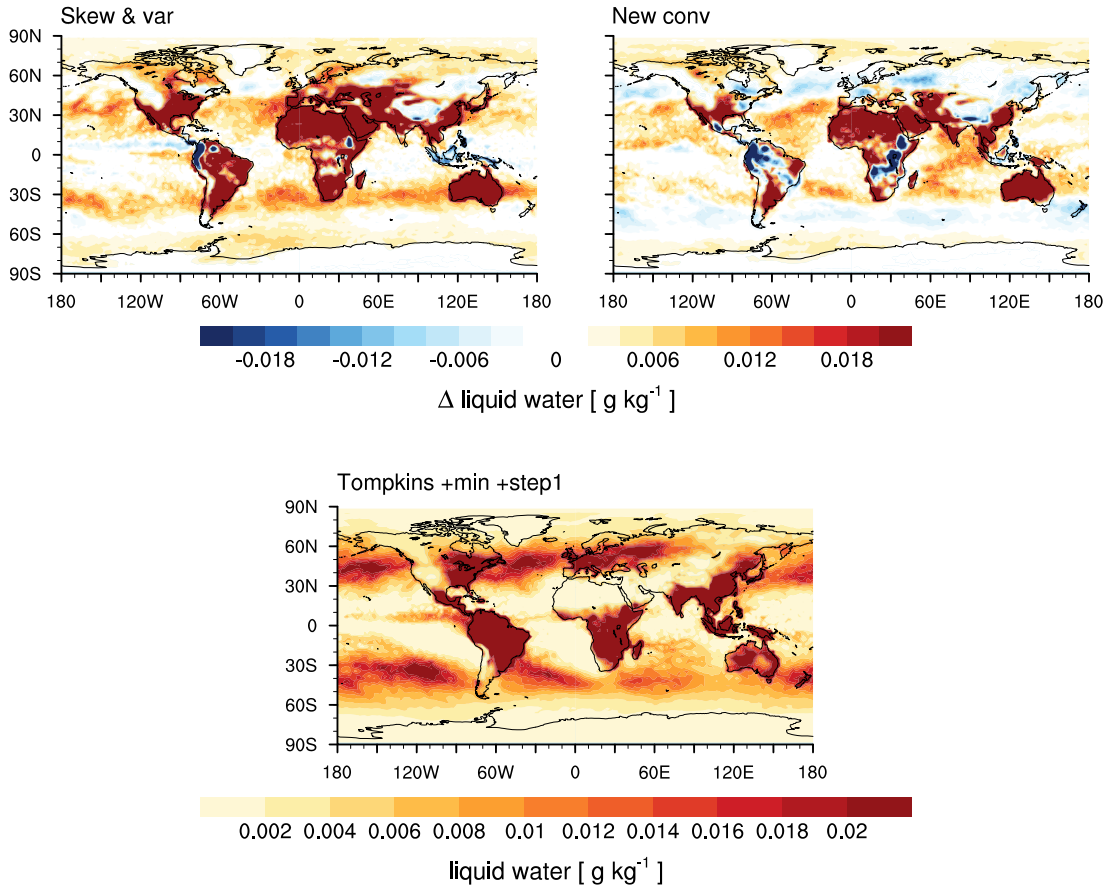

Figure 5.9: Top: Global distribution of the difference between the annual mean liquid cloud water for the revised schemes (Skew & var, New conv) and the annual mean liquid cloud water for the Tompkins scheme (+min +step1) at approximately 700 hPa. Bottom: Annual mean liquid water for the Tompkins scheme (+min +step1) at approximately 700 hPa.

scheme. As mentioned in section 2.1.1, the underlying PDF is used two times in the cloud physics of the GCM: first to transform the influence of turbulence to source and sink terms for the cloud water, and second for the large-scale condensation.

Figure 5.10 shows the sink term for liquid water caused by the influence of turbulence on the shape of the PDF. The relaxation to symmetry by turbulence leads to an evaporation of cloud water. This effect is strongest over the continents, and the evaporation is higher for the revised scheme than for the Tompkins scheme. Figure 5.11 shows the source term of liquid cloud water connected to large-scale condensation. Clearly, the condensation is higher for the revised schemes than for the Tompkins scheme – again especially over the continents – but also over the ocean in the Tropics. The strong

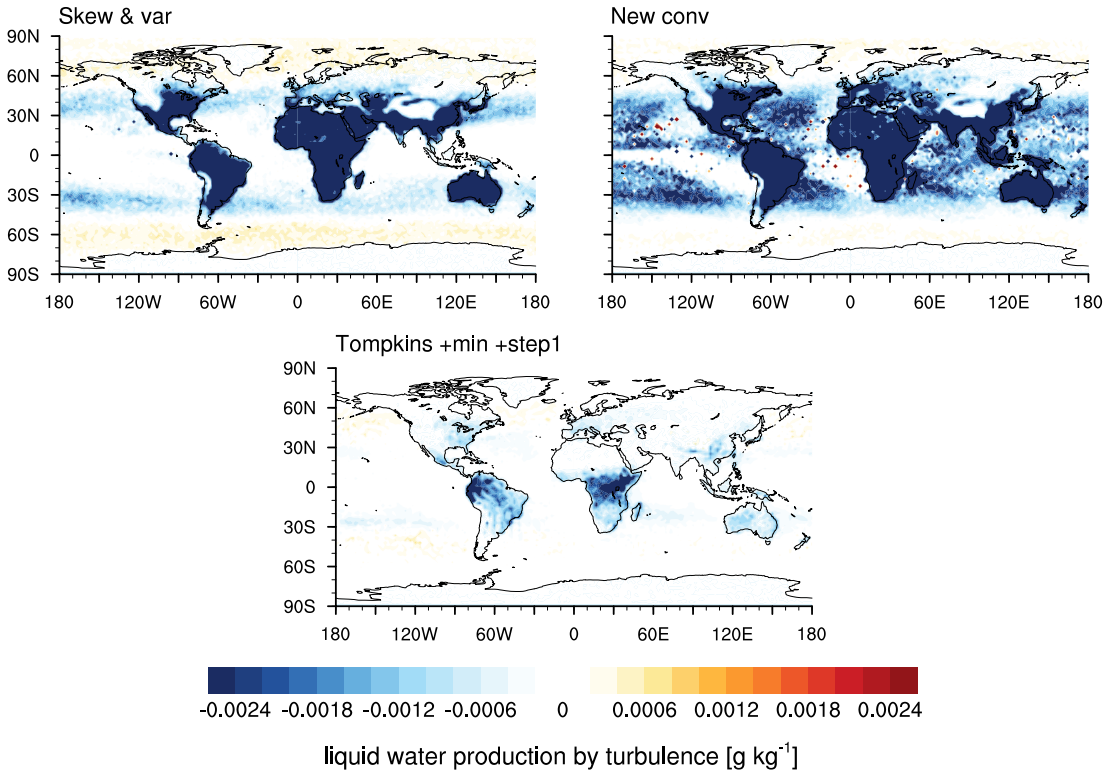

Figure 5.10: Global distribution of the annual mean production of liquid water by the turbulence tendency for skewness and variance of total water within one timestep at approximately 700 hPa; shown for the revised scheme using skewness and variance, the revised scheme with new convection source terms, and the modified Tompkins scheme (+min +step1).

increases over the continents have to be seen with caution, as the analyzed height of approximately 700 hPa can lead to numerical artifacts due to elevated areas. Nevertheless and especially over the ocean, the pattern of increased condensation for the revised schemes can explain in particular the increased cloud fraction in the Tropics. The enhanced processes of evaporation by turbulence and condensation could balance each other, but a comparison of Fig. 5.10 and Fig. 5.11 shows that the condensation is approximately one order of magnitude larger. The stronger condensation can cause a higher cloud fraction that will also enhance other microphysical processes. This can then lead to the changes in the water vapor and liquid water discussed above. One reason for the presented differences in the two specific source and sink terms for cloud water will be discussed in the following section.

Other possible explanations for the change in relative humidity and cloud fraction could be a change in the saturation mixing ratio or an enhanced convection, but no

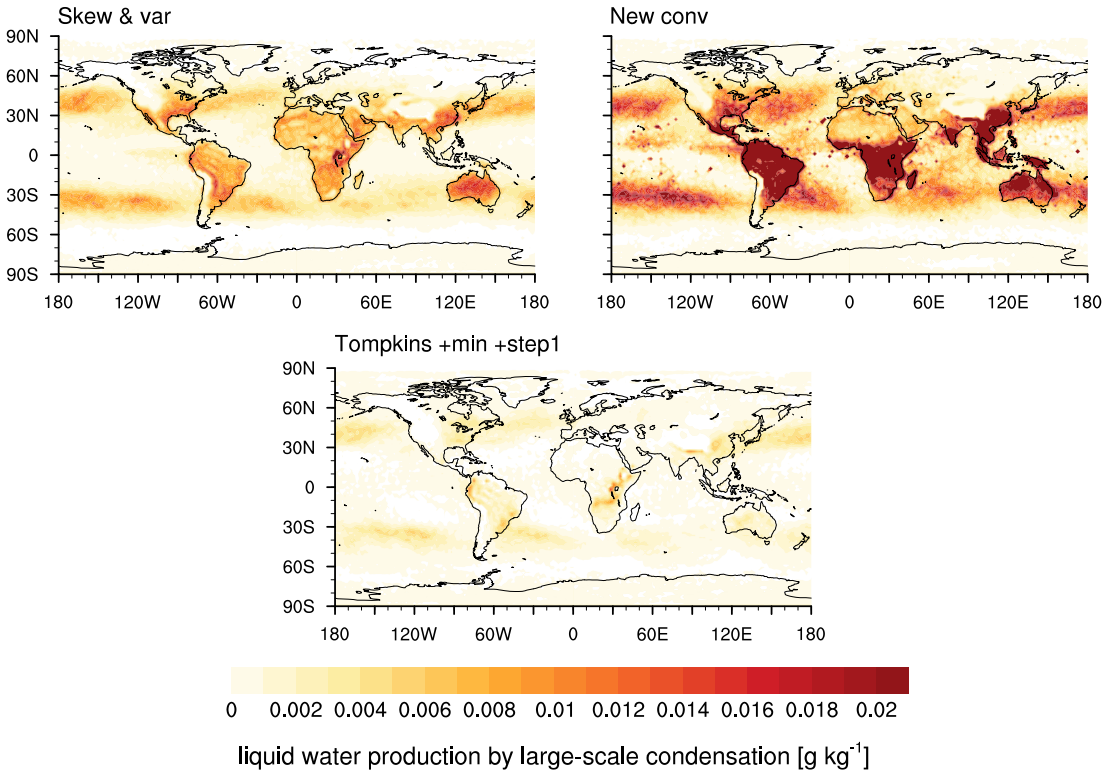

Figure 5.11: Global distribution of annual mean large-scale condensation within one timestep at approximately 700 hPa; shown for the revised scheme using skewness and variance, the revised scheme with new convection source terms, and the modified Tompkins scheme (+min +step1).

strong evidence of these two processes causing the pattern of Fig. 5.6 and Fig. 5.7 could be seen. Nevertheless, in a GCM different processes are interacting with each other and lead to enhancement or weakening of the initial perturbation. The two presented source and sink terms can be the initial reason for the changes observed in the cloud fraction and relative humidity, but the changes are certainly influenced by more processes.

Skewness

The main difference between the three statistical schemes discussed here is the skewness of the underlying PDF. The skewness has been changed to be a prognostic equation and additionally updated with new convective source terms. Figure 5.12 shows the global distribution of skewness at 700 hPa. The Tompkins scheme shows a strong positive skewness in the Tropics and more symmetric distributions at high latitudes and specific regions (at the west side of the continents, the stratocumulus decks). The two revised schemes show a high positive skewness in the Tropics and negative skewness at higher

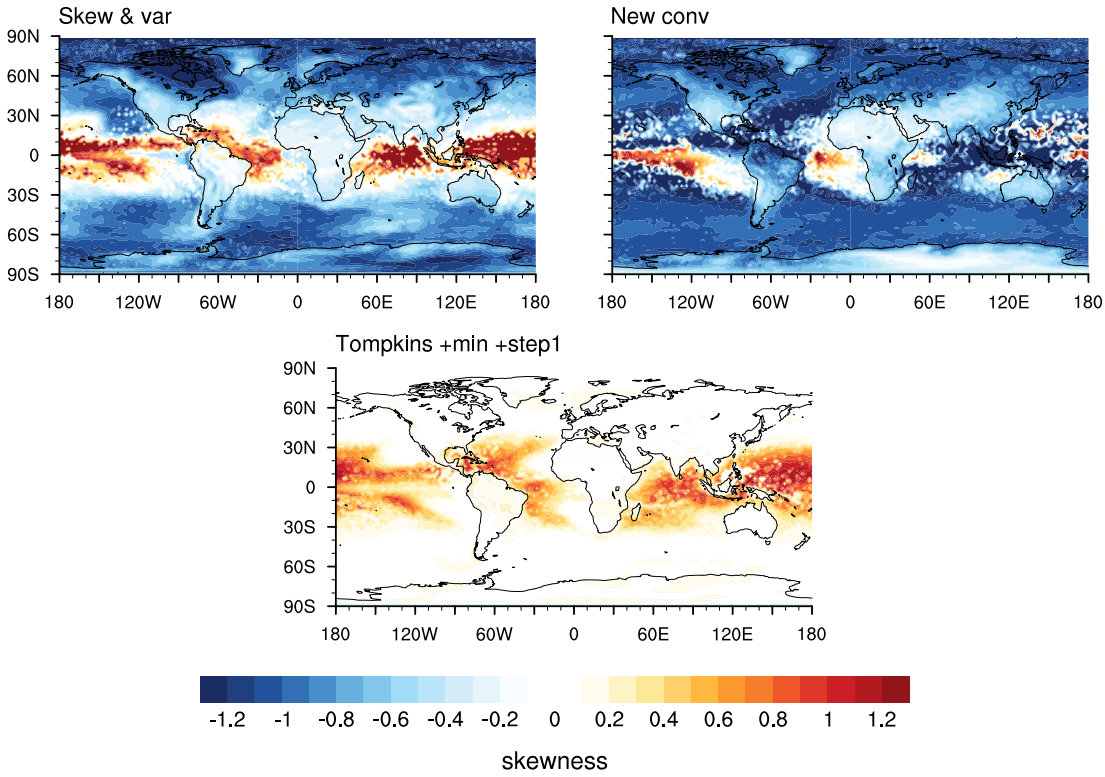

Figure 5.12: Global distribution of annual mean skewness at approximately 700 hPa; shown for the revised scheme using skewness and variance, the revised scheme with new convection source terms, and the modified Tompkins scheme (+min +step1).

latitudes. With the new convective source terms, the skewness in the Tropics is a lot more variable and also becomes negative. The increase in skewness for the revised schemes can partly be explained by the changed limits of the skewness. The minimum and maximum skewness that can be reached with the Tompkins scheme is symmetry ($\zeta_{\text{min}} = 0$) and a positive skewness of $\zeta_{\text{max}} \approx 1.3$. With the change to higher order moments, the skewness becomes a lot more flexible with minimal and maximal values of $\zeta_{\text{min}} \approx -1.8$ and $\zeta_{\text{max}} \approx 1.8$. With this, a broader spectrum of possible skewness values and more extreme values can be adopted. The dominant negative skewness in the two revised schemes seems rather surprising, especially as it was completely neglected in the Tompkins scheme. Weber et al. (2011) found negative integrated skewness in the Tropics by analyzing satellite data, but a thorough understanding of the vertical distribution of skewness is still missing.

With the differences in the skewness, the differences in condensation of water vapor (Fig. 5.11) can be explained. In this framework, a negatively skewed distribution reacts, for small saturated parts, more sensitive to a change in saturation mixing ratio or the

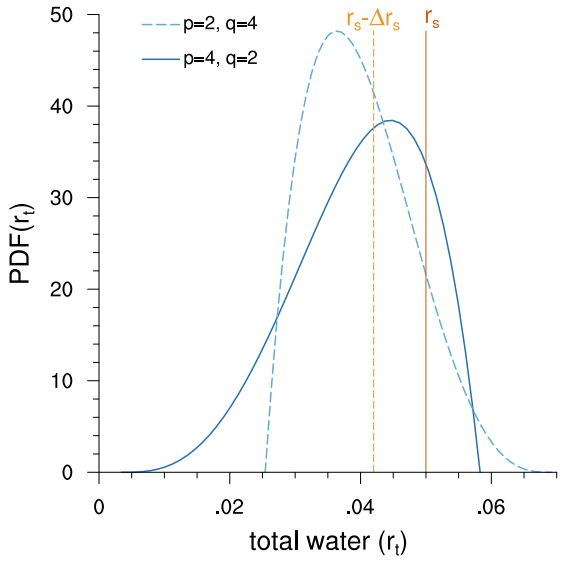

Figure 5.13: Sketch outlining the different sensitivities of a negatively skewed and a positively skewed distribution to a change in the saturation r_s.

mean total water. More specific, the reason for the increased sensitivity is the steep right side of the distribution. This is due to negative skewness, which leads to small values of the shape parameter q. For the same change in saturation mixing ratio, the revised schemes are producing a higher condensation amount, due to their negative skewness. A sketch of two distributions, one with a positive and one with a negative skewness, are shown in Fig. 5.13 to provide a graphical impression on the varying sensitivity of cloud water to a perturbation in the saturation mixing ratio. The decrease in skewness for the revised scheme compared to the Tompkins scheme additionally leads to a favoring of slightly higher cloud fractions, as the cloud fraction tends to increase with decreasing skewness assuming a similar environment. To understand the differences in the evaporation due to turbulence and also the causes for the dominant negative skewness in the revised scheme, a detailed analysis of the source and sink terms for the skewness is necessary.

Skewness tendencies

The temporal evolution of skewness is driven by the contributions from the three different physical processes: convection, turbulence, and microphysics. For the Tompkins scheme the evolution of the skewness is defined by the evolution of the shape parameter q. Due to this, all source terms are formulated as a change Δq to the shape parameter q, with $2 \leq q \leq 50$. For the revised schemes, the evolution is directly described by the prognostic equation and all sources and sinks are formulated as a change $\Delta\zeta$ to the

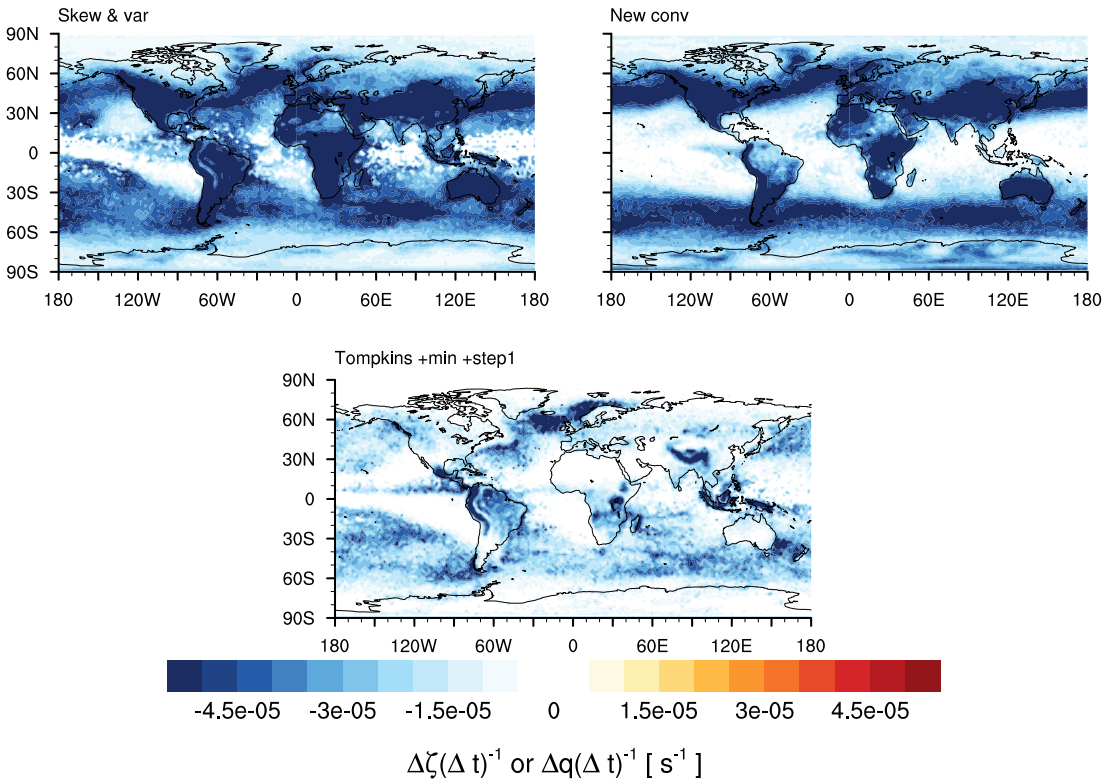

Figure 5.14: Global distribution of the annual mean microphysical tendency for the skewness ζ for the two revised schemes (Skew & var, New conv) and for the shape parameter q for the modified Tompkins scheme (+min +step1) at approximately 700 hPa.

skewness ζ, with $-1.8 \leq \zeta \leq 1.8$. If the source and sink terms from the three statistical schemes are compared, changes to q are compared with changes to ζ and due to this, weaker source terms for the revised schemes are expected compared to the Tompkins scheme.

The main driver for decreasing the skewness and causing negative skewness is the tendency for the microphysics. Figure 5.14 shows the global distribution at approximately 700 hPa. For the Tompkins scheme, the positive skewness can only be reduced until symmetry. For the revised schemes, the tendency for microphysics can also lead to negative skewness, as the skewness is no longer restricted to positive values. Additionally, the sensitivity of the skewness produced by the new closure in the revised schemes to a perturbation in the shape parameter q is higher than for the old closure in the Tompkins scheme (see section 4.2.1). This explains why the microphysics sink term is clearly stronger for the revised schemes than for the Tompkins scheme. For the revised scheme, the simple linear approach to describe the effect of microphysics on the skewness suggested by Tompkins (2002) was adopted. For a more flexible skew-

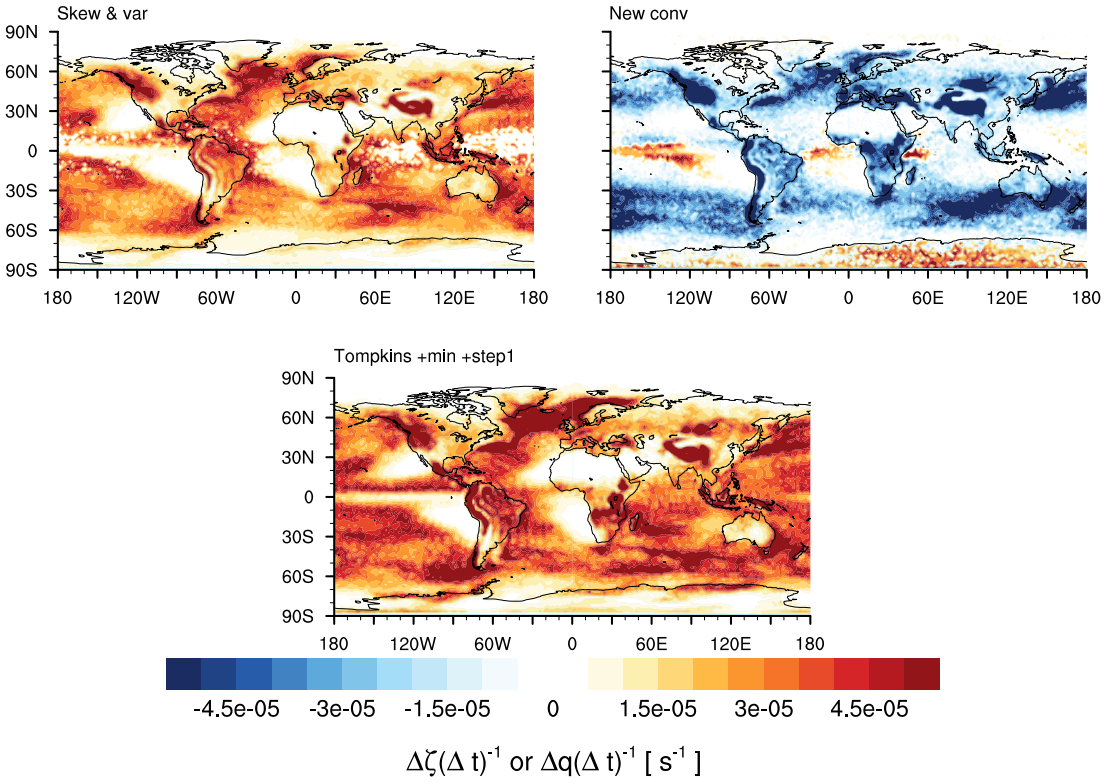

Figure 5.15: Global distribution of annual mean convection tendency for the skewness ζ for the two revised schemes (Skew & var, New conv) and for the shape parameter q for the modified Tompkins scheme (+min +step1) at approximately 700 hPa.

ness, this approach might be too simple and a more detailed investigation would be useful in the future. A possible change, or short term fix, could be to allow only a relaxation to symmetry for the microphysical tendency, to decrease the sensitivity to certain processes, or to include less processes.

The convection tendency (Fig. 5.15) is supposed to be the strongest source for skewness and variance. This is certainly true for the Tompkins scheme and the revised scheme, where the expected weakening of the source term can also be seen. But for the new convection source terms, only in the Tropics positive skewness tendencies can be found, while the main part is negative. With this the convection source term leads to a decrease of skewness. This is not completely unphysical, as instead of a continuous increase in skewness, convection might also lead to a decrease of skewness by contributing to a shift of the whole grid box to a rather moist environment. A mainly moist environment with some dry patches would be described by a PDF with a negative skewness. Nevertheless, as the parameterization of the source term is rather simple, the negative skewness observed here is probably due to a self-amplification of

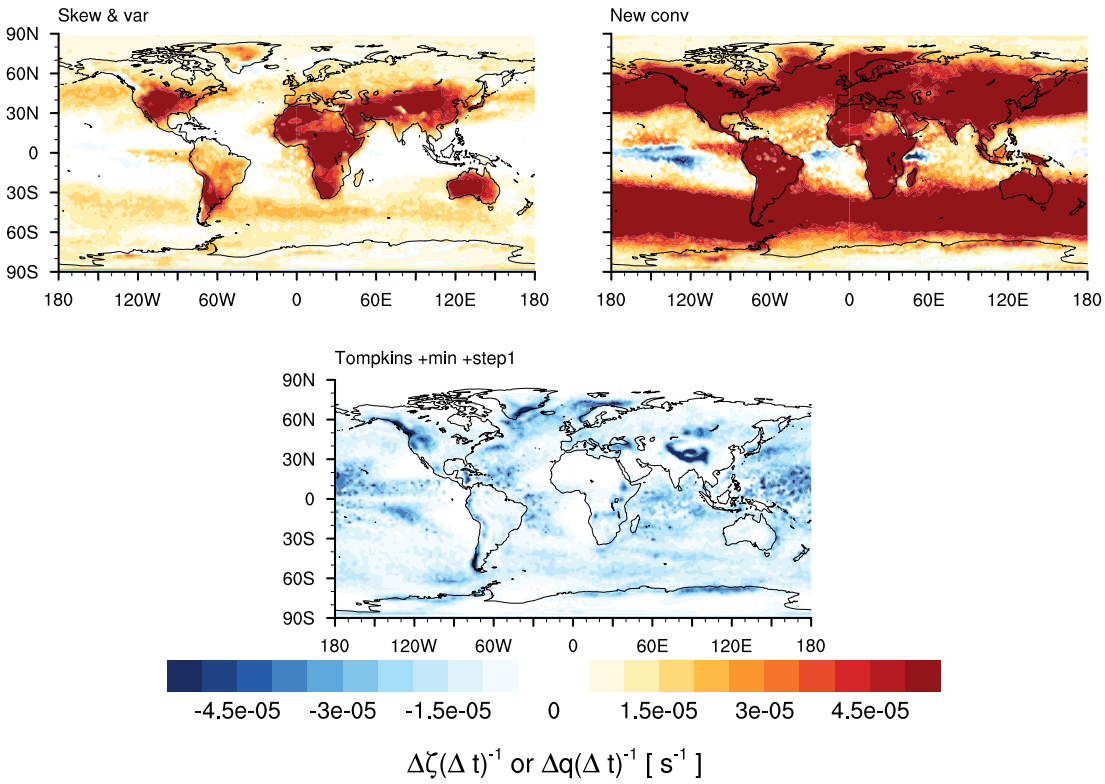

Figure 5.16: Global distribution of annual mean turbulence tendency for the skewness ζ for the two revised schemes (Skew & var, New conv) and for the shape parameter q for the modified Tompkins scheme (+min +step1) at approximately 700 hPa.

the negative skewness introduced by the microphysical tendency.

The turbulence tendency (Fig. 5.16) is at the moment implemented as a relaxation to symmetry. By this, the tendency has a sign opposed to the sign of the skewness. For the Tompkins scheme this leads to a negative forcing by the turbulence. For the revised schemes, the turbulence tendency produces mainly a positive forcing, as large parts of the globe show a negative skewness. Especially for the new convection source terms, the turbulence tendency produces a strong positive forcing, as both other tendencies are providing a negative contribution. This clearly stronger forcing of the turbulence tendency for the revised schemes compared to the Tompkins scheme is consistent with the higher evaporation of cloud water seen in Fig. 5.10.

While discussing the three different tendencies of prognostic skewness equations due to microphysics, convection and turbulence, also some drawbacks have been mentioned. Certainly, all presented parameterizations of the source terms offer some space for improvement. Some suggestions and ideas will be discussed in more detail in the outlook (section 6.2). Besides the effects of the negative skewness that are leading to

higher condensation and with this to a lower critical relative humidity, the negative skewness also has a less physical effect, discussed in the following section.

Distribution parameters

In this section, an overview of the changes in the actual distribution parameters will be given. The two shape parameters p and q (not shown) follow the expected behaviour with respect to the skewness (Fig. 5.12). For the revised schemes, the shape parameter p is often larger than the shape parameter q due to the negative skewness. And especially for the new convection source terms the shape parameter q is rather small, while the shape parameter p shows high values. But this is not the only effect of the dominant negative skewness. As the distribution maximum b is only slightly increasing for the revised schemes compared to the Tompkins scheme, the negative skewness causes large differences in the distribution minimum a, which are shown in Fig. 5.17. While for the Tompkins scheme the distribution minima are small positive values, already for the revised scheme the fraction of negative distribution minima is increasing especially in the high latitudes. With the new convection source terms, the distribution minima become more negative and only some regions at the west side of the continents, which are described by rather symmetric or positively skewed distributions, still show positive distribution minima. This is certainly an effect that needs to be investigated in more detail, as it shows that the forcing by the source terms and the closure almost always results in a distribution minimum outside of the physical range.

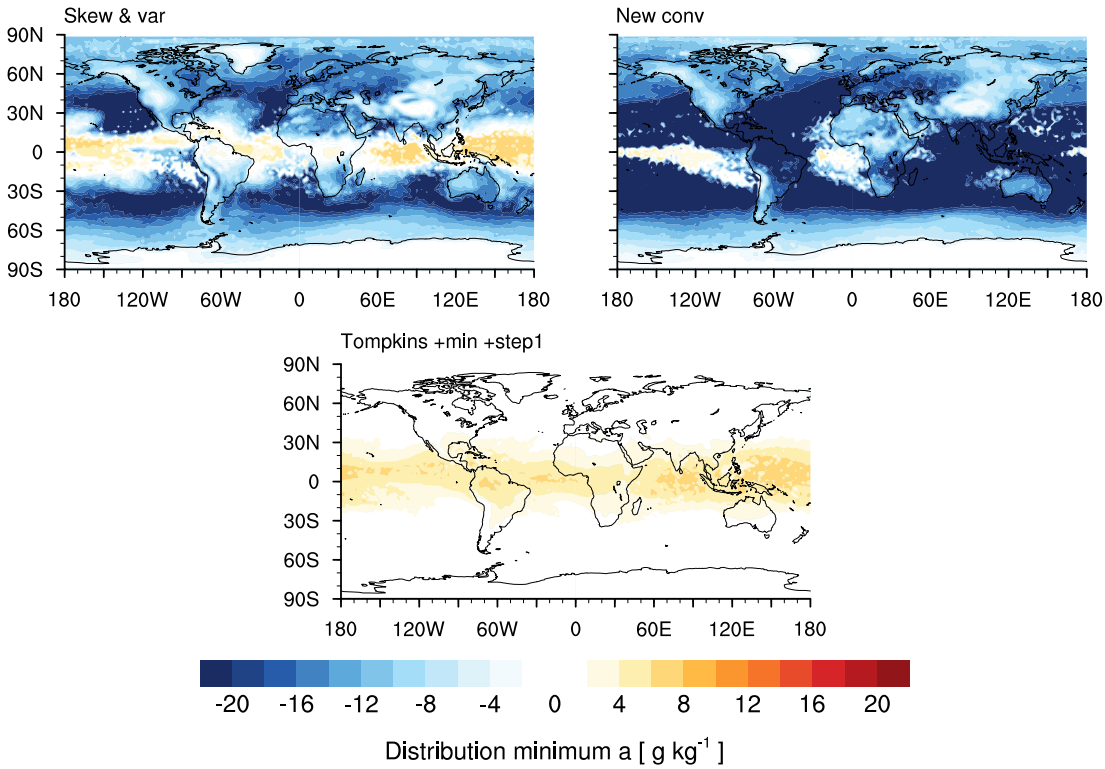

Figure 5.17: Global distribution of the annual mean distribution minimum a at approximately 700 hPa; shown for the revised scheme using skewness and variance, the revised scheme with new convection source terms, and the modified Tompkins scheme (+min +step1)

5.5 Conclusion and Outlook

The implementation of the statistical cloud scheme introduced by Tompkins (2002) in the ECHAM6 GCM has been revised in one minor and three major steps:

0. The original implementation has been changed by setting a lower threshold for the minimal amount of cloud water necessary for cloud formation.

1. The original assumption of an incomplete beta distribution in cases of a negative distribution minimum has been changed to the approximation of a truncated beta distribution by a general beta distribution.

2. The scheme has been revised to use prognostic equations for the two higher moments variance and skewness of the subgrid-scale PDF of total-water mixing ratio.

3. The convective source terms for the prognostic equations have been revised following Klein et al. (2005) with parameterizations for the higher moments of the detrained total water derived from LES diagnostics.

In this study the modifications of the Tompkins scheme (step 0 and 1) and the implementation of the revised scheme without (step 0 to 2) and with (step 0 to 3) new convective source terms in the ECHAM6 GCM are compared to the results from the default cloud cover scheme by Sundqvist and the original Tompkins scheme as well as two observational datasets (AIRS and a combination of ERA-Interim and CALIPSO).

The revision of the statistical cloud cover scheme by Tompkins (2002) in terms of the higher moments – skewness and variance – provides a basis for the introduction of more physical source terms. Additionally, the whole scheme becomes more flexible, as the range of possible values for the skewness is broadened and also negative values are allowed. One suggestion for more physically motivated source terms for the contribution by convection (Klein et al. (2005), and section 4.5) has been implemented. One big advantage of these new convection source terms is their formulation independent of the parameters of the specific distribution.

The representation of the subgrid-scale variability of humidity by the Tompkins scheme, by the introduced modifications, and by the two revised schemes is evaluated using the metric of critical relative humidity, used by Quaas (2012). The critical relative humidity describes a minimal threshold for the relative humidity when clouds start to form. With this a low critical relative humidity can be understood as a high subgrid-scale variability of humidity. The Sundqvist scheme is using a predefined profile of critical relative humidity that is decreasing with height but is independent of latitude and longitude. The values defining this profile are clearly higher than the critical relative humidity that can be observed. Also the original Tompkins scheme is overestimating the critical relative humidity and with this underestimating the subgrid-scale

variability of humidity. The results for both schemes are similar to what was shown by Quaas (2012).

By relaxing the constraint on the cloud water and especially by changing the treatment of cases with a negative distribution minimum to the approximation by a general beta distribution, lower values of critical relative humidity can be obtained for the Tompkins scheme. This improvement continues for the revised scheme using prognostic equations for skewness and variance of total water. The implementation of the new source terms for the contribution by convection shows a slight additional improvement. The two revised schemes are able to reproduce a global distribution and profile of the critical relative humidity more similar to the observational datasets.

The lower critical relative humidity values can be explained by changes in the relative humidity and cloud fraction produced by the development steps applied to the statistical cloud scheme. While the relative humidity is basically reduced during the development steps, the cloud fraction is increased, especially in the Tropics. By an overall improvement in the representation of variability in cloud fraction, especially for small cloud fractions, it became possible to produce the critical relative humidity close to the observed values.

The changed relative humidity and cloud fraction can be explained by the shift during the development steps towards an atmosphere containing less water vapor but more liquid water. A more detailed analysis showed an increased large-scale condensation for the revised schemes. This increased condensation could be an initial reason for the higher frequency of small cloud fractions, especially in the tropics. The large-scale condensation is calculated using the underlying PDF from the statistical scheme and the sensitivity to changes in the saturation mixing ratio or the total water mean is changing with the skewness of the PDF. Due to a strong forcing by the microphysical source term, the skewness of the revised schemes shows large areas with negative skewness and this leads, for rather small saturated parts, to a higher sensitivity to changes in saturation and total water mean. Additionally, the negatively skewed distributions tend to produce a larger cloud fraction compared to positively skewed distribution, as the cloud fraction should increase with decreasing skewness if no other changes are applied. Of course also the interaction with other processes is important for the changes in the mean atmospheric state, but the changed condensation and slightly increased cloud fraction could be the initial reasons.

The large influence of the coupling of the PDF to the microphysical processes (e.g. large-scale condensation) shows that the coupling between different processes and parameterizations is essential for the representation of subgrid-scale variability of humidity. Also the formerly introduced additional evaporation of cloud water by assuming an incomplete beta function in case of a negative distribution minimum, was influencing the microphysical processes and led to a strong restriction on the subgrid-scale variability of humidity.

The evaluation of the distribution parameter and source terms also showed, that even though the increased flexibility of the scheme is an advantage, it is important to refine the way this flexibility is used. As a next step the tendencies and with this the description and understanding of the contribution by physical processes to the evolution of skewness and variance has to be refined. The forcing by the microphysical term seems to be too strong and a new, more sophisticated approach, instead of the simple linear approach, might be necessary. Another possibility is to restrict the microphysical tendency to a relaxation to symmetry. The contribution of turbulence to the evolution of the skewness is for now only described by dissipation. For a more realistic and physical formulation the production and transport terms should be included as well. In this study a first approach to introduce more physically based terms describing the contribution by convection was made. Already the current simple parameterization provides the big advantage to be formulated exclusively in the space of the moments and with this to be independent of the specific assumed PDF family and the applied closures. Also the use of a tunable constant that was necessary in the old convection source terms could be avoided with the new parameterization of convection source terms. Nevertheless, a more sophisticated parameterization of the unknown higher moments of detrained total water might improve the results. Besides refining the parameterization, another open issue is the description and implementation of the contributions by entrainment and downdrafts.

This study and the revised schemes are providing a basis that can be used to introduce more physical tendencies and to refine the contributions of the physical processes. Due to the more physical description provided by prognostic equations for the higher moments, also the coupling to other parameterizations can now be investigated in more detail. By introducing the new convection source terms, an additional step to use more physically based source terms which are independent of the specific distribution has been made. The revised scheme is formulated in higher moments and is able, without any tuning, to reproduce the observed subgrid-variability of humidity measured by the metric of critical relative humidity.

Short summary of chapter 5:

- The three development steps improved the representation of subgrid-scale variability of total water in the metric of critical relative humidity.
- The revised statistical schemes based on prognostic equations for skewness and variance were able to reproduce observed values of critical relative humidity.
- The largest changes were produced by the coupling of the varying PDFs to microphysical processes (e.g. large-scale condensation).
- Refining the source terms of the prognostic equations for variance and skewness will be necessary. Especially the microphysics source terms seem to cause a too strong negative forcing.
- The new implementation of the revised schemes provides the basis for the introduction of new source terms and a more detailed investigation of the coupling to other processes.

Chapter 6

Summary, Conclusions and Outlook

In chapter 3, 4 and 5 several aspects of the evaluation and development of statistical cloud cover schemes are investigated and discussed. They are all motivated by the driving questions how to obtain a representation of subgrid-scale variability of humidity consistent across varying scales and processes. In this chapter an overall summary and conclusion of the thesis are given, following the structure introduced by the research questions, which are raised in the introduction. The summary is followed by an outlook presenting further possibilities to continue the work presented in this thesis.

6.1 Summary and Conclusions

How should the subgrid-scale variability of total water change with resolution? And how can this information be used for the evaluation and development of parameterizations?

A consistent and continuous scaling of the variance of total-water mixing ratio was seen at all analyzed scales, ranging from a general circulation model to large eddy simulations. Neither a spectral gap, nor evidence of a strong scale break was found. Especially for the coarser models, a common power law scaling with an exponent of approximately -2 could be estimated. This estimated scale dependency can be used for the evaluation of cloud parameterizations, as on average they should reproduce this expected scaling behaviour. The variability of the amount of resolved variance for different seasons (NWP) or heights (LES) and especially the spread in the exponents for the high resolution simulations give evidence for different physical processes influencing the amount and the scaling of variance. The aim should be to represent all these fluctuations and variability by using prognostic equations for the moments, but to also reproduce a mean scaling of -2. The presented evaluation of the statistical scheme by Tompkins (2002) showed that the parameterized variance did not produce any scale dependency. Nevertheless, the statistical schemes using flexible higher moments provide a great potential for the development of scale-aware parameterizations

as their representation of subgrid-scale variability can be adjusted to different scales. But before an expected scale dependency can be implemented, for the statistical cloud scheme by Tompkins (2002) it is more essential to improve the overall representation – and reduce the underestimation – of subgrid-scale variability of humidity.

How can the representation of subgrid-scale variability of total water by a statistical cloud scheme be improved?

Three development steps for the statistical cloud scheme have been presented and implemented in order to improve the representation of the subgrid-scale variability of total water. First, in the case of a negative distribution minimum, now an approximation of a truncated beta distribution by a general beta distribution is used. With this it is possible to keep a distribution consistent to all four input variables and avoid an additional evaporation of cloud water. Especially for the representation of small amounts of cloud water this change in the treatment of cases with a negative distribution minimum is essential. Second, prognostic equations for the higher moments skewness and variance of total water, instead of a shape parameter and distribution width, have been suggested and implemented. These new equations provide a better consistency with the other parameterizations, as the higher moments are containing information independent of a specific distribution. But more important is the increased flexibility of the scheme, which now allows negative skewness and can cover a broader spectrum of possible skewness values. Third, the consistency with other parameterizations was additionally increased by a new parameterization for the convection source terms. The original convection source terms proposed by Tompkins (2002) were rather ad-hoc by assuming a scaling between the detrainment of cloud water and the increase in skewness. This relation needed a tunable constant to restrict the efficiency. The new parameterization is based on more physical relations between the total water in the updraft and in the environment, as had been suggested by Klein et al. (2005). An additional advantage is the formulation of the new convection source terms exclusively in terms of the higher moments. This simplifies the exchange of e.g. the assumed PDF family and improves the flexibility of the scheme. Implementing these three development steps led to a representation of the subgrid-scale variability of total water close to observational data in the metric of critical relative humidity.

How does the sensitivity of the properties of the PDF depend on the chosen approach to determine the parameters? How should the parameterization respond to changes in the initial conditions?

Two different closures for the reduction of degrees of freedoms for the statistical scheme based on Tompkins (2002) have been compared. As our physical understanding

of the moments of the PDF of total water with an order higher than three is limited, it is a common approach to reduce the degrees of freedoms to three by additional closures. This study showed how this leads to different sensitivities on perturbations, as different closures project the solutions onto different subspaces. With this, the right source terms can potentially lead to wrong results if the sensitivity of the scheme restricted by the closure is over- or underestimated. This influence of the closure also shows the necessity to formulate the equations for the moments purely in terms of moments and keep the prognostic equations and the transformation to distribution parameters as separated as possible. This separation increases the flexibility and the consistency of the scheme. The differences caused by the application of different closures also underline that the comparison of different statistical schemes should not purely be based on the comparison of the assumed PDF families, but that it is also essential to evaluate and discuss the different ways of determining the parameters.

If the skewness of the statistical scheme is decreased, the cloud fraction should increase, assuming the rest of the environment stays unchanged. This relation was confirmed by analyzing three LES datasets. Furthermore, a good representation of the relation in the framework of the statistical scheme was found under idealized conditions. To understand those responses of the scheme or its output parameter to changes in the input parameter can be useful for the evaluation of the scheme in the framework of a GCM. If a lower skewness is seen in the evaluation of the parameterization in a GCM, a higher cloud fraction should be expected. Otherwise, this increase of cloud fraction had to be balanced by other changes, e.g. a drier or warmer atmosphere.

In the three main chapters, the scale dependency of total-water variance, which should be fulfilled by cloud parameterizations, has been investigated and several steps to improve the representation of subgrid-scale variability of total water have been introduced and implemented. The presented evaluation and development emphasized the great possibilities that are offered by statistical cloud schemes: their ability to reproduce subgrid-scale variability, the opportunities to interact with other parameterizations and their potential to adjust to different resolutions by a flexible description of the shape. Additionally, further interesting research questions and possibilities to improve the statistical cloud scheme have emerged.

6.2 Outlook

For the evaluation of the scale dependency of total-water variance, new upcoming datasets with high resolution on large domains could be a useful extension. In the analysis presented in this thesis, some gaps in the analyzed resolution appeared, due to restrictions by resolution and domain size. These gaps could be closed with the new upcoming datasets. Additionally, if the intermediate wavenumber space is increased

and more processes are represented, this type of analysis can be used to understand the distribution of variability on scales in more detail. Especially the spread in the exponents, which was seen in this study, could be analyzed in more detail, if the numerical uncertainty and the probability of excessive dissipation are reduced. A detailed investigation of how specific atmospheric situations differ in the distribution of variance on different scales, can provide new information for the understanding of physical processes and their interaction across different scales. This enhanced understanding is also essential for the required development of scale-aware cloud cover parameterizations.

The development of the statistical scheme presented in this thesis led to a great improvement of the representation of subgrid-scale variability. Additionally, it forms the basis for following development and possibilities to further improve the representation of physical processes and their interactions. The revised schemes are able to reproduce the same amount of subgrid-scale variability of total water that was seen in observational datasets. Now, the parameterization could benefit from a refining of the source terms in order to constrain and use the possible variability in a reasonable way. The turbulence source term in the skewness equation could be extended by including the production and transport terms. As now a reasonable amount of subgrid-scale variability is obtained, the dissipation term could be used to improve the scale dependency by introducing a stronger dependency on the grid-box size. The new parameterization of the convection source terms can certainly be refined. Nevertheless, a thorough analysis of the influence of convection on the shape of the PDF might be more important. Especially a detailed investigation of the timescales, on which the skewness operates, can provide new insights for the parameterization of the convection source terms. If the timescales are long enough also the possibility for a negative tendency should be included to describe the shift of the whole grid box to a rather humid environment. Another interesting point is the question if it is possible to find a sufficiently good parameterization based on known quantities or if it is necessary to include additional equations for the moments of total water in the updraft. Furthermore, the contributions by downdrafts and entrainment should be included in the convection source terms. In order to parameterize all source terms independent of a specific distribution member, it is most important to revise the microphysical source term as this is still coupled to a shift of the distribution maximum. Furthermore, the representation of the influence of microphysical processes on the shape of the PDF could benefit from a better separation of the individual processes. While some processes (e.g. phase changes) influence the cloud water and the cloud fraction, some might only influence the cloud water but not the cloud fraction (e.g. precipitation). Especially for the latter one, a reasonable tendency for the skewness could balance the decrease of cloud fraction by the decrease in the cloud water, as seen in chapter 4. More consistency for the overall prognostic equations could also be reached by including the advection term, which is still neglected at the moment.

On a long-term perspective, another aim for the development of statistical cloud

schemes should be to enhance the coupling to other parameterizations. For instance, the parameterization of radiation or autoconversion could certainly benefit from the information about spatial variability of total water described by the statistical cloud scheme. An enhanced and improved coupling has a great potential to actually improve the overall performance of the model as it provides a more realistic and consistent representation of the included physical processes.

This thesis has contributed to the evaluation of the scale-dependency of total-water variance and to the development of statistical cloud cover schemes. Several ways to improve the representation of subgrid-scale variability of humidity as well as our understanding of the expected behaviour of a statistical scheme have been introduced. Furthermore, the need for scale-aware parameterizations has clearly been shown, and the found scaling behaviour of total-water variance can be used for their evaluation. The presented revised scheme provides a good basis for following research on different source terms for the higher moments, on the coupling of the PDF to other parameterizations and on the scale-awareness of the statistical scheme.

Appendix A

Appendix

A.1 Source terms by Tompkins (2002)

Convection

The increase of skewness due to convection is related to the detrainment of cloud condensate by

$$\left(\frac{\partial q}{\partial t}\right)_{\text{conv}} = \frac{K}{\bar{\rho} r_s}\frac{\partial}{\partial z}(M^{\text{cu}} r_c^{\text{cu}}) \quad . \tag{A.1}$$

$K = 10$ is a dimensionless tunable constant, M^{cu} is the updraft mass flux, and r_c^{cu} the mean cloud water in the convective updraft, assuming ($r_c^{\text{cu}} \gg \overline{r_c}$).

The change of distribution width is associated with the increase in the shape parameter q, assuming that the distribution minimum does not change ($\Delta a = 0$). The new value for the distribution width can be calculated by using the shape parameter q updated with respect to convection (q_{n+1}^{conv}).

$$\begin{aligned}\left(\frac{\partial(b-a)}{\partial t}\right)_{\text{conv}} &= \frac{(\bar{r}_t - a)(p + q_{n+1}^{\text{conv}})p^{-1} - (b-a)}{\Delta t} \\ (b-a)_{n+1}^{\text{conv}} &= (b-a)_n \frac{p + q_{n+1}^{\text{conv}}}{p+q}\end{aligned} \tag{A.2}$$

Turbulence

The effects of production and vertical transport on the skewness budget are neglected and the dissipation term is formulated as a relaxation of the skewness to symmetry:

$$\left(\frac{\partial q}{\partial t}\right)_{\text{turb}} = (q_0 - q)\left(\frac{1}{\tau_v} + \frac{1}{\tau_h}\right) \quad \text{, with } q_0 = 2. \tag{A.3}$$

For the distribution width, the variance equation including production, vertical trans-

port and dissipation is transformed to be formulated in terms of distribution width:

$$\begin{aligned}\left(\frac{\partial(b-a)}{\partial t}\right)_{\text{turb}} = &-\frac{(p+q)^2}{(b-a)}\frac{p+q+1}{pq}\overline{w'r_t'}\frac{\partial \bar{r}_t}{\partial z} \\ &-\frac{1}{2}(b-a)\left(\frac{1}{\tau_v}+\frac{1}{\tau_h}\right)-\frac{\partial}{\partial z}\left(\Lambda\sqrt{e}\frac{\partial(b-a)}{\partial z}\right) \quad ,\end{aligned} \tag{A.4}$$

with τ_h and τ_v being time-scales, $\overline{w'r_t'}$ the turbulence moisture flux, e the turbulent kinetic energy and Λ a mixing length-scale.

Microphysics

It is assumed, that the microphysics is mainly changing the saturated part and with this the distribution maximum b, while the distribution minimum is assumed to stay unchanged ($\Delta a = 0$). If the whole cloud would be removed, the change of the distribution maximum should be $\Delta b_{\max} = (r_s - b)$ and with this $b_{n+1} = b + \Delta b_{\max} = r_s$. Therefore, the change of the distribution maximum is related to the relative change of cloud water:

$$\Delta b = \frac{\Delta \bar{r}_c^{\text{micro}}}{\bar{r}_c}(b - \bar{r}_s) \quad . \tag{A.5}$$

By using the equation for the mean value $\bar{r}_t = (b-a)\frac{p}{p+q} + a$ and assuming $\Delta a = 0$, a new value for the shape parameter q updated with respect to the microphysics can be calculated by:

$$q_{n+1}^{\text{micro}} = \frac{(b + \Delta b - a)p}{\bar{r}_t - a} - p \tag{A.6}$$

The actual source term for the microphysics is then

$$\left(\frac{\Delta q}{\Delta t}\right)_{\text{micro}} = \frac{q_n - q_{n+1}^{\text{micro}}}{\Delta t} \quad . \tag{A.7}$$

Bibliography

André, J. C., G. D. Moor, P. Lacarrère, and R. D. Vachat, 1976: Turbulence Approximation for Inhomogeneous Flows: Part I. The Clipping Approximation. *J. Atmos. Sci.*, **33**, 476–481, doi:10.1175/1520-0469(1976)033⟨0476:TAFIFP⟩2.0.CO;2.

Arakawa, A., J.-H. Jung, and C.-M. Wu, 2011: Toward unification of the multiscale modeling of the atmosphere. *Atmos. Chem. Phys.*, **11 (8)**, 3731–3742, doi:10.5194/acp-11-3731-2011.

Baldauf, M., A. Seifert, J. Foerstner, D. Majewski, M. Raschendorfer, and T. Reinhardt, 2011: Operational convective-scale numerical weather prediction with the COSMO model: Description and sensitivities. *Mon. Wea. Rev.*, **139**, 3887 – 3905, doi:10.1175/MWR-D-10-05013.1.

Blossey, P. N., et al., 2013: Marine low cloud sensitivity to an idealized climate change: The CGILS LES intercomparison. *J. Adv. Model. Earth Syst.*, **5 (2)**, 234–258, doi:10.1002/jame.20025.

Bony, S. and J.-L. Dufresne, 2005: Marine boundary layer clouds at the heart of tropical cloud feedback uncertainties in climate models. *Geophys. Res. Lett.*, **32**, doi:10.1029/2005GL023851.

Bony, S. and K. A. Emanuel, 2001: A parameterization of the cloudiness associated with cumulus convection; evaluation using toga coare data. *J. Atmos. Sci.*, **58**, 3158–3183, doi:10.1175/1520-0469(2001)058⟨3158:APOTCA⟩2.0.CO;2.

Chepfer, H., S. Bony, D. Winker, G. Cesana, J. L. Dufresne, P. Minnis, C. J. Stubenrauch, and S. Zeng, 2010: The GCM-Oriented CALIPSO Cloud Product (CALIPSO-GOCCP). *J. Geophys. Res.*, **115 (D4)**, doi:10.1029/2009JD012251.

Cho, J. Y. N., R. E. Newell, and G. W. Sachse, 2000: Anomalous scaling of mesoscale tropospheric humidity fluctuations. *Geophys. Res. Lett.*, **27 (3)**, 377–380, doi:10.1029/1999GL010846.

Cusack, S., J. M. Edwards, and R. Kershaw, 1999: Estimating the subgrid variance of saturation, and its parametrization for use in a GCM cloud scheme. *Q. J. R. Meteorol. Soc.*, **125 (560)**, 3057–3076, doi:10.1002/qj.49712556013.

de Roode, S. R., P. G. Duynkerke, and H. J. J. Jonker, 2004: Large-Eddy Simulation: How Large is Large Enough? *J. Atmos. Sci.*, **61**, 403–421, doi:10.1175/1520-0469(2004)061⟨0403:LSHLIL⟩2.0.CO;2.

de Rooy, W. C., et al., 2013: Entrainment and detrainment in cumulus convection: an overview. *Q. J. R. Meteorol. Soc.*, **139 (670)**, 1–19, doi:10.1002/qj.1959.

Fischer, L., C. Kiemle, and G. C. Craig, 2012: Height-resolved variability of midlatitude tropospheric water vapor measured by an airborne lidar. *Geophys. Res. Lett.*, **39 (6)**, doi:10.1029/2011GL050621.

Hourdin, F., et al., 2006: The LMDZ4 general circulation model: climate performance and sensitivity to parametrized physics with emphasis on tropical convection. *Climate Dynamics*, **27**, 787–813, doi:10.1007/s00382-006-0158-0.

Illingworth, A. J. and Coauthors, 2007: Cloudnet. *Bull. Amer. Meteor. Soc.*, **88**, 883–898, doi:10.1175/BAMS-88-6-883.

Jonker, H. J. J., P. G. Duynkerke, and J. W. M. Cuijpers, 1999: Mesoscale Fluctuations in Scalars Generated by Boundary Layer Convection. *J. Atmos. Sci.*, **56**, 801–808, doi:10.1175/1520-0469(1999)056⟨0801:MFISGB⟩2.0.CO;2.

Kahn, B., et al., 2011: Temperature and water vapor variance scaling in global models: Comparisons to satellite and aircraft data. *J. Atmos. Sci.*, **68**, 2156–2168, doi:10.1175/2011JAS3737.1.

Kahn, B. H. and J. Teixeira, 2009: A global climatology of temperature and water vapor variance scaling from the atmospheric infrared sounder. *J. Climate*, **22**, 5558–5576, doi:10.1175/2009JCLI2934.1.

Klein, S. A., R. Pincus, C. Hannay, and K.-M. Xu, 2005: How might a statistical cloud scheme be coupled to a mass-flux convection scheme? *J. Geophys. Res.*, **110 (D15S06)**, doi:10.1029/2004JD005017.

Larson, V. E. and J.-C. Golaz, 2005: Using Probability Density Functions to Derive Consistent Closure Relationships among Higher-Order Moments. *Mon. Wea. Rev.*, **133**, 1023–1042, doi:10.1175/MWR2902.1.

Larson, V. E., J.-C. Golaz, and W. R. Cotton, 2002: Small-Scale and Mesoscale Variability in Cloudy Boundary Layers: Joint Probability Density Functions. *J. Atmos. Sci.*, **59**, 3519–3539, doi:10.1175/1520-0469(2002)059⟨3519:SSAMVI⟩2.0.CO;2.

Larson, V. E., R. Wood, P. R. Field, J.-C. Golaz, T. H. V. Haar, and W. R. Cotton, 2001: Small-scale and mesoscale variability of scalars in cloudy boundary layers:

One-dimensional probability density functions. *J. Atmos. Sci.*, **58**, 1978–1994, doi: 10.1175/1520-0469(2001)058⟨1978:SSAMVO⟩2.0.CO;2.

Le Trent, H. and Z.-X. Li, 1991: Sensitivity of an atmospheric general circulation model to prescribed sst changes: feedback effects associated with the simulation of cloud optical properties. *Climate Dynamics*, **5 (3)**, 175–187, doi:10.1007/BF00251808.

Lohmann, U. and E. Roeckner, 1996: Design and performance of a new cloud microphysics scheme developed for the ECHAM general circulation model. *Climate Dynamics*, **12 (8)**, 557–572, doi:10.1007/s003820050128.

Mellado, J. P., 2010: The evaporatively driven cloud–top mixing layer. *J. Fluid Mech.*, **660**, 5–36, doi:10.1017/S0022112010002831.

Moeng, C.-H. and B. Stevens, 2000: Representing the stratocumulus-topped boundary layer in GCMs. *General circulation model development: past, present, and future*, D. A. Randall, Ed., Academic Press, San Diego, 577 – 603.

Möbis, B. and B. Stevens, 2012: Factors controlling the position of the intertropical convergence zone on an aquaplanet. *J. Adv. Model. Earth Syst.*, **4**, doi:10.1029/2012MS000199.

Nastrom, G. D., W. H. Jasperson, and K. S. Gage, 1986: Horizontal spectra of atmospheric tracers measured during the global atmospheric sampling program. *J. Geophys. Res.*, **91 (D12)**, 13,201–13,209, doi:10.1029/JD091iD12p13201.

Naumann, A. K., A. Seifert, , and J. P. Mellado, 2013: A refined statistical cloud closure using double-gaussian probability density functions. *Geosci. Model Dev. Discuss.*, **6**, 1085–1125, doi:10.5194/gmdd-6-1085-2013.

NCAR Command Language, 2012: (version 6.0.0) [software]. Boulder, Colorado: UCAR/NCAR/CISL/VETS, doi:10.5065/D6WD3XH5, boulder, Colorado: UCAR/NCAR/CISL/VETS.

Nordeng, T. E., 1994: Extended versions of the convective parameterization scheme at ECMWF and their impact on the mean and transient activity of the model in the tropics. *Tech. Memo.*, **206**.

Perraud, E., F. Couvreux, S. Malardel, C. Lac, V. Masson, and O. Thouron, 2011: Evaluation of statistical distributions for the parametrization of subgrid boundary-layer clouds. *Boundary-Layer Meteorology*, **140 (2)**, 263–294, doi:10.1007/s10546-011-9607-3.

Pincus, R., H. W. Barker, and J.-J. Morcrette, 2003: A fast, flexible, approximate technique for computing radiative transfer in inhomogeneous cloud fields. *J. Geophys. Res.*, **108 (D13)**, doi:10.1029/2002JD003322.

Pressel, K. G. and W. D. Collins, 2012: First-Order Structure Function Analysis of Statistical Scale Invariance in the AIRS-Observed Water Vapor Field. *J. Climate*, **25**, 5538–5555, doi:10.1175/JCLI-D-11-00374.1.

Quaas, J., 2012: Evaluating the "critical relative humidity" as a measure of subgrid-scale variability of humidity in general circulation model cloud cover parameterizations using satellite data. *J. Geophys. Res.*, **117, D09208**, doi:10.1029/2012JD017495.

Randall, D., et al., 2007: Climate models and their evaluation. *Climate Change 2007: The Physical Science Basis. Contribution of Working Group I to the Fourth Assessment Report of the Intergovernmental Panel on Climate Change*, S. Solomon, D. Qin, M. Manning, Z. Chen, M. Marquis, K. Averyt, M.Tignor, and H. Miller, Eds., Cambridge University Press, Cambridge, United Kingdom and New York, NY, USA., chap. 8.

Rauber, R. M., et al., 2007: Rain in shallow cumulus over the ocean: The RICO campaign. *Bull. Am. Meteorol. Soc.*, **88**, 1912–1928, doi:10.1175/BAMS-88-12-1912.

Satoh, M., T. Matsuno, H. Tomita, H. Miura, T. Nasuno, and S. Iga, 2008: Nonhydrostatic icosahedral atmospheric model (NICAM) for global cloud resolving simulations. *J. Comput. Phys.*, **227 (7)**, 3486 – 3514, doi:10.1016/j.jcp.2007.02.006.

Schlemmer, L. and C. Hohenegger, in revision: The formation of wider and deeper clouds through cold-pool dynamics. *J. Atmos. Sci.*

Seifert, A. and K. D. Beheng, 2001: A double-moment parameterization for simulating autoconversion, accretion and selfcollection. *Atmos. Res.*, **9–60 (0)**, 265 – 281, doi:10.1016/S0169-8095(01)00126-0.

Seifert, A. and K. D. Beheng, 2006: A two-moment cloud microphysics parameterization for mixed-phase clouds. part 1: Model description. *Meteorol Atmos Phys*, **92 (1-2)**, 45–66, doi:10.1007/s00703-005-0112-4.

Seifert, A. and T. Heus, 2013: Large-eddy simulation of organized precipitating trade wind cumulus clouds. *Atmos. Chem. Phys.*, **13 (11)**, 5631–5645, doi:10.5194/acp-13-5631-2013.

Siebesma, A. P., et al., 2009: Cloud-controlling factors. *Clouds in the perturbed climate system*, J. Heintzenberg and R. Charlson, Eds., MIT Press, Cambridge, Mass., Strüngmann Forum Reports.

Smith, R. N. B., 1990: A scheme for predicting layer clouds and their water content in a general circulation model. *Q. J. R. Meteorol. Soc.*, **116 (492)**, 435–460, doi: 10.1002/qj.49711649210.

Sommeria, G. and J. W. Deardorff, 1977: Subgrid-Scale Condensation in Models of Nonprecipitating Clouds. *J. Atmos. Sci.*, **34**, 344–355, doi:http://dx.doi.org/10.1175/1520-0469(1977)034⟨0344:SSCIMO⟩2.0.CO;2.

Stevens, B. and S. Bony, 2013: Water in the atmosphere. *Physics Today*, **66 (6)**, 29–34, doi:10.1063/PT.3.2009.

Stevens, B., C.-H. Moeng, and P. P. Sullivan, 1999: Large-eddy simulations of radiatively driven convection: sensitivities to the representationi of small scales. *J. Atmos. Sci.*, **56**, 3963–3984.

Stevens, B. and A. Seifert, 2008: On the sensitivity of simulations of shallow cumulus convection to their microphysical representation. *J. Meteorol. Soc. Japan*, **86A**, 143–162.

Stevens, B., et al., 2005: Evaluation of large-eddy simulations via observations of nocturnal marine stratocumulus. *Mon. Wea. Rev.*, **133**, 1443–1462.

Stevens, B., et al., 2013: Atmospheric component of the MPI-M Earth System Model: ECHAM6. *J. Adv. Model. Earth Syst.*, **5 (2)**, 146–172, doi:10.1002/jame.20015.

Sundqvist, H., 1978: A parameterization scheme for non-convective condensation including prediction of cloud water content. *Q. J. R. Meteorol. Soc.*, **104 (441)**, 677–690, doi:10.1002/qj.49710444110.

Sundqvist, H., E. Berge, and J. E. Kristjánsson, 1989: Condensation and Cloud Parameterization Studies with a Mesoscale Numerical Weather Prediction Model. *Mon. Wea. Rev.*, **117**, 1641–1657, doi:/10.1175/1520-0493(1989)117⟨1641:CACPSW⟩2.0.CO;2.

Tiedtke, M., 1989: A Comprehensive Mass Flux Scheme for Cumulus Parameterization in Large-Scale Models. *Mon. Wea. Rev.*, **117**, 1779–1800, doi:10.1175/1520-0493(1989)117⟨1779:ACMFSF⟩2.0.CO;2.

Tiedtke, M., 1993: Representation of clouds in large-scale models. *Mon. Wea. Rev.*, **121**, 3040–3061, doi:10.1175/1520-0493(1993)121⟨3040:ROCILS⟩2.0.CO;2.

Tompkins, A. M., 2002: A prognostic parameterization for the subgrid-scale variability of water vapor and clouds in large-scale models and its use to diagnose cloud cover. *J. Atmos. Sci.*, **59**, 1917–1942.

Tompkins, A. M., 2003: Impact of temperature and humidity variability on cloud cover assessed using aircraft data. *Q. J. R. Meteorol. Soc.*, **129 (592)**, 2151–2170, doi: 10.1256/qj.02.190.

Tompkins, A. M., 2008: Cloud Parametrization. *ECMWF Seminar on Parametrization of subgrid physical processes.*

Wan, H., et al., 2013: The ICON-1.2 hydrostatic atmospheric dynamical core on triangular grids – Part 1: Formulation and performance of the baseline version. *Geosci. Model Dev.*, **6 (3)**, 735–763, doi:10.5194/gmd-6-735-2013.

Weber, T., J. Quaas, and P. Räisänen, 2011: Evaluation of the statistical cloud scheme in the ECHAM5 model using satellite data. *Q. J. R. Meteorol. Soc.*, **137**, 2079–2091, doi:10.1002/qj.887.

Xu, K.-M., 1995: Partitioning mass, heat, and moisture budgets of explicitly simulated cumulus ensembles into convective and stratiform components. *J. Atmos. Sci.*, **52**, 551–573, doi:10.1175/1520-0469(1995)052⟨0551:PMHAMB⟩2.0.CO;2.

Acknowledgements

First of all I would like to thank my supervisors Prof. Dr. Bjorn Stevens, Dr. Verena Grützun and Prof. Dr. Johannes Quaas for their support and scientific advice. Thank you, for giving me the possibility to work on my PhD in this for me new and existing field and for your patient guidance through the topics of atmospheric physics and cloud parameterizations.

I would also like to especially thank the German Weather Service (Deutscher Wetterdienst, DWD) for the financial support through the extramural research program, and Dr. Matthias Raschendorfer, Dr. Dmitrii Mironov, Dr. Ekaterina Machulskaya and Dr. Martin Köhler for many fruitful discussions.

It was great to become and be a part of the IMPRS on Earth System Modelling and I would like to thank Antje Weitz, Connie Kampmann and Wiebke Böhm for their support and organisational effort.

Writing the last sentences of my thesis also makes me aware of the great time I had at this institute and of all the people who contributed to this. And even though I will not mention all the names, I am thankful to everyone contributing to the nice and friendly environment at this institute. I would like to thank Johannes Quaas and the Ex-CCF group for giving me a nice welcome and for their company during my first year at the institute. And I would like to thank Cathy Hohenegger and Axel Seifert and the whole Herz group for adopting me during the last two years. I am thankful to all the people from the former OPS, and the current HOT and LSD seminar, for giving me the chance to present and discuss my work, but also for all the interesting discussions and talks in the seminar. Thanks to Dagmar Popke and Tobias Becker for the discussions about the Tompkins scheme during their work on their Bachelorthesis, and to my 'meteorologists' office for answering all my questions about acronyms and processes.

It would be difficult to write so many pages without people volunteering for proofreading: Thanks to Linda, Thijs, Florian, Julia, Katrin and Felix for spending their time on my drafts. And for the last and personal words: Thanks to Suvarchal for beeing such a great officemate, thanks to Thijs for having always an 'open ear' and to all the people making the lunch- and coffeebreaks, the kicker and tennis games such great events. And thanks to my parents and sisters for always supporting me.



ISSN 1614-1199